

RICE UNIVERSITY

**Transfer-of-approximation Approaches for Subgrid Modeling**

by

**Xin Wang**

A THESIS SUBMITTED  
IN PARTIAL FULFILLMENT OF THE  
REQUIREMENTS FOR THE DEGREE

**Doctor of Philosophy**

APPROVED, THESIS COMMITTEE:

---

Dr. William W. Symes, Chairman  
Noah G. Harding Professor of  
Computational and Applied Mathematics

---

Dr. Tim Warburton  
Associate Professor of Computational and  
Applied Mathematics

---

Dr. Béatrice M. Rivière  
Associate Professor of Computational and  
Applied Mathematics

---

Dr. Colin Zelt  
Professor of Earth Science

HOUSTON, TEXAS

APRIL 2012



## Abstract

### Transfer-of-approximation Approaches for Subgrid Modeling

by

Xin Wang

I propose two Galerkin methods based on the transfer-of-approximation property for static and dynamic acoustic boundary value problems in seismic applications. For problems with heterogeneous coefficients, the polynomial finite element spaces are no longer optimal unless special meshing techniques are employed. The transfer-of-approximation property provides a general framework to construct the optimal approximation subspace on regular grids.

The transfer-of-approximation finite element method is theoretically attractive for that it works for both scalar and vectorial elliptic problems. However the numerical cost is prohibitive. To compute each transfer-of-approximation finite element basis, a problem as hard as the original one has to be solved. Furthermore due to the difficulty of basis localization, the resulting stiffness and mass matrices are dense.

The 2D harmonic coordinate finite element method (HCFEM) achieves optimal second-order convergence for static and dynamic acoustic boundary value problems with variable coefficients at the cost of solving two auxiliary elliptic boundary value problems. Unlike the conventional FEM, no special domain partitions, adapted to discontinuity surfaces in coefficients, are required in HCFEM to obtain the optimal convergence rate. The resulting stiffness and mass matrices are constructed in a systematic procedure, and have the same sparsity pattern as those in the standard finite element method. Mass-lumping in HCFEM maintains the optimal order of convergence, due to the smoothness property of acoustic solutions in harmonic coordinates, and overcomes the numerical obstacle of inverting the mass matrix every time update, results in an efficient, explicit time step.

## Acknowledgements

First and foremost I would like to offer my sincerest gratitude to my advisor Dr. William Symes, who has provided me guidance and advice for the past 4 years. His passion, knowledge and patience make this thesis become ever possible.

I am very grateful to my thesis committee, Dr. Tim Warburton, Dr. Béatrice M. Rivière and Dr. Colin Zelt for overseeing this work, and for their suggestion and advice.

I would like to thank all professors, staffs and fellow graduate students in the CAAM department for providing such a warm and friendly atmosphere for study during the last five years.

I would like to thank Dr. Dan Sorensen and Dr. Jan Hewitt and Dr. Symes for their help on improving my writing and presentation at the Thesis Writing class.

I would like to show my gratitude to Michael O'Brien and Keith Gray for their mentorship during my internships at BP, America.

I am indebted to my family. Without their love and support, I would never be possible to go this far. This thesis is dedicated to my wife, Xuan.

This work was partially supported by The Rice Inversion Project (TRIP) and NSF grant DMS-0714193. I greatly appreciate their support.



# Contents

<b>Abstract</b>	<b>iii</b>
<b>Acknowledgements</b>	<b>v</b>
<b>List of Figures</b>	<b>ix</b>
<b>List of Tables</b>	<b>xii</b>
<b>1 Introduction</b>	<b>1</b>
1.1 Motivation . . . . .	2
1.2 Claim . . . . .	5
1.3 Organization of the thesis . . . . .	7
<b>2 Literature Review</b>	<b>9</b>
2.1 Analytical upscaling . . . . .	10
2.2 Numerical upscaling . . . . .	14
2.3 Summary . . . . .	18
<b>3 Theory of Transfer-of-approximation</b>	<b>21</b>
3.1 Introduction . . . . .	21
3.2 Model problems . . . . .	23
3.3 Flux norm and transfer property . . . . .	25
3.4 Transfer property through intertwining operators . . . . .	29

3.5	Scalar wave equation . . . . .	35
3.6	Summary . . . . .	40
<b>4</b>	<b>Transfer-of-approximation Finite Element Method</b>	<b>41</b>
4.1	Introduction . . . . .	41
4.2	Transfer-of-approximation finite element method . . . . .	42
4.3	Numerical results . . . . .	45
<b>5</b>	<b>Harmonic Coordinate Finite Element Method</b>	<b>63</b>
5.1	Introduction . . . . .	63
5.2	Harmonic coordinates . . . . .	65
5.3	Elliptic equation in non-divergence form . . . . .	67
5.4	Harmonic coordinate finite element method . . . . .	72
5.5	Approximation error of the harmonic coordinates . . . . .	76
5.6	Numerical results for elliptic interface problems . . . . .	83
<b>6</b>	<b>HCFEM for Scalar Wave Equation</b>	<b>93</b>
6.1	Introduction . . . . .	93
6.2	Error estimate of HCFEM for scalar wave equation . . . . .	94
6.3	HCFEM Galerkin approximation . . . . .	95
6.4	Mass-lumping for HCFEM . . . . .	97
6.5	Numerical results for scalar wave equation . . . . .	105
<b>7</b>	<b>Conclusion</b>	<b>113</b>
7.1	Future work . . . . .	115
	<b>Bibliography</b>	<b>117</b>

# List of Figures

1.1	A velocity model with interfaces. . . . .		4
1.2	A log of compressional wave velocity from a well in West Texas, supplied to TRIP by Total E&P USA and used by permission. . . . .		5
2.1	2D checkerboard model, $\epsilon = 0.1$ . . . . .	<code>./fig/metapost/checkerboard.pdf</code>	12
4.1	2D checkerboard model, $\epsilon = 0.1$ . . . . .	<code>./metapost/checkerboard.pdf</code>	46
4.2	Initial value $p(x, 0)$ . . . . .	<code>./initValue</code>	48
4.3	Snapshot of $p(x, t)$ at $t = 1.0$ s. . . . .	<code>./solComparisonAll</code>	48
4.4	Solution's detail from $-0.55$ to $-0.35$ of Figure (4.3) . . . . .	<code>./solComparisonLeft</code>	49
4.5	Sound velocity field for the dipping interface model. Source locates at $(0.65, 0.65)$ . . . . .		50
4.6	Locally refined mesh . . . . .		50
4.7	Difference between solutions by the $P_1$ finite element method on the locally refined mesh and on the regular mesh at $t = 0.4$ s. . . . .		51
4.8	Difference between solutions by the $P_1$ finite element method on the locally refined mesh and the transfer-of-approximation finite element method on the regular mesh at $t = 0.4$ s. . . . .		51
4.9	A patch $\mathcal{P}_k^h$ associated with the node $x_k^h$ is illustrated by the union of elements with red boundaries. . . . .		54

4.10	A patch $\mathcal{Q}_k^h$ associated with the node $x_k^h$ is illustrated by the union of elements with red boundaries. . . . .	55
4.11	Convergence tests for the checkerboard example with $\epsilon = 0.5$ . $P_1$ finite element space is used to construct the global transfer finite element space $S_C^h$ defined in (4.4) as well as $S_C^{0,h}$ in (4.12) and $S_C^{1,h}$ in (4.15). .	58
4.12	Convergence tests for the checkerboard example with $\epsilon = 0.5$ . $P_2$ finite element space is used to construct the global transfer finite element space $S_C^h$ defined in (4.4) as well as the damping transfer finite element space $S_C^{d,h}$ defined in (4.9). . . . .	59
4.13	Convergence tests for the checkerboard example with $\epsilon = 0.1$ . $P_1$ finite element space is used to construct the global transfer finite element space $S_C^h$ defined in (4.4) as well as $S_C^{0,h}$ in (4.12) and $S_C^{1,h}$ in (4.15). .	60
4.14	Convergence tests for the checkerboard example with $\epsilon = 0.1$ . $P_2$ finite element space is used to construct the global transfer finite element space $S_C^h$ defined in (4.4) as well as the damping transfer finite element space $S_C^{d,h}$ defined in (4.9). . . . .	61
5.1	An example of $C(x)$ . . . . .	66
5.2	Left: regular grid $(x_1, x_2) = (jh_x, kh_y)$ . Right: harmonic grid $(y_1, y_2) = (F_1(jh_x, kh_y), F_2(jh_x, kh_y))$ . The coefficient $C(x)$ in equation (5.3) is showed in Figure (5.1), and $C_1 = 20, C_2 = 1$ . . . . .	66
5.3	Illustration of 1D HCFE bases . . . . .	73
5.4	Convergence test for 1D interface problem using $P_1$ finite element method.	81
5.5	Convergence test of HCFEM for the square-circle model when $C_1 = 20, C_2 = 1$ . HCFEM is applied on the regular grid of diameter $h$ . Harmonic coordinates are approximated on the locally refined grid, in which the grid size is $\delta$ ( $\delta = h^2$ ) near interfaces. . . . .	85
5.6	Convergence test of the standard $Q_1$ FEM for the square-circle model when $C_1 = 20, C_2 = 1$ . . . . .	86
5.7	HCFEM is applied on a regular grid of diameter $h = 2^{-6}$ for the square-circle model when $C_1 = 20, C_2 = 1$ . Different locally refined grids of diameter $\delta$ near the interface are tested to show the error effect of harmonic coordinates' approximation. . . . .	87

5.8	Convergence test of HCFEM for the square-circle model when $C_1 = 2, C_2 = 1$ . HCFEM is applied on the regular grid of diameter $h$ . Harmonic coordinates are approximated on the locally refined grid, in which the grid size is $\delta$ ( $\delta = h^2$ ) near interfaces. . . . .	88
5.9	Convergence test of the standard $Q_1$ FEM for the square-circle model when $C_1 = 2, C_2 = 1$ . . . . .	89
5.10	HCFEM is applied on a regular grid of diameter $h = 2^{-6}$ for the square-circle model when $C_1 = 2, C_2 = 1$ . Different locally refined grids of diameter $\delta$ near the interface are tested to show the error effect of harmonic coordinates' approximation. . . . .	90
5.11	Two-layer dip model. . . . .	90
6.1	Illustration of $\Omega_1^{m,n}, \Omega_2^{m,n}, \Omega_3^{m,n}, \Omega_4^{m,n}$ . . . . .	99
6.2	Dipping model . . . . .	107
6.3	Velocity model for dome model . . . . .	108
6.4	Density model for dome model . . . . .	108
6.5	$Q_1$ FEM solution snapshot at $T = 0.75$ s on the dipping model, regular grid quadrature for mass and stiffness matrices. . . . .	109
6.6	$Q_1$ FEM solution snapshot at $T = 0.75$ s on the dipping model, accurate quadrature for mass and stiffness matrices. . . . .	109
6.7	HCFEM solution snapshot at $T = 0.75$ s on the dipping model. . . . .	110
6.8	Difference of $Q_1$ FEM solution on a regular grid $\mathcal{T}^h$ and on a locally refined grid $\mathcal{T}_\delta^h$ around interfaces at $T = 1.3$ s on the dome model. . . . .	111
6.9	Difference of HCFEM solution on $\mathcal{T}^h$ and $Q_1$ FEM solution on $\mathcal{T}_\delta^h$ at $T = 1.3$ s on the dome model. . . . .	111



# List of Tables

4.1	Convergence test for $\epsilon = 0.1$ : $u^\delta, u^h$ are $P_1$ finite element solutions on triangulations of diameter $\delta$ and $h$ , respectively. $u_t^h$ is the transfer-of-approximation finite element solution on the triangulation of diameter $h$ . . . . .	47
5.1	Convergence test of HCFEM for the two-layer dip model. HCFEM is applied on the regular grid of diameter $h$ . Harmonic coordinates are approximated on the locally refined grid, in which the grid size is $\delta$ ( $\delta = h^2$ ) near interfaces. . . . .	91
5.2	Convergence test of the standard $Q_1$ FEM for the two-layer dip model.	91
6.1	RMS error and estimated convergence rate over the region within the red box shown in Figure (6.6) and (6.7). The $Q_1$ FEM here is the one with accurate quadrature for mass and stiffness matrices . . . . .	110

# Chapter 1

## Introduction

Solutions of partial differential equations depend on material coefficients occurring in them. These coefficients also influence the computational cost of a numerical solution for a given level of accuracy. For example an elliptic equation with a highly oscillatory conductivity tensor has a solution that varies on many fine scales. If the solution does not have important structures on the fine scales, this property requires a numerical grid commensurate with the scale of oscillations in the coefficients. As a result the computational cost corresponding to the large number of grid points could become prohibitive even for modern computers. For decades scientists and engineers have been searching for methods that can provide accurate numerical solutions for multiscale problems with acceptable computational cost. In this thesis I explore two new upscaling approaches, using grids on the length scale of solutions features, not medium textures, that intend to accomplish this goal in their designs.

## 1.1 MOTIVATION

Many fundamental problems can be mathematically described by partial differential equations (PDEs). However analytic solutions for them are only available for ideally theoretical settings. Thus approximate solutions play very important roles in science and engineering. However, numerical simulation of these equations in practical applications may require prohibitive cost of computation possibly beyond the capability of contemporary computing technologies. One of the reasons is the wide range of space and time scales characteristic to these applications. For example, the spatial scale in seismic wave simulations is usually several hundred times the dominant wavelength. For homogeneous media both the spatial grid size and the time stepping size are proportional to the shortest wavelength according to the rule of thumb proposed by Alford et al. (1974) and the Courant-Friedrichs-Lewy condition for numerical stability. Another reason is the fine scale nature of media. The fine scale material heterogeneities force us to use even finer grids. Consequently a finite difference modeling in 3D for a single shot would then require a huge amount of memories and computation time, not to mention the inversion process which often involves thousands of such simulations.

This thesis attempts to find efficient and accurate ways of solving problems with many scales, especially those without separation of scales. In problems with separation of scales the characteristic length of the medium heterogeneities is far less than that of the volume of material or of the phenomenon of interest. Homogenization (or analytic upscaling) from the microscopic scale to the macroscopic scale then becomes possible. Given  $\epsilon$  the ratio of the characteristic length of the macroscopic scale over that of the microscopic scale, the coefficient in a scale-separated problems can be

represented reasonably in the form of  $C(x, x/\epsilon, \dots)$ , in which “ $\dots$ ” stand for other possible smaller scales.

In seismic applications the scale of material parameters is not separated since the earth’s material varies in every scale. This thesis focuses on problems that exhibit variance on a continuum of scales and occur in seismic and other applications. Two classes of these problems can be defined. One class consists of *interface problems*, in which medium parameters are piece-wise smooth with discontinuities at interfaces (see Figure (1.1) for example). As known, spatial length scales correspond roughly to frequencies in localized spatial *Fourier transformation*. The Fourier constituent frequencies decay slowly when the material parameter is localized in neighborhood of a discontinuity point. Consequently in interface problems all scales are present, with no separation possible. The widely used time-domain finite difference methods applied to models with interfaces produce the first order interface error (Brown, 1984; Symes and Vdovina, 2009). Symes and Vdovina (2009) pointed out that errors of 100% or more in finite difference wave modelings may be observed using grids which would yield very small error for homogeneous media, and for heterogeneous media finite difference methods converge, but slowly. This interface error manifests itself as the time shift in the solution and can be corrected in no obvious way. For an extensive assessment of the importance of this type of error in 3D finite difference modeling, see Fehler and Keliher (2011). Galerkin-type methods for interface problems have an immediate cure, that is to use a proper domain partition adapted to material parameters. In my master thesis (Wang, 2010) I investigated that the time-domain discontinuous Galerkin method on interface-fitting meshes produces accurate solutions with lower cost in comparison with the finite difference method. However the interface-fitting meshing requires accurate explicit location information about the interfaces, which

finite difference methods do not. For constant density acoustics there is an exception. Symes and Terentyev (2009b) show that finite difference methods derived from mass-lumped finite element method on regular grids achieve second order convergence even with interfaces. This exception does not extend to variable density acoustics at least not in theory, much less to any more complex elastic wave propagation model.

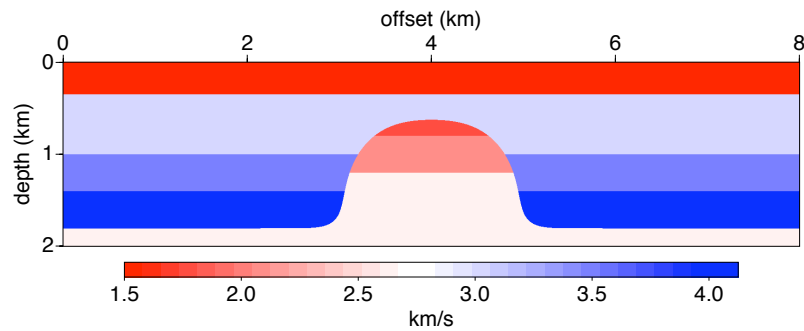


**Figure 1.1:** A velocity model with interfaces.

Beside the interface problems, the other class of problems of this thesis's interest are *rough media problems*, where the material parameters vary over many scales, locally everywhere in a volume, as opposed to on a set of positive co-dimension as in the interface problems. Figure (1.2) illustrates a measurement of velocity of rocks, and attempts to show what the real earth looks like (sound velocity of the real earth may vary on every scale). The oscillatory feature of the subsurface is expected to appear later in the solution of the corresponding problem. A typical temporal frequency in this setting might be 30 Hz corresponding to a wavelength of about 100 m at an average velocity of 3 km/s. So we should not have to use a 1 m grid or smaller to represent the most important features of the seismic wave-field. Yet accurate regular grid finite difference simulation of 30 Hz waves on a material model in Figure (1.2) may require 1 m grid cells.

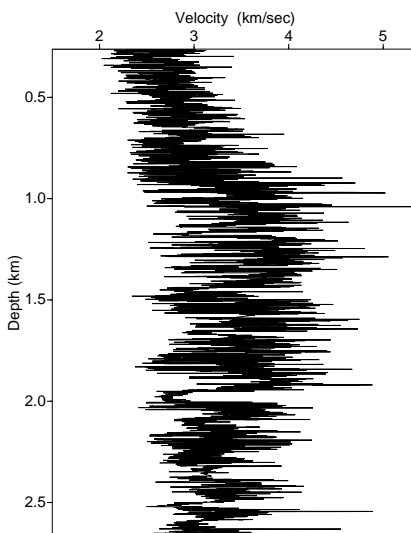


**Figure 1.2:** A log of compressional wave velocity from a well in West Texas, supplied to TRIP by Total E&P USA and used by permission.

## 1.2 CLAIM

I study the numerical Galerkin-type upscaling methods that are based on the transfer-of-approximation property. The two proposed methods in this thesis achieve the optimal convergence rate on regular grids for problems in heterogeneous media. I apply the transfer-of-approximation finite element method to both the scalar elliptic equation and the scalar wave equation, and experiment with two localization strategies for the transfer basis construction. I conclude that though theoretically attractive the transfer-of-approximation finite element method is not practically useful in seismic applications. I also propose the harmonic coordinate finite element method (HCFEM) and present the full analysis over it including the effect of errors from the harmonic coordinates' approximation. I apply HCFEM to elliptic interface problems and obtain the optimal second order convergence. For the scalar wave interface problem I

show that HCFEM with mass-lumping not only provides accurate solutions, but also achieves the numerical efficiency.

I list the main results of this thesis as follows.

- I summarize the transfer-of-approximation results derived by Symes (2011, 2012). My contribution is to show that under certain technical assumptions which are hard to verify, the HCFEM for scalar elliptic problems with  $L^\infty$  coefficients converges at optimal order because of Corollary 3.8, Theorem 5.4. In them, I must assume the chain rule and change of variable formula to be valid for the harmonic coordinate map  $\mathbf{F}$ , which is a priori only of class  $H^1$ . My results depend on estimates for the solution of non-divergence form problems due to Bernstein (1910) and various others.
- I modify the proof of the approximation theorem in Symes and Terentyev (2009a) for the scalar wave equation to show that the key assumption is an approximation property for solutions of an elliptic equation (Theorem 3.9), as opposed to the specific finite element spaces ( $Q_1$  finite element space) assumed in Symes and Terentyev (2009a).
- I implement the simple transfer-of-approximation FEM for scalar elliptic and wave interface problems, and find that even with the localization strategy suggested by Owhadi and Zhang (2011), it is so expensive as to be impractical.
- I treat the approximation error of the harmonic coordinate map for the first time, for interface problems only (not for texture problems). My results completely justify the HCFEM in 1D with optimal order convergence (but not in 2D, since we do not have any results which say that the harmonic coordinate

map  $\mathbf{F}$  is in the Besov space mentioned). Given these results, I suggest a practical computation of harmonic coordinates in the case of interface problems, which is optimally efficient.

- I implement HCFEM with adaptive gridding for harmonic coordinates' computation as suggested, and show that the convergence is as expected by theory.
- I extend the results of Symes and Terentyev (2009a) on mass-lumping with  $Q_1$  elements for constant density acoustics, to HCFEM for variable density acoustics, showing that the lumped mass solution is just as accurate as the consistent mass solution (asymptotically).
- I implement the lumped mass HCFEM for 2D acoustics and verify convergence.
- Most importantly my experiments strongly suggest that standard lumped mass  $Q_1$  Galerkin method is nearly as accurate as lumped mass HCFEM when the density contrasts are small (2:1), of the type that occur in sedimentary rocks. This suggests that for such problems the expensive harmonic coordinates' computations can be avoided.

### 1.3 ORGANIZATION OF THE THESIS

This thesis is organized as follows. In the next chapter I present a brief review of upscaling approaches. Chapter 3 discusses the theory of transfer-of-approximation. Chapter 4 describes the transfer-of-approximation finite element method and presents its numerical results. Chapter 5, 6 introduces the harmonic coordinate finite element method for elliptic and scalar wave equations. For both equations numerical experiments are presented. Conclusions and future work are discussed in the last chapter.



# Chapter 2

## Literature Review

This thesis explores upscaling approaches (Efendiev and Hou, 2009; Engquist et al., 2011; Allaire and Brizzi, 2005; Vdovina et al., 2005; Owhadi and Zhang, 2008), which are designed to achieve numerical accuracy for complex material parameter fields on regular coarse grids. In general upscaling approaches don't incorporate the microscopic material structure itself (that would require a "fine" grid), but rather its effects on the solution on a coarse grid. The goal is to solve the original problem over an affordable computational (regular, coarse) grid so as to suppress the overall computation load. The subgrid information either is averaged under certain rules, or encoded into numerical schemes. In this chapter I give a brief overview of upscaling approaches.

Upscaling approaches fall into two categories, that are, the *analytical upscaling approach* and the *numerical upscaling approach*. The analytical upscaling approach, which homogenizes the multiscale problem first and then discretizes, use the numerical solution of the homogenized problem as an approximation to the solution of the

original continuous problem with many fine scales. The numerical upscaling approach works directly on the multiscale problems. It captures the small scale effect on the large scales on a relatively coarse grid without resolving all the small scale characteristics. The numerical upscaling approach is the focus of this proposal.

## 2.1 ANALYTICAL UPSCALING

I take the mathematical treatment from Bensoussan et al. (1978) to illustrate the analytical upscaling idea. They considered a family of elliptic problems

$$-\nabla \cdot C^\epsilon \nabla u^\epsilon = f \tag{2.1}$$

with the periodic coefficient tensor  $C^\epsilon(x) = C(x/\epsilon)$ , where  $C(y)$  is 1-periodic and uniformly coercive and bounded, i.e., there exist positive constants  $\alpha, \beta$  such that,

$$\alpha|\xi|^2 \leq \xi^T C(y)\xi \leq \beta|\xi|^2, \quad \forall \xi, y \in \mathbb{R}^n.$$

The solution  $u^\epsilon$  is in the form of a power series expansion in  $\epsilon$ ,

$$u^\epsilon = u_0 + \epsilon u_1 + \epsilon^2 u_2 + \dots .$$

For small  $\epsilon$ ,  $u_0 + \epsilon u_1$  provides a reliable approximation to  $u^\epsilon$ . A *two-scale asymptotic expansion* claims that  $u_i (i = 0, 1, \dots)$  depends explicitly on  $x$  and  $y = x/\epsilon$  and is periodic with respect to the fast variable  $y$ , and hence

$$u^\epsilon(x) = u_0(x, y) + \epsilon u_1(x, y) + \epsilon^2 u_2(x, y) + \dots .$$

It can be deduced that  $u_0$  is independent of  $y$  and satisfies the homogenized equation as  $\epsilon \rightarrow 0$ ,

$$-\nabla \cdot C^* \nabla u_0 = f, \quad (2.2)$$

where the constant effective coefficient  $C^* = \int_{\mathbb{T}^n} (C(y) + C(y) \nabla \chi(y)^T) dy$  with  $\mathbb{T}^n$  the  $n$ -dimension unit cube.  $\chi(y) = [\chi_1(y), \dots, \chi_n(y)]^T$  is called the *first-order corrector* and each component  $\chi_i$  is 1-periodic and is the weak solution of the *cell problem*,

$$-\nabla_y \cdot C(y) \nabla_y \chi_i(y) = \nabla_y \cdot C(y) e_i, \quad (2.3)$$

where  $\{e_i\}_{i=1}^n$  is the canonical basis of the Euclidean space  $\mathbb{R}^n$ . The name *first order corrector* of  $\chi(y)$  comes from the fact that  $u_1$  can be expressed as a linear combination of  $\chi$ 's components, i.e.,

$$u_1(x, y) = \sum_{i=1}^n \frac{\partial u_0}{\partial x_i} \chi_i(y).$$

It is worthwhile pointing out that  $y_i + \chi_i(y)$  satisfies the harmonic condition,

$$-\nabla_y \cdot C(y) \nabla_y (y_i + \chi_i(y)) = 0.$$

Later it'll be seen that such condition plays a very important role in deriving numerical upscaling approaches.

## An example

The example of the 2D checkerboard (Craster and Obnosov, 2001) can be used to illustrate the homogenization theory described in Bensoussan et al. (1978). In Figure (2.1) red and black squares represent two materials with quantitative values  $c_r$  and  $c_b$  respectively. Suppose the checkerboard occupies the domain  $\Omega = [0, 1] \times [0, 1]$  and  $\epsilon$  denote the side length of each little square. Denote by  $C^\epsilon(x) = c^\epsilon(x)I$  the material coefficient matrix, where  $c^\epsilon$  is defined by

$$c^\epsilon(x_1, x_2) = \begin{cases} c_r, & \lfloor x_1/\epsilon \rfloor + \lfloor x_2/\epsilon \rfloor \text{ odd} \\ c_b, & \lfloor x_1/\epsilon \rfloor + \lfloor x_2/\epsilon \rfloor \text{ even} \end{cases} \quad (2.4)$$

By the homogenization theory the effective coefficient for (2.1) is a constant matrix,  $C^* = \sqrt{c_r c_b}I, \forall x \in \Omega$ . The solution of the homogenized problem (2.2) can be calculated readily from the perspective of computational effort and by theory provides an admissible approximation when  $\epsilon$  is very small.

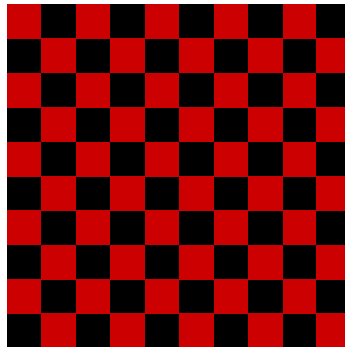


**Figure 2.1:** 2D checkerboard model,  $\epsilon = 0.1$ . `./fig/metapost/checkerboard.pdf`

## Backus upscaling

Even earlier Backus (1962) presented an effective media statement for horizontally layered media in the context of geophysical application, that is, large wavelength waves ignore local fluctuations of medium parameters over small vertical height, and act like passing through a homogeneous, transversely isotropic medium ( “A horizontally layered inhomogeneous medium, isotropic or transversely isotropic, is considered, whose properties are constant or nearly so when averaged over some vertical height  $l$ . For waves longer than  $l$  the medium is shown to behave like a homogeneous, or nearly homogeneous, transversely isotropic medium”). Schoenberg and Muir (1989) generalized the Backus averaging rule and apply it for near-layered structure. Besides simplifying the wave modeling procedure in Muir et al. (1992), the Schoenberg-Muir calculus justifies the transverse anisotropy.

## Separation of scales

Periodicity in coefficients is only used to simplify the mathematical treatment in the homogenization theory. The essential assumption for problems that can be homogenized analytically is *separation of scales*, that is, the length scale of the medium heterogeneities is far less than the length scale of the volume of material or the phenomena of interest. The *separation of scales* concept can be illustrated by a real life experience (for details see p77 in Auriault et al. (2009)). Think a man and an ant are both running on a pebble road. As long as the size of the pebbles is quite small compared to the man’s stride, the man’s speed and trajectory can be described without the information of the precise positions and shapes (local fluctuations) of the pebbles. This is the case where the scales are separated. As far as the ant is

concerned, since its scale is less than that of the pebbles, its trajectory is dependent of the local medium information (position and shape of individual pebble).

## 2.2 NUMERICAL UPSCALING

Instead of applying averaging rules to material parameters for an equivalent medium, several authors developed numerical methods that capture the small scale effect on the large scale phenomena without resolving all the small scale characteristics. In general these *numerical upscaling* approaches encode the multiscale information into the numerical schemes.

For interface problems, the immersed interface finite difference methods, proposed by Leveque and Li (1994) for elliptic problems and by Zhang and LeVeque (1997); Zhang and Symes (1998) for waves, modify the standard finite difference schemes in accordance with appropriate jumps of the solution across interfaces, and consequently improve the numerical accuracy. The cost is the additional physical memory for storing special scheme coefficients near interfaces and lowering code efficiency due to conditional branches and/or post-processing over the numerical solution near interfaces. The immersed finite element method by Li and Ito (2006) also focuses on interface problems. The idea is to element by element construct special basis functions that have appropriate jumps across interfaces. Like the interface-fitting meshing immersed interface methods need accurate location information about interfaces to construct numerical schemes that have optimal order convergence. In 1D, it is identical to the harmonic coordinate approach (Ohwadi and Zhang, 2007) described in Chapter 5 (this observation is due to T. Binford - see Binford (2011)).

For problems with highly oscillatory coefficients polynomial finite element spaces

are inefficient. Presumably the inefficiency is due to using a grid on the scale of the coefficient oscillations to represent solution features that exhibit on a much larger scale. For rough coefficient problems arising from composite materials and flows in porous media, Hou and Wu (1997) proposed the *multiscale finite element method*, in which the basis function  $\phi_i$  is the weak solution of the local elliptic problem (similar to the cell problem (2.3)) within the grid cell  $K$  in a domain partition,

$$\begin{aligned} \nabla \cdot C \nabla \phi_i &= 0, \quad \text{in } K \\ \phi_i(x_j) &= \delta_{ij} \end{aligned} \tag{2.5}$$

where  $x_j \in \bar{K}$  is the nodal points of  $K$ . Each calculation of these new basis functions is completely independent and so it is easy for parallelization. Notice that the boundary condition in (2.5) is incomplete and hence the simple linearly interpolated Dirichlet conditions is imposed on element boundaries. Such artificial boundary condition introduces boundary layers or resonance effects, which corrupt the numerical accuracy of this special finite element method. To suppress them Hou and Wu (1997) proposed an oversampling strategy, which first calculates the temporary basis function  $\psi_i$  satisfying (2.5) over a larger domain and then constructs the actual basis function  $\phi_i$  that is a linear combination of  $\psi_i$ s. Though the multiscale finite element method is designed for general problems, Hou et al. (1999) only provide the convergence analysis for periodic media using the homogenization theory introduced by Bensoussan et al. (1978).

Allaire and Brizzi (2005) also explored the possibility of constructing multiscale basis functions locally and independently. They started from the general homogenization theory, and realized that the two-scale asymptotic expansion is just like the

first order Taylor expansion, i.e.,

$$u^\epsilon(x) \approx u_0(x) + \epsilon \sum_{i=1}^n \chi_i\left(\frac{x}{\epsilon}\right) \frac{\partial u_0}{\partial x_i} \approx u_0\left(x + \epsilon \chi\left(\frac{x}{\epsilon}\right)\right), \quad (2.6)$$

They then define the *oscillating finite element basis*  $\phi_i^\epsilon$  by the composition rule,

$$\phi_i^\epsilon(x) = \phi_i\left(x + \epsilon \chi\left(\frac{x}{\epsilon}\right)\right)$$

with  $\phi_i$  the classical conforming finite element basis. This change-of-variable strategy can be used to generate high order multiscale finite element spaces naturally. Like the multiscale finite element method by Hou and Wu (1997), the error estimate analysis of this method only works for periodic coefficients.

Babuška et al. (1994) noticed that the change-of-variable through the global harmonic mapping transforms the elliptic boundary value problem with highly oscillatory coefficients into a non-divergence form, and proposed to use the composition of the standard finite element basis with the harmonic mapping to formulate the approximation space for the original oscillatory problem. The restriction of their method is to assume that the coefficient depends only on one spatial coordinate, perhaps after a smooth change of coordinates (e.g., curved interfaces). In the geophysical literature, such models are known as layered media, for which Backus (1962) also used a global harmonic change of coordinates to derive an averaging rule. This change-of-variable idea is obviously related to Allaire and Brizzi (2005); Kozlov (1980), in which solutions of cell problems are used to apply the change-of-variable locally.

Similar to the work by Babuška et al. (1994), Ohwadi and Zhang (2007) used harmonic coordinates as new variables to convert the elliptic boundary value problems

with the general bounded and measurable coefficient  $C$  into a non-divergence form. They first define *harmonic coordinates*  $\mathbf{F} = [F_1(x), \dots, F_n(x)]$  that form an identity operator on the boundary and satisfy  $\nabla \cdot C(x)\nabla F_i(x) = 0$  ( $i = 1, \dots, n$ ) inside the domain and then express the solution  $u$  of the original problem as a composite function  $\tilde{u} \circ \mathbf{F}$ , in which  $\tilde{u}$  solves the non-divergence elliptic problem,

$$-\sum_{j,k=1}^n \left[ [\nabla \mathbf{F} C (\nabla \mathbf{F})^T]_{jk} \circ \mathbf{F}^{-1} \right] \frac{\partial^2 \tilde{u}}{\partial F_j \partial F_k} = f \circ \mathbf{F}^{-1}. \quad (2.7)$$

The special finite element that Ohwadi and Zhang (2007) proposed is composition of the  $P_1$  finite element with harmonic coordinates, the latter being calculated numerically. Their approach truncates the basis function to make it have the same support as the  $P_1$  element, and results in a non-conforming finite element method and degenerates the convergence order. The localized basis in Ohwadi and Zhang (2007) is very similar to that in Hou and Wu (1997), with different boundary conditions. Binford (2011) showed that by using full, untruncated basis function the harmonic coordinate finite element method achieves the optimal order convergence on triangular meshes for 2D static interface problems.

Another numerical upscaling framework proposed by E and Engquist (2003) is called the heterogeneous multiscale method (HMM). HMM appears to be justified only when scales are separated, and is really aimed at problems where the physics is different at the different scales (e.g., molecular dynamics and continuum mechanics). Therefore it is not very close to my proposed work. In the HMM framework, the multiscale problem is approximated by two interactive model solvers. One is the macro model solver on a coarse grid, which can produce coarse scale or low frequency solution components. The other is the micro model solver that accurately describes

the solution of the original multiscale problem, but is computationally expensive. The micro model solver is only applied to a limit number (proportional to the element number in the coarse grid) of small sub-domains in order to provide the missing data in the macro model solver on the coarse grid. Engquist et al. (2011) proposed a method in this framework for wave propagation in rapidly oscillating media. Their method with minor change is also applied for a long time integration problem and correctly catch the dispersive phenomena.

## 2.3 SUMMARY

Of all the approaches to upscaling reviewed in the previous section, only the ideas of Ohwadi and Zhang (2007); Berlyand and Owhadi (2010) have been shown rigorously to lead to upscaling with a continuum of scales. So I will use those approaches to upscaling for the acoustic wave equation, and test the resulting methods on the two classes of problems explained at the beginning.

Ohwadi and Zhang (2007); Berlyand and Owhadi (2010) have proposed two general approaches. Both of them are really instances of the same basic idea, transfer of approximation, in which the approximation properties of one boundary value problem are transferred to another. I will explain this property in Chapter 3, and summarize my investigation of the first (chronologically, the second) of Owhadi's approaches in Chapter 4. In the first approach, the regularity of the constant coefficient boundary value problem is transferred into the special finite element space for the problem with variable coefficients. This works, but is very expensive, because the stiffness matrix resulting from it are generally dense. The reason is that the two problems are too different - the "source" problem (the constant coefficient problem) has none of

the non-smooth features of the “transfer” problem (the variable coefficient problem). The second approach, via harmonic coordinates, produces stiffness and mass matrices having the same sparsity pattern as for the standard continuous finite element method. I describe the harmonic coordinate approach in Chapter 5 and 6.



# Chapter 3

## Theory of

## Transfer-of-approximation

### 3.1 INTRODUCTION

Polynomial approximation spaces in finite element methods achieve the optimal rate of convergence under the assumption that the true solution has proper smoothness.

For example, consider the scalar elliptic problem,

$$\begin{aligned} -\nabla \cdot C \nabla u &= f, \quad \text{in } \Omega \subset \mathbb{R}^d \\ u &= 0, \quad \text{on } \partial\Omega \end{aligned} \tag{3.1}$$

in which for some positive constants  $\alpha, \beta$

$$\alpha_s |\xi|^2 \leq \xi^T C(x) \xi \leq \beta_s |\xi|^2, \quad \text{a.e. } x \in \Omega, \quad \forall \xi \in \mathbb{R}^d.$$

Denote by  $S^h$  the  $P_1$  (or  $Q_1$ ) finite element space on a triangulation of diameter  $h$ . If the solution  $u \in H_0^1(\Omega) \cap H^2(\Omega)$ , then Céa's Lemma and approximation theory yield that for some constant  $K$  independent of  $h$

$$\|u - u^h\|_{H^1(\Omega)} \leq Kh \|u\|_{H^2(\Omega)}$$

The property that  $u \in H^2(\Omega)$  follows if the coefficient  $C(x)$  is smooth, e.g.,  $C(x) \in C^\infty(\Omega, \mathbb{R}^{d \times d})$ . However in general  $C(x) \in L^\infty(\Omega, \mathbb{R}^{d \times d})$ , one can only conclude that  $u \in H_0^1(\Omega)$ . Polynomial finite element methods fail to converge at the rate given above because  $u \notin H^{1+\epsilon}(\Omega), \forall \epsilon > 0$ . For example one dimensional elliptic interface problem with  $f = 0$  in equation (3.1) has a solution that is piecewise linear. As mentioned in Melenk and Babuška (1996) a good finite element method relies on basis functions with good local approximation properties. Apparently polynomials bases are not always the best choice.

Several authors have developed special finite element methods, in which their bases are no longer polynomials, but adapt to features of the true solution. The transfer-of-approximation property, first formulated by Berlyand and Owhadi (2010) and later generalized by Symes (2012) provides a general framework to construct finite dimensional approximation space with the prescribed rate of convergence for bounded and measurable coefficients. This property basically states that if the spaces mapping from two finite dimensional Galerkin approximating subspaces under two respective self-adjoint operators are the same, then the approximation errors of these two self-adjoint systems with the same right hand side are equivalent.

For scalar elliptic problems, it is possible to obtain optimal Galerkin subspaces through function composition. For example, Babuška et al. (1994) constructed spe-

cial finite elements for rapidly varied coefficient  $C(x)$  depending only on one spatial coordinate (in the geophysical literature, such models are known as *layered media*), perhaps after a coordinate transformation. The special finite elements are composition of  $P_1$  elements with a  $C$ -harmonic function, that is, a solution of  $\nabla \cdot C \nabla f = 0$ . For layered media, the  $C$ -harmonic function may be constructed by quadrature. Ohwadi and Zhang (2007) extended the harmonic coordinate idea to problems with general bounded and measurable coefficients. The global harmonic mapping associated with the coefficient as the new set of variables transforms the problem into a non-divergence form. The above change of variables (function composition) technique can be generalized by the transfer property through intertwining relations (see Symes (2012) for details).

In this chapter I present two forms of the transfer-of-approximation property (see Berlyand and Ohwadi (2010); Symes (2012) for more details). One is the basic transfer lemma, which is later used to construct the transfer-of-approximation finite element method. The other is the transfer property through intertwining relations, which provides the fundamental for the harmonic coordinate finite element method. I also describe in details the application of the transfer property to the scalar wave equation for optimal convergence rate at the end of this chapter.

## 3.2 MODEL PROBLEMS

Berlyand and Ohwadi (2010) consider the scalar and vectorial elliptic problems in divergence forms with bounded and measurable coefficients. In the scalar case, the equation reads as in equation (3.1). The coefficient  $C(x)$  in it belongs to  $\in L^\infty(\Omega, \mathbb{R}^{d \times d})$  and is uniformly elliptic, i.e., for all  $\xi \in \mathbb{R}^d$  and  $x \in \Omega$ , there exist some positive

constants  $\alpha_s, \beta_s$  such that

$$\alpha_s |\xi|^2 \leq \xi^T C(x) \xi \leq \beta_s |\xi|^2. \quad (3.2)$$

In the vectorial case, the static elastic equation is considered,

$$\begin{aligned} -\nabla \cdot (C : \epsilon(u)) &= f, \quad \text{in } \Omega \subset \mathbb{R}^d \\ u &= 0, \quad \text{on } \partial\Omega \end{aligned} \quad (3.3)$$

In the static elastic equation,  $u$  is the particle displacement during equilibrium deformation. The strain tensor  $\epsilon(u) = \frac{1}{2}(\nabla u + \nabla u^T)$ .  $C(x) = \{C_{ijkl}\}$  is a 4th order *Hooke tensor* with each entry  $C_{ijkl} \in L^\infty(\Omega)$ .  $C : \epsilon(u)$  gives the *infinitesimal stress*  $\sigma$ , where

$$\sigma_{ij} = \sum_{k,l} C_{ijkl} \epsilon_{kl}.$$

By conservation of linear momentum, angular momentum and energy, etc (see Symes (2006) for more details),  $C$  has the symmetric properties

$$C_{ijkl} = C_{ijlk} = C_{jikl} = C_{klij}, \quad \forall i, j, k, l.$$

For each  $x \in \Omega$ ,  $C(x)$  is a linear mapping on the space  $\mathbb{R}_{\text{symm}}^{d \times d}$  of symmetric  $d \times d$  matrices.  $C(x)$  is also assumed to be uniformly elliptic, i.e., for some positive constants  $\alpha_v, \beta_v$ ,

$$\alpha_v \sum_{k,l} \eta_{k,l} \leq \sum_{i,j,k,l} C_{ijkl} \eta_{i,j} \eta_{k,l} \leq \beta_v \sum_{k,l} \eta_{k,l}, \quad \forall \eta \in \mathbb{R}_{\text{symm}}^{d \times d} \quad (3.4)$$

### 3.3 FLUX NORM AND TRANSFER PROPERTY

Berlyand and Owhadi (2010) introduced the transfer property through the flux norms associated with the scalar and vectorial elliptic operators as follows.

In the scalar case, for  $u \in (L^2(\Omega))^d$  by Weyl-Helmholtz decomposition

$$u = \Pi u + (I - \Pi)u \quad (3.5)$$

with  $\Pi$  the projection from  $(L^2(\Omega))^d$  on the closure of its subspace  $\{\nabla f : f \in C_0^\infty(\Omega)\}$ .

**Definition 3.1.** (Definition 2.1 in Berlyand and Owhadi (2010)) *for  $\psi \in H_0^1(\Omega)$ , the flux norm associated with the scalar elliptic operator is defined by*

$$\|\psi\|_{C\text{-flux}} := \|\Pi(C\nabla\psi)\|_{(L^2(\Omega))^d}$$

The above flux norm is a norm on  $H_0^1(\Omega)$ , equivalent to  $\|\cdot\|_{H^1(\Omega)}$  (Proposition 2.1 in Berlyand and Owhadi (2010)).

**Theorem 3.2.** (Theorem 2.1 in Berlyand and Owhadi (2010)) *Let  $V_0, V_1$  be finite dimensional subspaces of  $H_0^1(\Omega)$ . For  $f \in L^2(\Omega)$  let  $u_0$  be the solution of equation (3.1) with coefficient  $C_0$  and  $u_1$  be the solution of equation (3.1) with coefficient  $C_1$ . Define*

$$\nabla \cdot C_0 \nabla V_0 := \{\nabla \cdot C_0 \nabla v_0 : \forall v_0 \in V_0\}, \quad \nabla \cdot C_1 \nabla V_1 := \{\nabla \cdot C_1 \nabla v_1 : \forall v_1 \in V_1\}.$$

If  $\nabla \cdot C_0 \nabla V_0 = \nabla \cdot C_1 \nabla V_1$ , then

$$\sup_{f \in L^2(\Omega)} \inf_{v \in V_0} \frac{\|u_0 - v\|_{C_0\text{-flux}}}{\|f\|_{L^2(\Omega)}} = \sup_{f \in L^2(\Omega)} \inf_{v \in V_1} \frac{\|u_1 - v\|_{C_1\text{-flux}}}{\|f\|_{L^2(\Omega)}}$$

Furthermore, there exist positive constants  $K_1, K_2$  dependent of the largest and smallest eigenvalues of  $C_0, C_1$  such that,

$$K_1 \inf_{v \in V_0} \|u_0 - v\|_{H^1(\Omega)} \leq \inf_{v \in V_1} \|u_1 - v\|_{H^1(\Omega)} \leq K_2 \inf_{v \in V_0} \|u_0 - v\|_{H^1(\Omega)}$$

In the vectorial case, for  $u \in (L^2(\Omega))^{d \times d}$  similarly by Weyl-Helmholtz decomposition

$$u = \Pi u + (I - \Pi)u \tag{3.6}$$

with  $\Pi$  the projection from  $(L^2(\Omega))^{d \times d}$  on the closure of its subspace  $\{\nabla f : f \in (C_0^\infty(\Omega))^d\}$ .

**Definition 3.3.** (equation (2.27) in Berlyand and Owhadi (2010)) for  $\psi \in (H_0^1(\Omega))^d$ , the flux norm associated with the vectorial elliptic operator is defined by

$$\|\psi\|_{C\text{-flux}} := \|\Pi(C : \nabla \psi)\|_{(L^2(\Omega))^{d \times d}}$$

The above flux norm is a norm on  $(H_0^1(\Omega))^d$ , equivalent to  $\|\cdot\|_{(H_0^1(\Omega))^d}$  (see Proposition 2.3 in Berlyand and Owhadi (2010)).

**Theorem 3.4.** (Theorem 2.3 in Berlyand and Owhadi (2010)) Let  $V_0, V_1$  be finite dimensional subspaces of  $(H_0^1(\Omega))^d$ . For  $b \in (L^2(\Omega))^d$  let  $u_0$  be the solution of equation (3.3) with coefficient  $C_0$  and  $u_1$  be the solution of equation (3.3) with coefficient  $C_1$ .

Define

$$\begin{aligned}\nabla \cdot (C_0 : \epsilon(V_0)) &:= \{\nabla \cdot (C_0 : \epsilon(v_0)) : \forall v_0 \in V_0\}, \\ \nabla \cdot (C_1 : \epsilon(V_1)) &:= \{\nabla \cdot (C_1 : \epsilon(v_1)) : \forall v_1 \in V_1\}.\end{aligned}$$

If  $\nabla \cdot (C_0 : \epsilon(V_0)) = \nabla \cdot (C_1 : \epsilon(V_1))$ , then

$$\sup_{b \in (L^2(\Omega))^d} \inf_{v \in V_0} \frac{\|u_0 - v\|_{C_0\text{-flux}}}{\|f\|_{(L^2(\Omega))^d}} = \sup_{b \in (L^2(\Omega))^d} \inf_{v \in V_1} \frac{\|u_1 - v\|_{C_1\text{-flux}}}{\|f\|_{(L^2(\Omega))^d}}$$

Furthermore, there exist positive constants  $K_1, K_2$  dependent of the largest and smallest eigenvalues of  $C_0, C_1$  such that,

$$K_1 \inf_{v \in V_0} \|u_0 - v\|_{(H^1(\Omega))^d} \leq \inf_{v \in V_1} \|u_1 - v\|_{(H^1(\Omega))^d} \leq K_2 \inf_{v \in V_0} \|u_0 - v\|_{(H^1(\Omega))^d}$$

From the above discussion we see similarities in the process of deriving the transfer property on different systems. First with the Weyl-Helmholtz decomposition the remainder after removing the divergence free portion from a function is used to define the flux norm. Then by the uniform ellipticity of coefficients the equivalence of the flux norm and the usual norm of the functional space can be established. Finally provided that the two finite dimensional spaces are mapped to the same space under the respective elliptic operators, the transfer property is formulated.

Symes (2012) generalized the transfer-of-approximation property in a general setting: Hilbert spaces  $V, W$  replace the specific Sobolev spaces  $H_0^1(\Omega), L^2(\Omega)$  in scalar case, and  $(H_0^1(\Omega))^d, (L^2(\Omega))^d$  in vectorial case, and isomorphisms replace the scalar and vectorial elliptic operators.

Suppose  $A$  is an isomorphism of  $V$  onto  $W$ . For  $u \in V$  define

$$\|u\|_A := \|Au\|_W. \quad (3.7)$$

We have the following *basic transfer lemma* (Symes, 2012).

**Theorem 3.5.** *Suppose that  $V, W$  are Hilbert spaces,  $A_0, A_1 : V \rightarrow W$  are isomorphisms, and  $S_0, S_1 \subset V$  are subspaces satisfying the condition  $A_0 S_0 = A_1 S_1$ . Then for any  $f \in W$ ,*

$$\inf_{v \in S_0} \|A_0^{-1}f - v\|_{A_0} = \inf_{v \in S_1} \|A_1^{-1}f - v\|_{A_1}.$$

*Proof.* Refer to Symes (2012) for proof. □

Both Theorem (3.2) and Theorem (3.4) can be derived from this theorem. Take Theorem (3.2) for example. Suppose  $V = H_0^1(\Omega)$ ,  $W = V^* = H^{-1}(\Omega)$ ,  $H = (L^2(\Omega))^d$ . Denote by  $G$  the gradient operator that maps  $V$  onto  $H$ . Its adjoint  $G^*$  is the divergence operator that maps  $H$  onto  $V^*$ .  $C_0, C_1 \in L^\infty(\Omega, \mathbb{R}^{d \times d})$  are uniformly elliptic, i.e., satisfying equation (3.2) for some positive constants. They thus form two self-adjoint bounded positive definite operators from  $H$  to itself.

Define  $A_0 = -G^*C_0G$  and  $A_1 = -G^*C_1G$ . By Lax-Milgram theorem (Yosida (1996), p. 92ff),  $A_0, A_1, G^*G$  are all isomorphisms:  $V \rightarrow V^*$ .

Denote by  $\|\cdot\|_{V^*}$  the dual norm on  $V^*(= H^{-1}(\Omega))$ . For any  $f \in V^*$

$$\|f\|_{V^*} = \sup_{\|v\|_V=1} \int_{\Omega} f(x)v(x) \, dx,$$

Let  $u$  be the weak solution of the Laplace problem  $-G^*Gu = -\Delta u = f$ . By Lax-Milgram theorem,  $\|Gu\|_H \leq \|f\|_{V^*}$ . By the definition of the dual norm,

$$\|f\|_{V^*} = \sup_{\|v\|_V=1} \int_{\Omega} f(x)v(x) \, dx = \sup_{\|v\|_V=1} \int_{\Omega} \nabla u \cdot \nabla v \, dx \leq \|Du\|_H$$

Whence

$$\|f\|_{V^*} = \|Gu\|_H = \|G(G^*G)^{-1}f\|_H.$$

With these notations, the projection operator  $\Pi$  in equation (3.5) has an explicit expression,  $\Pi = G(G^*G)^{-1}G^*$ . The definition of the flux norm and the above analysis then yield

$$\begin{aligned} \|A_0^{-1}f - v\|_{C_0-flux} &= \|\Pi(C_0G(A_0^{-1}f - v))\|_H = \|G(G^*G)^{-1}G^*C_0G(A_0^{-1}f - v)\|_H \\ &= \|G(G^*G)^{-1}A_0(A_0^{-1}f - v)\|_H = \|A_0(A_0^{-1}f - v)\|_{V^*} \\ &= \|A_0^{-1}f - v\|_{A_0} \end{aligned}$$

Finally by Theorem (3.5) Theorem (3.2) is proved.

Generic Applications of *the transfer property* have been illustrated in Berlyand and Owhadi (2010); Symes (2012). In the next chapter I describe one of them - the transfer-of-approximation finite element method.

### 3.4 TRANSFER PROPERTY THROUGH INTERTWINING OPERATORS

The conventional finite element method fails to achieve the optimal order of convergence when the analytical solution of the problem does not have the required prop-

erty of smoothness. This often occurs in problems with bounded and measurable coefficients. Babuška et al. (1994); Ohwadi and Zhang (2007) used the change-of-variable technique to transform these problems into those (e.g., equation (2.7)) with smooth solutions, for which the  $P_1$  or  $Q_1$  finite element method would produce numerical solutions with second order convergence. Consequently the composition of  $P_1$  or  $Q_1$  bases with the new variables provides an optimal Galerkin subspace for the original problem. Evidently this change-of-variable technique implies the transfer-of-approximation idea. Symes (2011) generalized this technique within the framework of the transfer property through intertwining relations. In the following I first describe the transfer property through intertwining relations. Then I elaborate its connection with the change-of-variable technique in Babuška et al. (1994); Ohwadi and Zhang (2007).

**Theorem 3.6.** (transfer property through intertwining relations (Symes, 2011)) *Suppose that  $V, W$  are Hilbert spaces.  $A : V \rightarrow W$  is an isomorphism.  $D$  is a dense subspace of  $V$ .  $B : D \rightarrow W$  is an injection. Isomorphisms  $T : V \rightarrow V$  and  $R : W \rightarrow W$  intertwine  $A$  and  $B$ , i.e.,  $B = RAT|_D$ . There exists  $K > 0$  so that for any  $f \in R^{-1}(B(D))$  and any subspace  $S$  of  $V$ ,*

$$\inf_{t \in TS} \|t - A^{-1}f\|_A \leq K \inf_{s \in S} \|s - B^{-1}Rf\|_B.$$

*Proof.* Let  $r_* > 0$  be lower bound for the isomorphism  $R$ . Because  $T$  is an isomorphism, for any  $t \in TS$ , there exists  $s \in S$  such that  $t = Ts$ . Then with equation (3.7) we have

$$\|t - A^{-1}f\|_A = \|At - f\|_W \leq \frac{1}{r_*} \|RAt - Rf\|_W = \frac{1}{r_*} \|RATs - Rf\|_W = \frac{1}{r_*} \|s - B^{-1}Rf\|_B$$

Taking  $K = 1/r_*$  concludes the proof.  $\square$

Now let us see how the change-of-variable technique in Babuška et al. (1994); Ohwadi and Zhang (2007) can be induced from the transfer property through intertwining relations. Assume  $\Omega \subset \mathbb{R}^2$ . Let  $V = H_0^1(\Omega)$ ,  $W = H^{-1}(\Omega)$ ,  $D = H^2(\Omega) \cap H_0^1(\Omega)$ ,  $A = -\nabla \cdot C\nabla$ , where  $C(x)$  is uniformly elliptic.  $\mathbf{F}$  are harmonic coordinates, i.e.,  $\mathbf{F} = \text{identity}$  on the boundary of  $\Omega$  and in  $\Omega$  its component  $F_i$  satisfies the equation  $\nabla \cdot C\nabla F_i = 0$ . Set  $\tilde{\sigma} = [|\det \nabla \mathbf{F}|^{-1} \nabla \mathbf{F} C (\nabla \mathbf{F})^T] \circ \mathbf{F}^{-1}$  and

$$B = \sum_{i,j=1}^2 \tilde{\sigma}_{ij} \frac{\partial^2}{\partial y_i \partial y_j} : D \rightarrow L^2(\Omega)$$

with the dummy variable  $y = \mathbf{F}(x)$ .

The preceding manipulations make sense when  $\nabla \mathbf{F}$  is continuous and all of its values are invertible. In general  $\mathbf{F} \in (H^1(\Omega))^d$ . In order to apply the change-of-variable, I assume  $\mathbf{F} \in (W^{1,\infty}(\Omega))^d$  and  $\mathbf{F}^{-1} \in (W^{1,\infty}(\Omega))^d$ . Then we can define an isomorphism  $T : H_0^1(\Omega) \rightarrow H_0^1(\Omega)$  by  $Tv = v \circ \mathbf{F}$  for any  $v \in H_0^1(\Omega)$ . Denote its adjoint by  $R : H^{-1}(\Omega) \rightarrow H^{-1}(\Omega)$ , i.e., for any  $f \in H^{-1}(\Omega)$

$$Rf = T^*f = (|\det \nabla \mathbf{F}|^{-1} f) \circ \mathbf{F}^{-1}.$$

Then we have the intertwining condition

$$B = RAT|_D \tag{3.8}$$

The legitimacy of definition of  $R$  depends on the validity of the change-of-variable

theorem for integrals, i.e., for any  $v \in H_0^1(\Omega)$

$$\int_{\Omega} (Rf)v \, dy = \int_{\Omega} (|\det \nabla \mathbf{F}|^{-1}f) \circ \mathbf{F}^{-1}(y)v(y) \, dy = \int_{\Omega} f(Tv) \, dx. \quad (3.9)$$

This is true if  $\mathbf{F}$  is smooth. Also for smooth  $\mathbf{F}$  equation (3.8) holds by applying chain rule on the operator  $A$  (Theorem 4.(ii) in Evans and Gariepy (1992), pp 130ff). In the following discussion I assume  $F$  is well defined such that both equation (3.8) and (3.9) hold.

Theorem 1.2.1 in Maugeri et al. (2000) is used in the proof of the following Corollary 3.8 and also later. For completeness I quote this theorem in full.

**Theorem 3.7.** (Theorem 1.2.1 in Maugeri et al. (2000)) *Suppose  $\Omega \in \mathbb{R}^d$  to be a bounded and convex domain of class  $C^2$  and the coefficient  $a_{ij}(x) \in L^\infty(\Omega)$  is coercive, i.e., for some positive constant  $\lambda$ ,*

$$\lambda|\xi|^2 \leq \sum_{i,j=1}^d a_{ij}\xi_i\xi_j, \quad a.a. \, x \in \Omega, \, \forall \xi \in \mathbb{R}^d$$

*and also satisfies the Cordes condition, i.e., there exists a positive number  $\epsilon < 1$  such that*

$$\frac{\sum_{i,j=1}^d a_{ij}^2(x)}{\left(\sum_{i=1}^d a_{ii}(x)\right)^2} \leq \frac{1}{d-1+\epsilon}, \quad a.e. \, \Omega.$$

*Then there exists a unique solution  $u \in H^2(\Omega) \cap H_0^1(\Omega)$  to the equation  $\sum_{i,j=1}^d a_{ij} \frac{\partial^2 u}{\partial x_i \partial x_j} = f \in L^2(\Omega)$  and*

$$\left( \int_{\Omega} \sum_{i,j=1}^d \frac{\partial^2 u}{\partial x_i \partial x_j} \, dx \right)^{1/2} \leq \frac{\text{esssup}_{\Omega} \alpha(x)}{1 - \sqrt{1 - \epsilon}} \|f\|_{L^2(\Omega)}$$

where  $\alpha(x) = \sum_{i=1}^d a_{ii}(x) / \sum_{i,j=1}^d a_{ij}^2(x)$ .

I prove the following corollary to establish the equivalence of norms  $\|\cdot\|_A$ ,  $\|\cdot\|_B$  and  $\|\cdot\|_{H^1(\Omega)}$ .

**Corollary 3.8.** *Assume that the harmonic coordinate map  $\mathbf{F}$  is well defined such that equation (3.8) and (3.9) hold. With the above notations, the norm  $\|\cdot\|_A$  and  $\|\cdot\|_B$  are norms equivalent to  $\|\cdot\|_{H^1(\Omega)}$ .*

*Proof.* For any  $v \in H_0^1(\Omega)$ , by Lax-Milgram theorem there exists a constant  $K$  such that

$$\|v\|_{H^1(\Omega)} \leq K \|Av\|_{H^{-1}(\Omega)} = K \|v\|_A$$

Also

$$\begin{aligned} \|v\|_A = \|Av\|_{H^{-1}(\Omega)} &= \sup_{\|w\|_{H^1(\Omega)}=1} \left| \int_{\Omega} (Av)w \, dx \right| = \sup_{\|w\|_{H^1(\Omega)}=1} \left| \int_{\Omega} \nabla v^T C \nabla w \, dx \right| \\ &= \beta_C \sup_{\|w\|_{H^1(\Omega)}=1} \left| \int_{\Omega} \nabla v \cdot \nabla w \, dx \right| \leq \beta_C \|v\|_{H^1(\Omega)}, \end{aligned}$$

where  $\beta_C$  is the upper bound in equation (3.2) for  $C(x)$ .

Next we establish the equivalence between  $\|\cdot\|_B$  and  $\|\cdot\|_{H^1(\Omega)}$ . For any  $v \in H^2(\Omega) \cap H_0^1(\Omega)$ , by Theorem 1.2.1 in Maugeri et al. (2000) there exists a constant  $K$  dependent of  $\sigma$  and  $C(x)$  such that

$$\|v\|_{H^1(\Omega)} \leq K \|Bv\|_{H^{-1}(\Omega)} = K \|v\|_B.$$

On the other hand,

$$\begin{aligned}
\|v\|_B = \|Bv\|_{H^{-1}(\Omega)} &= \sup_{\|w\|_{H_0^1(\Omega)}=1} \left| \int_{\Omega} (Bv)w \, dy \right| \\
&= \sup_{\|w\|_{H_0^1(\Omega)}=1} \left| \int_{\Omega} |\det \nabla \mathbf{F}(x)|^{-1} (\nabla_x (w \circ \mathbf{F}(x)))^T C \nabla_x (v \circ \mathbf{F}(x)) \, dy \right| \\
&= \sup_{\|w\|_{H_0^1(\Omega)}=1} \left| \int_{\Omega} (\nabla_x (w \circ \mathbf{F}))^T C \nabla_x (v \circ \mathbf{F}) \, dx \right| \\
&\leq \frac{\beta_C}{\inf_{x \in \Omega} \sqrt{|\det \nabla \mathbf{F}|}} \|v \circ \mathbf{F}\|_{H^1(\Omega)} \leq \frac{\beta_C}{\inf_{x \in \Omega} |\det \nabla \mathbf{F}|} \|v\|_{H^1(\Omega)}.
\end{aligned}$$

□

Denote by  $\tilde{S}^h$  (e.g.,  $P_1$  or  $Q_1$  finite element space) associated with  $h$  the characteristics length (e.g., the diameter of a triangulation) a finite dimensional subspace in  $H_0^1(\Omega)$ . Suppose the error estimate,

$$\inf_{v \in \tilde{S}^h} \|v - B^{-1}Rf\|_{H^1(\Omega)} = O(h).$$

holds. Then we construct  $S^h = \tilde{S}^h = \{\tilde{v}^h \circ \mathbf{F} : \tilde{v}^h \in \tilde{S}^h\}$ . The resulted subspace  $S^h$  therefore contains an approximation of the solution of equation (3.1) with a comparable error estimate, i.e.,

$$\inf_{u \in S^h} \|u - A^{-1}f\|_{H^1(\Omega)} = O(h). \quad (3.10)$$

The above discussion actually presents the harmonic coordinate finite element method first proposed by Ohwadi and Zhang (2007); Binford (2011). Chapter (5) provides the discussion in details about this unconventional finite element method.

### 3.5 SCALAR WAVE EQUATION

I consider the scalar wave equation

$$\frac{1}{\kappa} \frac{\partial^2 u}{\partial t^2} - \nabla \cdot \frac{1}{\rho} \nabla u = f, \quad \text{in } \Omega \subset \mathbb{R}^d \quad (3.11)$$

where  $u$  is the excess pressure,  $\kappa$  ( $\log \kappa \in L^\infty(\Omega)$ ) is the bulk modulus and  $\rho$  ( $\log \rho \in L^\infty(\Omega)$ ) is the material density, and the source term  $f \in L^2(\mathbb{R}, L^2(\Omega))$  is *causal*, i.e.,  $f(t, \cdot) = 0$  for  $t < 0$ . In this case with the previous notation the coefficient  $C(x) = 1/\rho I$  is a diagonal  $d \times d$  matrix, and the operator  $A = -G^*CG$ .

In this section I assume that we have found a finite dimensional subspace  $S^h$  that validates equation (3.10) for the operator  $-G^*CG$ . In the following I prove that in  $S^h$  an approximation of the scalar wave solution is spatially second-order accurate in  $L^2$  norm.

The following argument is patterned after that given by Symes and Terentyev (2009a), but replace the  $Q_1$  finite element space used there with an arbitrary family of finite dimensional approximating spaces  $S^h$  satisfying estimate (3.10). It is important to point out that it is this estimate which derives the result proven by Symes and Terentyev (2009a), not any other special properties of  $Q_1$  elements.

We seek a *causal* weak solution  $u \in C^1(\mathbb{R}, L^2(\Omega)) \cap C^0(\mathbb{R}, H_0^1(\Omega))$  of (3.11), vanishing on the boundary  $\partial\Omega$ , such that

$$0 = \int dt \left( \left\langle \frac{u(t)}{\kappa}, \frac{\partial^2 v}{\partial t^2} \right\rangle_{L^2(\Omega)} + \left\langle \frac{1}{\rho} \nabla u(t), \nabla v(t) \right\rangle - \langle f(t), v(t) \rangle_{L^2(\Omega)} \right)$$

for all  $v \in C_0^2(\mathbb{R}, H_0^1(\Omega))$ . The existence and uniqueness of the causal weak solution

of (3.11) can be found in the pioneered work by Lions and Magenes (1972).

For  $u \in C^1(\mathbb{R}, L^2(\Omega)) \cap C^0(\mathbb{R}, H_0^1(\Omega))$ , define the energy  $e_{\kappa, \rho}[u]$  by

$$e_{\kappa, \rho}[u](t) = \frac{1}{2} \left( \left\| \frac{1}{\sqrt{\kappa}} \frac{\partial u}{\partial t}(t) \right\|_{L^2(\Omega)}^2 + \left\| \frac{1}{\sqrt{\rho}} \nabla u \right\|_{L^2(\Omega)}^2 \right),$$

Stolk (2000) showed that if  $u$  is a weak solution of (3.11), then for any  $T > 0$ ,

$$e_{\kappa, \rho}[u](t) \leq K_T \int_0^T \|f(s)\|_{L^2(\Omega)}^2 ds, \quad 0 \leq t \leq T, \quad (3.12)$$

where the constant  $K_T$  grows exponentially with  $T$  and also depends on other bounds in the problem. For simplicity the same  $K_T$  will be used for any other such constant.

If  $f \in H^1(\mathbb{R}, L^2(\Omega))$ , i.e., it has one  $L^2$  derivative in time, then from (3.12) we have

$$\left\| \frac{1}{\sqrt{\kappa}} \frac{\partial^2 u}{\partial t^2}(t) \right\|_{L^2(\Omega)}^2 + \left\| \frac{1}{\sqrt{\rho}} \frac{\partial}{\partial t} \nabla u \right\|_{L^2(\Omega)}^2 \leq K_T \int_0^T \left\| \frac{\partial f}{\partial t}(s) \right\|_{L^2(\Omega)}^2 ds, \quad 0 \leq t \leq T,$$

and  $u \in C^2(\mathbb{R}, H_0^1(\Omega))$ . Therefore the following elliptic problem resulting from rearranging (3.11) holds point-wise in time.

$$Au = -\nabla \cdot \frac{1}{\rho} \nabla u = -\frac{1}{\kappa} \frac{\partial^2 u}{\partial t^2} + f \quad (3.13)$$

For each  $t$  in (3.13) an error estimate for approximation in the subspace  $S^h$  has been provided in (3.10):

$$\inf_{v^h \in S^h} \|u(t) - v^h\|_{H^1(\Omega)} \leq K_T h \left( \int_0^T \left\| \frac{\partial f}{\partial t}(s) \right\|_{L^2(\Omega)}^2 ds \right)^{1/2}, \quad 0 \leq t \leq T.$$

If we assume  $f \in H^3(\mathbb{R}, L^2(\Omega))$ , then

$$\inf_{v^h \in S^h} \left\| \frac{\partial u}{\partial t}(t) - v^h \right\|_{H^1(\Omega)} \leq K_T h \left( \int_0^T \left\| \frac{\partial^2 f}{\partial t^2}(s) \right\|_{L^2(\Omega)}^2 ds \right)^{1/2}, \quad 0 \leq t \leq T, \quad (3.14)$$

and

$$\inf_{v^h \in S^h} \left\| \frac{\partial^2 u}{\partial t^2}(t) - v^h \right\|_{H^1(\Omega)} \leq K_T h \left( \int_0^T \left\| \frac{\partial^3 f}{\partial t^3}(s) \right\|_{L^2(\Omega)}^2 ds \right)^{1/2}, \quad 0 \leq t \leq T, \quad (3.15)$$

The Galerkin solution  $u^h \in C^2(\mathbb{R}, S^h)$  satisfies the spatially discrete weak formulation, which in turn forms a system of ODEs in time,

$$\frac{d^2}{dt^2} \left\langle \frac{1}{\kappa} u^h, v^h \right\rangle + \left\langle \frac{1}{\rho} \nabla u^h, \nabla v^h \right\rangle = \langle f, v^h \rangle, \quad \forall v^h \in S^h. \quad (3.16)$$

Denote by  $P^h$  the projection of  $H_0^1(\Omega)$  onto  $S^h$  such that for any  $u \in H_0^1(\Omega)$

$$\left\langle \frac{1}{\rho} \nabla(P^h u), \nabla v^h \right\rangle = \left\langle \frac{1}{\rho} \nabla u, \nabla v^h \right\rangle, \quad \forall v^h \in S^h \quad (3.17)$$

We can show that (see Strang and Fix (1973), or Symes and Terentyev (2009a), equation A-4)

$$\frac{d}{dt} e_{\kappa, \rho}[u^h - P^h u] \leq \frac{2}{\alpha} e_{\kappa, \rho}[u^h - P^h u] + 2\alpha \left\| \frac{d}{dt^2}(u - P^h u) \right\|_{L^2(\Omega)}^2$$

for any  $\alpha > 0$ . A standard differential inequality yields

$$e_{\kappa, \rho}[u^h - P^h u](t) \leq K_T \int_0^t dt \left\| \frac{d^2}{dt^2}(u - P^h u)(t) \right\|_{L^2(\Omega)}^2 \quad (3.18)$$

For each  $t \in [0, T]$ , we have that

$$\begin{aligned}
\left\| \frac{1}{\sqrt{\kappa}} \frac{d^2}{dt^2} (u - P^h u) \right\|_{L^2(\Omega)}^2 &\leq C_1 \left\| \frac{d^2}{dt^2} (u - P^h u) \right\|_{H^1(\Omega)}^2 \\
&\leq C_2 \left\langle \frac{1}{\rho} \nabla \left( \frac{d^2}{dt^2} (u - P^h u) \right), \nabla \left( \frac{d^2}{dt^2} (u - P^h u) \right) \right\rangle \\
&= C_3 \inf_{v^h \in S^h} \left\langle \frac{1}{\rho} \nabla \left( \frac{d^2 u}{dt^2} - v^h \right), \nabla \left( \frac{d^2 u}{dt^2} - v^h \right) \right\rangle \\
&\leq C_4 \inf_{v^h \in S^h} \left\| \frac{d^2 u}{dt^2} - v^h \right\|_{H^1(\Omega)}^2,
\end{aligned}$$

where the second inequality is guaranteed by Poincaré inequality, and the third equality holds for that  $P^h$  is a projection of  $H_0^1(\Omega)$  onto  $S^h$  defined by equation (3.17). We can also prove that

$$\left\langle \frac{1}{\rho} \nabla (u - P^h u), \nabla (u - P^h u) \right\rangle = \inf_{v^h \in S^h} \left\langle \frac{1}{\rho} \nabla (u - v^h), \nabla (u - v^h) \right\rangle \leq C_5 \inf_{v^h \in S^h} \|u - v^h\|_{H^1(\Omega)}^2$$

In these inequalities, the constants  $C_1, C_2, C_3, C_4, C_5$  independent of  $t$  depend only on  $\Omega$  and  $\rho, \kappa$ .

Combining the last two inequalities with (3.14), (3.15) and (3.18) gives

$$e_{\kappa, \rho}[u^h - P^h u] \leq K_T h^2 \int_0^T ds \left\| \frac{\partial^3 f}{\partial t^3}(s) \right\|_{L^2(\Omega)}^2, \quad 0 \leq t \leq T,$$

and

$$e_{\kappa, \rho}[u - P^h u](t) \leq K_T h^2 \int_0^T ds \left\| \frac{\partial^2 f}{\partial t^2}(s) \right\|_{L^2(\Omega)}^2, \quad 0 \leq t \leq T.$$

Finally by the triangle inequality we conclude the optimal order of approximation in

energy,

$$e_{\kappa,\rho}[u - u^h]^{1/2}(t) \leq K_T h \left\| \frac{\partial^3 f}{\partial t^3} \right\|_{L^2(\Omega \times [0, T])}, \quad 0 \leq t \leq T.$$

We can prove the optimal optimal order approximation in  $L^2$  norm following the proof of the Nitsche-Aubin lemma (Ciarlet (2002), pp. 136ff) (see Symes and Terentyev (2009a), Appendix B for details), provided that  $f$  has more smoothness, i.e.,  $f \in H^5(\mathbb{R}, L^2(\Omega))$ ,

$$\|u - u^h\|_{L^2(\Omega)}(t) \leq K_T h^2 \left\| \frac{\partial^5 f}{\partial t^5} \right\|_{L^2(\Omega \times [0, T])}, \quad 0 \leq t \leq T. \quad (3.19)$$

Again, this estimate is a consequence of the abstract approximation property (3.10), and does not require the explicit choice of  $Q_1$  elements made by Symes and Terentyev (2009a).

I summarize the above analysis by the following theorem.

**Theorem 3.9.** *Let  $\kappa, \rho$  be bounded and measurable ( $\log \kappa, \log \rho \in L^\infty(\Omega)$ ). Suppose  $S^h$  is a subspace of  $H_0^1(\Omega)$  satisfying equation (3.10) with  $A = -\nabla \cdot \frac{1}{\rho} \nabla$  and  $u^h(t) \in S^h$  is the Galerkin solution of equation (3.16). Then for any  $t \in [0, T]$  there exist a constant  $K_T$  dependent of  $T$  such that*

- if  $f \in H^3(\mathbb{R}, L^2(\Omega))$ ,  $e_{\kappa,\rho}[u - u^h]^{1/2}(t) \leq K_T h \left\| \frac{\partial^3 f}{\partial t^3} \right\|_{L^2(\Omega \times [0, T])}$ ;
- if  $f \in H^5(\mathbb{R}, L^2(\Omega))$ ,  $\|u - u^h\|_{L^2(\Omega)}(t) \leq K_T h^2 \left\| \frac{\partial^5 f}{\partial t^5} \right\|_{L^2(\Omega \times [0, T])}$ .

### 3.6 SUMMARY

For systems with heterogeneous coefficients polynomial basis functions are not always the best ingredients to formulate the approximate solution. The transfer properties provide a general framework to find the optimal subspace for a specific static system. Such subspace also can be used to approximate the solution of the associated dynamic system (e.g., the scalar wave equation). In the following chapters I'll discuss the numerical methods derived from the transfer property, and present numerical results to manifest the theoretical analysis.

# Chapter 4

## Transfer-of-approximation Finite Element Method

### 4.1 INTRODUCTION

The transfer-of-approximation (transfer property), first established by Berlyand and Owhadi (2010) and later generalized by Symes (2011), states that the approximation property of one Galerkin subspace for one self-adjoint system can be transferred to another provided the two subspaces are related in a specific way. This property provides a way to construct the optimal finite dimensional Galerkin subspace to approximate the solution of a problem with a heterogeneous coefficient.

The transfer-of-approximation finite element method is a direct application of the transfer property discussed in the previous chapter. Berlyand and Owhadi (2010) first formulated this method without any numerics. Owhadi and Zhang (2011) explored the possibility to localize the transfer bases for problems with non-separated and high

contrast coefficients. In the following I first introduce the transfer-of-approximation finite element method for the scalar elliptic equation and scalar wave equation, and then present numerical experiments. I also test some basis localization strategies

## 4.2 TRANSFER-OF-APPROXIMATION FINITE ELEMENT METHOD

First consider the Laplace problem with the Dirichlet boundary condition,

$$\begin{aligned} -\Delta u &= f, \quad \text{in } \Omega \subset \mathbb{R}^d \\ u &= 0, \quad \text{on } \partial\Omega \end{aligned} \tag{4.1}$$

which has a weak solution  $u_I \in H^2(\Omega) \cap H_0^1(\Omega)$  for any  $f \in L^2(\Omega)$  provided that  $\Omega$  is convex and  $\partial\Omega$  is Lipschitz continuous. Denote by  $S_I^h (\subset H_0^1(\Omega))$  the  $P_1$  or  $Q_1$  finite element space on a mesh of diameter  $h$ , with bases  $\phi_i^h, i = 0, \dots, N^h$ . Thus the approximation theory of Sobolev spaces yields the error estimate,

$$\inf_{v^h \in S_I^h} \|u_I - v^h\|_{H^1(\Omega)} = O(h). \tag{4.2}$$

For the scalar elliptic operator  $A_C = -\nabla \cdot C \nabla$ , the global transfer-of-approximation finite element space  $S_C^h = \text{span}\{\psi_i^h, i = 0, \dots, N^h\}$ , in which  $\psi_i^h \in H_0^1(\Omega), i = 0, \dots, N^h$  and satisfies,

$$\nabla \cdot C(x) \nabla \psi_i^h = \Delta \phi_i^h, \quad \text{in } \Omega \tag{4.3}$$

Denote by  $u_C \in H_0^1(\Omega)$  the solution of  $-\nabla \cdot C(x)\nabla u = f$  with zero Dirichlet boundary condition. By Theorem (3.2), for any  $f \in L^2(\Omega)$ ,

$$\inf_{v^h \in S_C^h} \|u_C - v^h\|_{H^1(\Omega)} = O(h).$$

In other words the finite dimensional Galerkin approximating space  $S_C^h$  achieves the optimal first order approximation error in  $H^1(\Omega)$  norm for the elliptic operator  $A_C$ . Actually if  $u_I$  has more smoothness,  $S_C^h$  can be constructed with high order approximation property by choosing a high order finite element space  $S_I^h$ . By Céa's lemma (Ciarlet (2002), pp. 104ff) and Theorem (3.9) we can construct a finite element method with the optimal order of convergence for both the scalar elliptic equation (3.1) and the scalar wave equation (3.11) with bounded and measurable coefficients.

## Transfer basis construction

To obtain the transfer basis, we need to solve equation (4.3) for every  $\phi_i^h$ . Numerically each of these problems is as difficult as the original elliptic problem. Since  $\Delta\phi_i^h$  is merely a  $H^{-1}(\Omega)$  function, theoretically no asymptotic convergence behavior exists for any finite element method applied to equation (4.3). I use a very fine mesh to solve equation (4.3).

Denote by  $S_I^\delta = \text{span}\{\phi_i^\delta, i = 0, \dots, N^\delta\}$  and  $S_I^h = \text{span}\{\phi_i^h, i = 0, \dots, N^h\}$  the standard finite element spaces on a triangulation of diameter  $\delta$  and  $h$  ( $\delta \ll h$ ), respectively, such that  $S_I^h \subset S_I^\delta \subset H_0^1(\Omega)$ .

Let

$$S_C^h = \text{span}\{\psi_i^h, i = 0, \dots, N^h\} \subset S_I^\delta \quad (4.4)$$

be the discretized transfer finite element space associated with  $S_I^h$ . For each  $\phi_i^h \in S_I^h$ ,  $\psi_i^h \in S_I^\delta$  satisfies,

$$\langle C\nabla\psi_i^h, \nabla\phi_k^\delta \rangle = \langle \nabla\phi_i^h, \nabla\phi_k^\delta \rangle, \quad k = 0, \dots, N^\delta. \quad (4.5)$$

## Stiffness and mass matrices

By solving equation (4.5),  $\psi_i^h$  can be expressed as,

$$\psi_i^h = \sum_{k=0}^{N^\delta} \beta_{ik} \phi_k^\delta.$$

We write  $B^h = (\beta_{ik}) \in \mathbb{R}^{N^h \times N^\delta}$

Denote by  $N^\delta = (n_{kl}^\delta), M^\delta = (m_{kl}^\delta) \in \mathbb{R}^{N^\delta \times N^\delta}$  the stiffness and mass matrices derived from  $S_I^\delta$ , and

$$n_{kl}^\delta = \langle C\nabla\phi_k^\delta, \nabla\phi_l^\delta \rangle, \quad m_{kl}^\delta = \langle \phi_k^\delta, \nabla\phi_l^\delta \rangle.$$

Denote by  $N^h = (n_{ij}^h), M^h = (m_{ij}^h) \in \mathbb{R}^{N^h \times N^h}$  the stiffness and mass matrices derived

from the transfer-of-approximation finite element space  $S_C^h$ , and

$$\begin{aligned} n_{ij}^h &= \langle C \nabla \psi_i^h, \nabla \psi_j^h \rangle = \left\langle C \sum_{k=0}^{N^\delta} \beta_{ik} \nabla \phi_k^\delta, \sum_{l=0}^{N^\delta} \beta_{jl} \nabla \phi_l^\delta \right\rangle = \sum_{k=0}^{N^\delta} \sum_{l=0}^{N^\delta} \beta_{ik} n_{kl}^h \beta_{jl}, \\ m_{ij}^h &= \langle \psi_i^h, \psi_j^h \rangle = \left\langle \sum_{k=0}^{N^\delta} \beta_{ik} \phi_k^\delta, \sum_{l=0}^{N^\delta} \beta_{jl} \phi_l^\delta \right\rangle = \sum_{k=0}^{N^\delta} \sum_{l=0}^{N^\delta} \beta_{ik} m_{kl}^h \beta_{jl}. \end{aligned}$$

In the matrix multiplication form, we have

$$N^h = B^h N^\delta (B^h)^T, \quad M^h = B^h M^\delta (B^h)^T. \quad (4.6)$$

Without assumptions on the support of  $\psi_i^h$ ,  $N^h$  and  $M^h$  are dense. This presents a major obstacle of the transfer-of-approximation finite element method: huge amount of memory required for storing the stiffness and mass matrices, and prohibitive cost for inverting a dense matrix (recent developments of iterative methods, e.g., multigrid method, are not applicable).

### 4.3 NUMERICAL RESULTS

In this section, I first present numerical experiments of the transfer-of-approximation finite element method for both the elliptic boundary value problem and the acoustic wave equation. Then I tested two localization strategies for the transfer basis construction. One is proposed by Owhadi and Zhang (2011) based on the decay of Green's functions with distance. The other is the direct truncation of the construction region.

I first consider the 2D elliptic boundary-value equation (3.1) on  $[0, 1] \times [0, 1]$  with

$f = -1$ . The coefficient function  $C = c_\epsilon(x, y)I$  where (see Figure (4.1))

$$c_\epsilon(x, y) = \begin{cases} 1.0 & \text{floor}(x/\epsilon) + \text{floor}(y/\epsilon) \text{ odd} \\ 0.2 & \text{floor}(x/\epsilon) + \text{floor}(y/\epsilon) \text{ even} \end{cases} \quad (4.7)$$

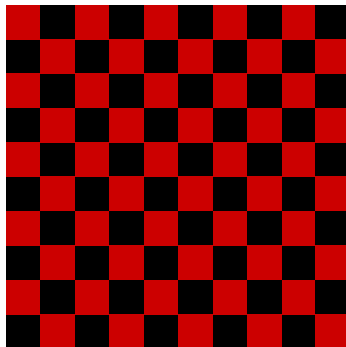


**Figure 4.1:** 2D checkerboard model,  $\epsilon = 0.1$ . `./metapost/checkerboard.pdf`

The  $P_1$  finite element method on a triangulation of diameter  $\delta = \frac{1}{80}$  is employed to calculate transfer bases and the reference solution  $u^\delta$  for error analysis. Table 4.1 shows the convergence test for  $\epsilon = 0.1$ . In this case the  $P_1$  finite element solution  $u^h$  poorly approximates the reference solution compared with the transfer-of-approximation finite element solution  $u_t^h$ . The transfer-of-approximation finite element method almost retains the optimal rate of convergence as predicted by analysis, while the  $P_1$  finite element method shows low rate of convergence.

Next I test the transfer-of-approximation finite element method for the one di-

$u_t^h - u^\delta$				
$h$	$L^2$ -error	$L^2$ -rate	$H^1$ -error	$H^1$ -rate
0.2	5.90e-2	-	2.78e-1	-
0.1	1.72e-2	1.78	1.53e-1	0.86
0.05	4.77e-3	1.85	8.21e-2	0.90
$u^h - u^\delta$				
$h$	$L^2$ -error	$L^2$ -rate	$H^1$ -error	$H^1$ -rate
0.2	2.19e-1	-	4.72e-1	-
0.1	1.59e-1	0.46	3.85e-1	0.29
0.05	1.06e-1	0.58	3.03e-1	0.35

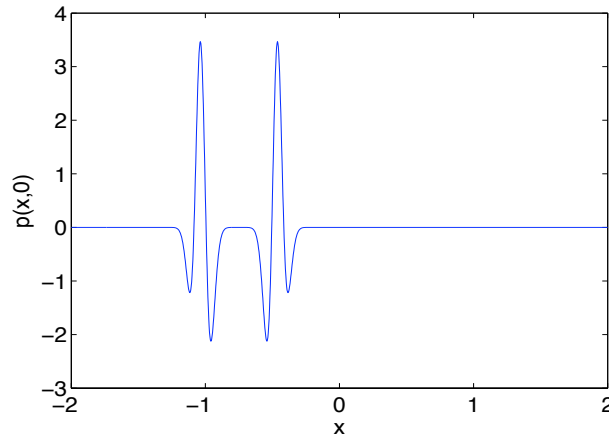
**Table 4.1:** Convergence test for  $\epsilon = 0.1$ :  $u^\delta, u^h$  are  $P_1$  finite element solutions on triangulations of diameter  $\delta$  and  $h$ , respectively.  $u_t^h$  is the transfer-of-approximation finite element solution on the triangulation of diameter  $h$ .

mensional acoustic wave equation,

$$\begin{cases} p_{tt} - \left(\frac{1}{\rho} p_x\right)_x = 0, & -2 \leq x \leq 2 \\ p(-2, t) = p(2, t) = 0, & t \geq 0 \\ p(x, 0) = p_0(x, 0), & \frac{\partial p}{\partial t}(x, 0) = \frac{\partial p_0}{\partial t}(x, 0) \end{cases}$$

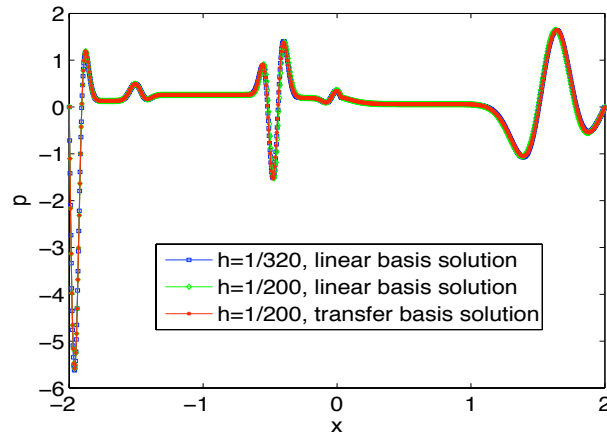
$$\text{where } \rho = \begin{cases} 1 & x < 1/32 \\ 0.1 & x \geq 1/32 \end{cases}.$$

Figure (4.2) shows the initial pressure ( $t = 0$ ), which is made up of two distorted Ricker wavelets with center frequency 5 Hz. Figure (4.3) displays numerical solutions at  $t = 1.0$  s computed by the linear finite element method on meshes of diameter  $h = 1/320$  and  $h = 1/200$  as well as by the transfer-of-approximation finite element method on the mesh of diameter  $h = 1/200$ . The transfer basis functions are calculated on a locally refined mesh around the media jump at  $x = 1/32$ . Since the  $P_1$  finite element method can produce very accurate solution on the interface-fitting mesh, I thus use the  $P_1$  finite element solution on a mesh of diameter  $h = 1/320$



**Figure 4.2:** Initial value  $p(x, 0)$ . `./initValue`

(a interface-fitting mesh in this case) as the reference solution. Figure (4.4) shows details of these solutions on the left part of Figure (4.3), the reflected wave. We can see that the transfer-of-approximation finite element method greatly reduces the time shift effect.



**Figure 4.3:** Snapshot of  $p(x, t)$  at  $t = 1.0$  s. `./solComparisonAll`

I also apply the transfer-of-approximation finite element method to the 2D acoustic wave equation with constant bulk modulus on a simple density dipping interface model of a  $1 \text{ km} \times 1 \text{ km}$  square (see Figure (4.5)). The sound velocity in this case

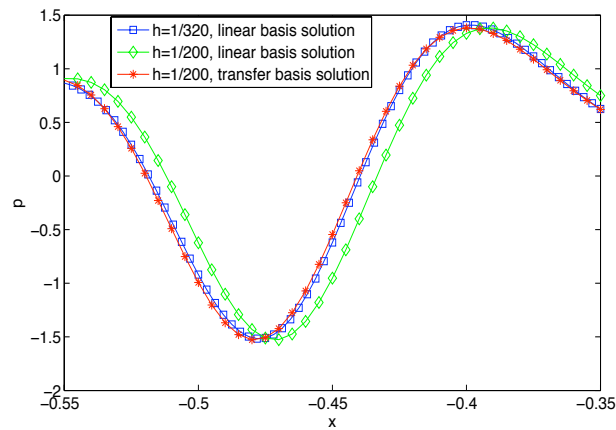


**Figure 4.4:** Solution's detail from  $-0.55$  to  $-0.35$  of Figure (4.3) `./solComparisonLeft`

is  $c(\mathbf{x}) = \sqrt{1/\rho(x)}$ . I use a point source at  $\mathbf{x}_s = (0.65, 0.65)$  to generate Ricker wavelet with central frequency 5 Hz. The transfer basis functions are computed on a locally refined mesh. At the non-refined region the mesh grid size is 20 m as shown in Figure (4.6). Local mesh refinement technique helps reduce the interface error, but leads to small time step according to Courant-Friedrichs-Lewy condition. By using transfer basis functions, I put the fine media information into the basis functions on a coarse mesh and hence don't have to deal with the small time step. This feature of the transfer-of-approximation finite element method is very important when it is applied to time-dependent problems. Here I compare the solution  $u_t^h$  by the transfer-of-approximation finite element method with  $u^\delta$ , the solution by the  $P_1$  finite element method on the locally refined mesh. Figure (4.7) and Figure (4.8) manifest that  $u_t^h$  is much closer to  $u^\delta$  with less diffraction than the standard finite element solution on the same mesh of diameter 20 m.

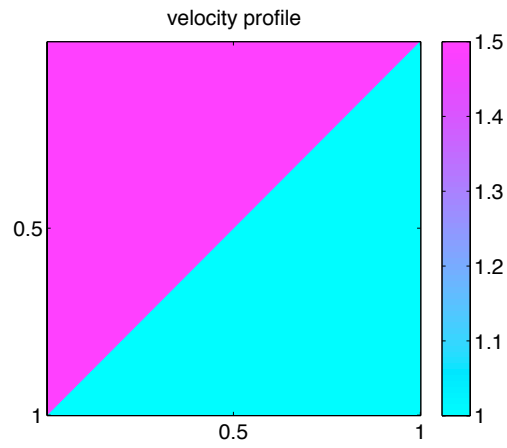


**Figure 4.5:** Sound velocity field for the dipping interface model. Source locates at  $(0.65, 0.65)$ .

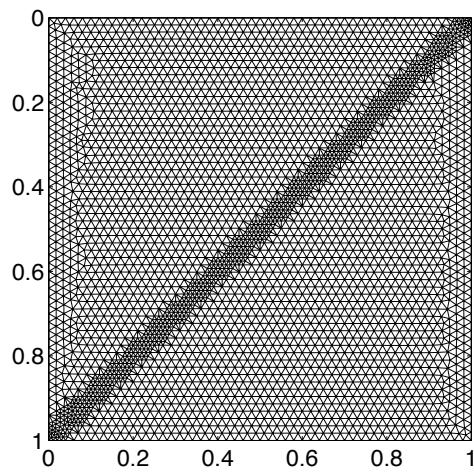


**Figure 4.6:** Locally refined mesh

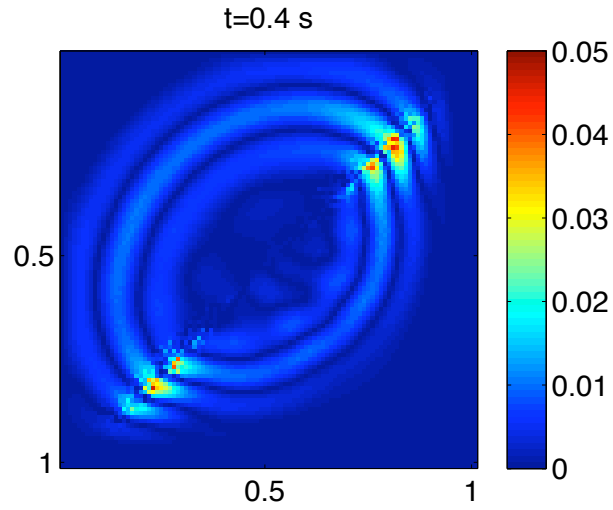


**Figure 4.7:** Difference between solutions by the  $P_1$  finite element method on the locally refined mesh and on the regular mesh at  $t = 0.4$  s.

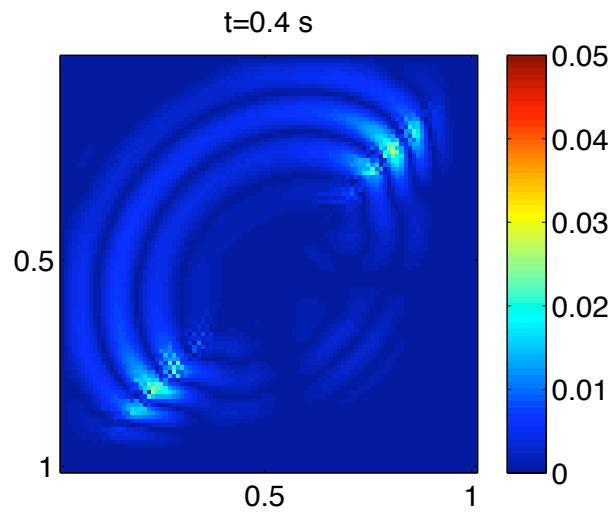


**Figure 4.8:** Difference between solutions by the  $P_1$  finite element method on the locally refined mesh and the transfer-of-approximation finite element method on the regular mesh at  $t = 0.4$  s.

## Transfer Basis Localization

The practical drawbacks of the transfer-of-approximation finite element method are visible. Construction of the transfer basis entails solutions of ( $O((h)^{-n})$  elliptic problems, each as difficult as the original - essentially, the construction of a discrete Green's function. Moreover, the transfer basis is not localized but spreads over the entire domain  $\Omega$ . As a result the stiffness and mass matrices in the finite element formulation are dense. In this part I experiment with two localization strategies for the transfer basis construction. One is the localization procedure proposed by Owhadi and Zhang (2011). The other is to construct the transfer basis on the truncated sub-domain of  $\Omega$ .

Owhadi and Zhang (2011) proposed a localization procedure based on the decay of Green's functions with distance. Denote by  $\mathcal{T}^h$  a conforming triangulation of  $\Omega$  containing non-overlapping tetrahedral elements  $\{T_m^h\}$  of diameter bounded by  $h$ , and denote by  $\{x_k^h, k = 0, 1, \dots, N^h\}$  the nodal points of  $\mathcal{T}^h$ . The *damping transfer basis* is defined by,

$$\begin{aligned} h^{-1}\psi_i^{d,h} - \nabla \cdot C(x)\nabla\psi_i^{d,h} &= -\Delta\phi_i^h & x \in B(x_i^h, C_1\sqrt{h}\ln(\frac{1}{h})) \cap \Omega \\ \psi_i^{d,h} &= 0 & x \in \partial B(x_i^h, C_1\sqrt{h}\ln(\frac{1}{h})) \cap \Omega. \end{aligned} \quad (4.8)$$

with the assumption (see Owhadi and Zhang (2011), section 3.1) that the finite element space  $S^h = \text{span}\{\phi_i^h, i = 0, 1, \dots, N^h\}$  has the following approximation properties: for any  $f \in H_0^1(\Omega) \cap H^2(\Omega)$

$$\inf_{v \in S^h} \|f - v\|_{H_0^1(\Omega)} \leq C_1 h \|f\|_{H^2(\Omega)}$$

and for all  $f \in H_0^1(\Omega) \cap H^3(\Omega)$

$$\inf_{v \in S^h} \|f - v\|_{H_0^1(\Omega)} \leq C_2 h^2 \|f\|_{H^3(\Omega)}.$$

Notice that the  $P_1$  (or  $Q_1$ ) finite element space does not have these properties. The quadratic finite element space or higher order finite element spaces have to be employed in order to use this localization strategy.

Denote by

$$S_C^{d,h} := \text{span}\{\psi_k^{d,h}, k = 0, 1, \dots, \} \quad (4.9)$$

the *damping* transfer-of-approximation finite element space. The error estimate result for  $S_C^{d,h}$  (see Owhadi and Zhang (2011), Theorem 3.1) states that: *for any  $f \in L^2(\Omega)$ , let  $u$  be the solution of (3.1) and  $u^{d,h}$  the finite element solution in  $S_C^{d,h}$ ,*

$$\|u - u^{d,h}\|_{H_0^1(\Omega)} \leq C_0 h \|f\|_{L^2(\Omega)}$$

where the constant  $C_0$  depends on the coefficient  $C(x)$  and  $\Omega$  but not on  $h$ .

The error estimate with this localization strategy exhibits first order convergence with respect to the energy norm even though the quadratic finite element space is employed to construct *damping* transfer bases. In addition the radius of the sub-domain region in (4.8) is of order  $\sqrt{h} \ln(1/h)$ . For small  $h$  the sub-domain in (4.8) contains a large number of mesh elements. Therefore this strategy is not computationally efficient.

The second localization strategy I attempt is directly truncating the region of

transfer basis construction. Denote by  $\mathcal{T}^h$  a conforming triangulation of  $\Omega$  containing non-overlapping tetrahedral elements  $\{T_m^h\}$  of diameter bounded by  $h$ , and denote by  $\{x_k^h, i = 0, 1, \dots, N^h\}$  the nodal points of  $\mathcal{T}^h$ . Associated with each  $x_k^h$  is a  $P_1$  basis function  $\phi_k^h$ . Denote by  $\mathcal{P}_k^h$  the union of tetrahedral elements  $\{T_m^h\}$  that have common vertex  $x_k^h$ ,

$$\mathcal{P}_k^h = \bigcup_{\forall T_m^h \ni x_k^h} T_m^h. \quad (4.10)$$

See Figure (4.9) for example.

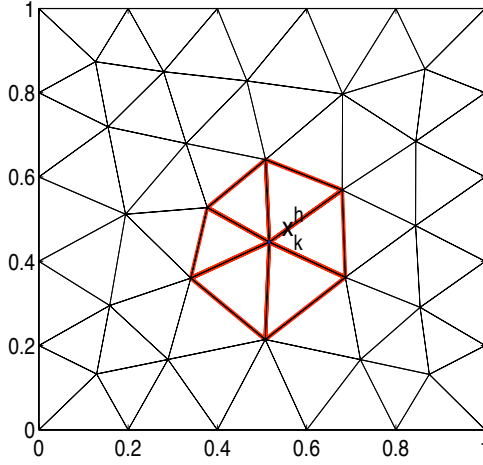


**Figure 4.9:** A patch  $\mathcal{P}_k^h$  associated with the node  $x_k^h$  is illustrated by the union of elements with red boundaries.

The local transfer basis  $\psi_k^{0,h}$  associated with the node  $x_k^h$  on  $\mathcal{P}_k^h$  is the weak solution of

$$\begin{aligned} \nabla \cdot C(x) \nabla \psi_k^{0,h}(x) &= \Delta \phi_k^h(x) \quad x \in \mathcal{P}_k^h \\ \psi_k^{0,h} &= 0 \quad x \in \partial \mathcal{P}_k^h \end{aligned} \quad (4.11)$$

Define

$$S_C^{0,h} := \text{span}\{\psi_k^{0,h}, k = 0, 1, \dots, \}. \quad (4.12)$$

This localization brings error into the transfer-of-approximation finite element method due to the boundary layer effect. The local transfer basis has large difference from the global transfer basis defined in (4.3) provided that the coefficient  $C$  is oscillatory near the boundary of  $\mathcal{P}_k^h$ . It is of interest to see if enlarging the sub-domain could reduce the error.

Denote by  $\mathcal{Q}_k^h$  the union of patches  $\{\mathcal{P}_i^h, i = 0, 1, \dots\}$  that have common vertex  $x_k^h$ ,

$$\mathcal{Q}_k^h = \bigcup_{\forall \mathcal{P}_i^h \ni x_k^h} \mathcal{P}_i^h \quad (4.13)$$

See Figure (4.10) for example.

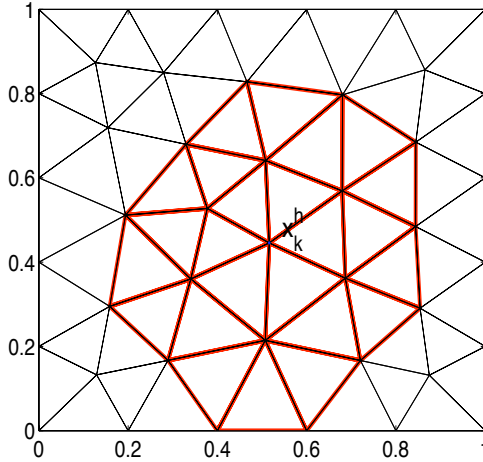


**Figure 4.10:** A patch  $\mathcal{Q}_k^h$  associated with the node  $x_k^h$  is illustrated by the union of elements with red boundaries.

The local transfer basis  $\psi_k^{1,h}$  associated with  $x_k^h$  on  $\mathcal{Q}_k^h$  is defined as the weak solution of

$$\begin{aligned} \nabla \cdot C(x) \nabla \psi_k^{1,h}(x) &= \Delta \phi_k^h(x) \quad x \in \mathcal{Q}_k^h \\ \psi_k^{1,h} &= 0 \quad x \in \partial \mathcal{Q}_k^h \end{aligned} \quad (4.14)$$

Define

$$S_C^{1,h} := \text{span}\{\psi_k^{1,h}, k = 0, 1, \dots, \}. \quad (4.15)$$

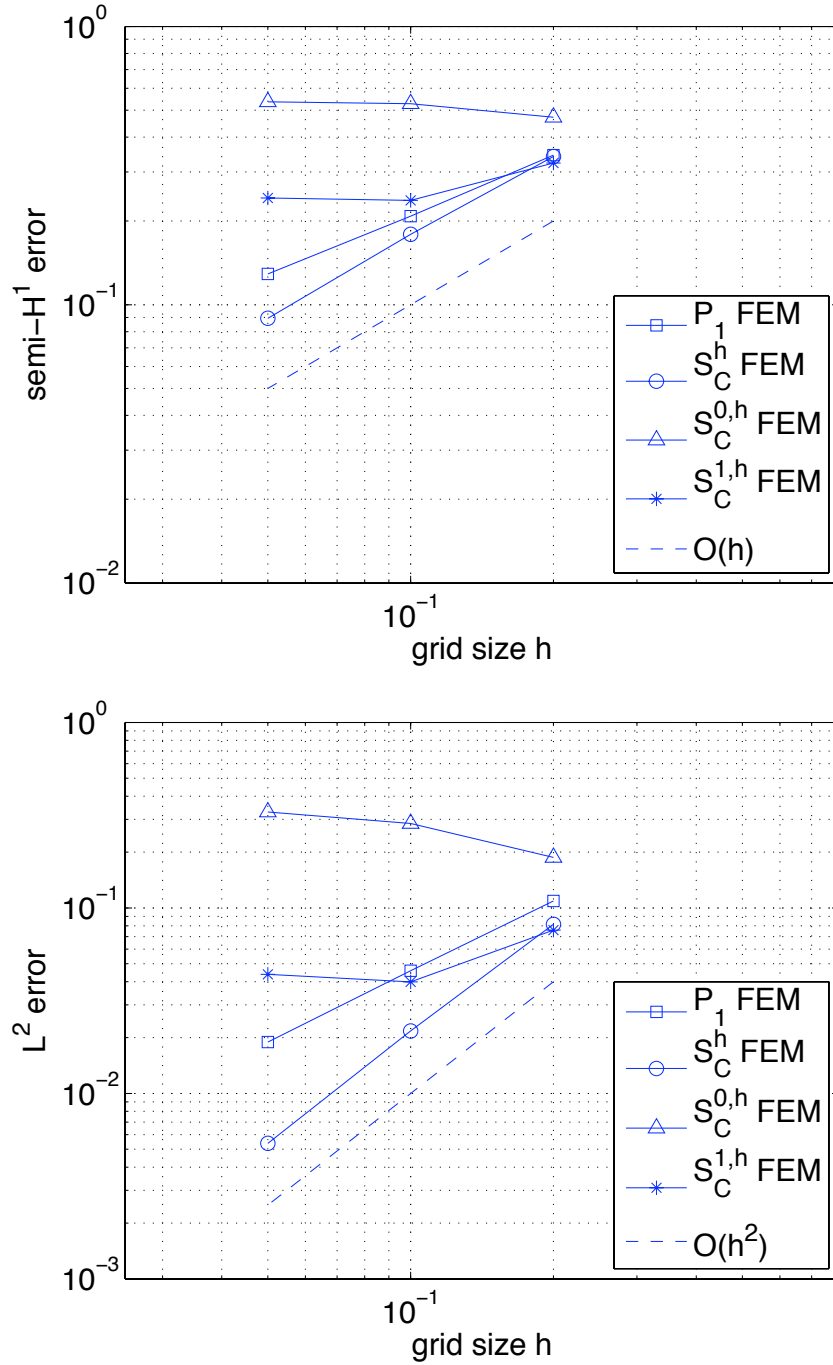
These localization strategies are applied to the elliptic boundary value problem with the 2D checkerboard coefficient (4.7). Two examples are tested with  $\epsilon = 0.5$  and  $\epsilon = 0.1$ .

Figure (4.11), (4.13) show the results for the localization strategy of direct truncating domain. The  $P_1$  finite element space is employed to construct transfer bases  $S_C^{0,h}$  and  $S_C^{1,h}$ . Figure (4.12), (4.14) show the results for the damping localization strategy by Owhadi and Zhang (2011). The  $P_2$  finite element space is employed to construct *damping* transfer bases  $S_C^{d,h}$ .

In these tests the convergence order of the standard finite element methods degenerates, while the global transfer-of-approximation finite element method achieves the theoretical optimal order convergence. The convergence property of the global transfer-of-approximation finite element method can not be replicated by simply truncating the domain (see Figure (4.11), (4.13)). The damping localization strategy in Owhadi and Zhang (2011) shows the predicted behavior when the coefficient is less oscillatory ( $\epsilon = 0.5$ ) (see Figure (4.12)), but breaks down for the high oscillatory

coefficient ( $\epsilon = 0.1$ ) (see Figure (4.14)). The unsuccessful localization suggests the transfer-of-approximation finite element method does not appear to achieve optimal order convergence at reasonable expense.

In summary global transfer-of-approximation finite element method achieves optimal order convergence on regular grids for non-smooth variable coefficients, but is computational prohibitive, and so is not feasible to apply to waves. The localization strategy of direct truncating the construction domain of the transfer basis doesn't work at all. Using the local transfer basis construction proposed by Owhadi and Zhang (2011), the transfer-of-approximation finite element method associated with the  $P_2$  finite element method yields  $O(h)$  error in energy. The support diameter of their local transfer basis leads to huge bandwidth ( $O(h^{-3/2})$ ) of 3D stiffness and mass matrices. Therefore it is not practical.



**Figure 4.11:** Convergence tests for the checkerboard example with  $\epsilon = 0.5$ .  $P_1$  finite element space is used to construct the global transfer finite element space  $S_C^h$  defined in (4.4) as well as  $S_C^{0,h}$  in (4.12) and  $S_C^{1,h}$  in (4.15).

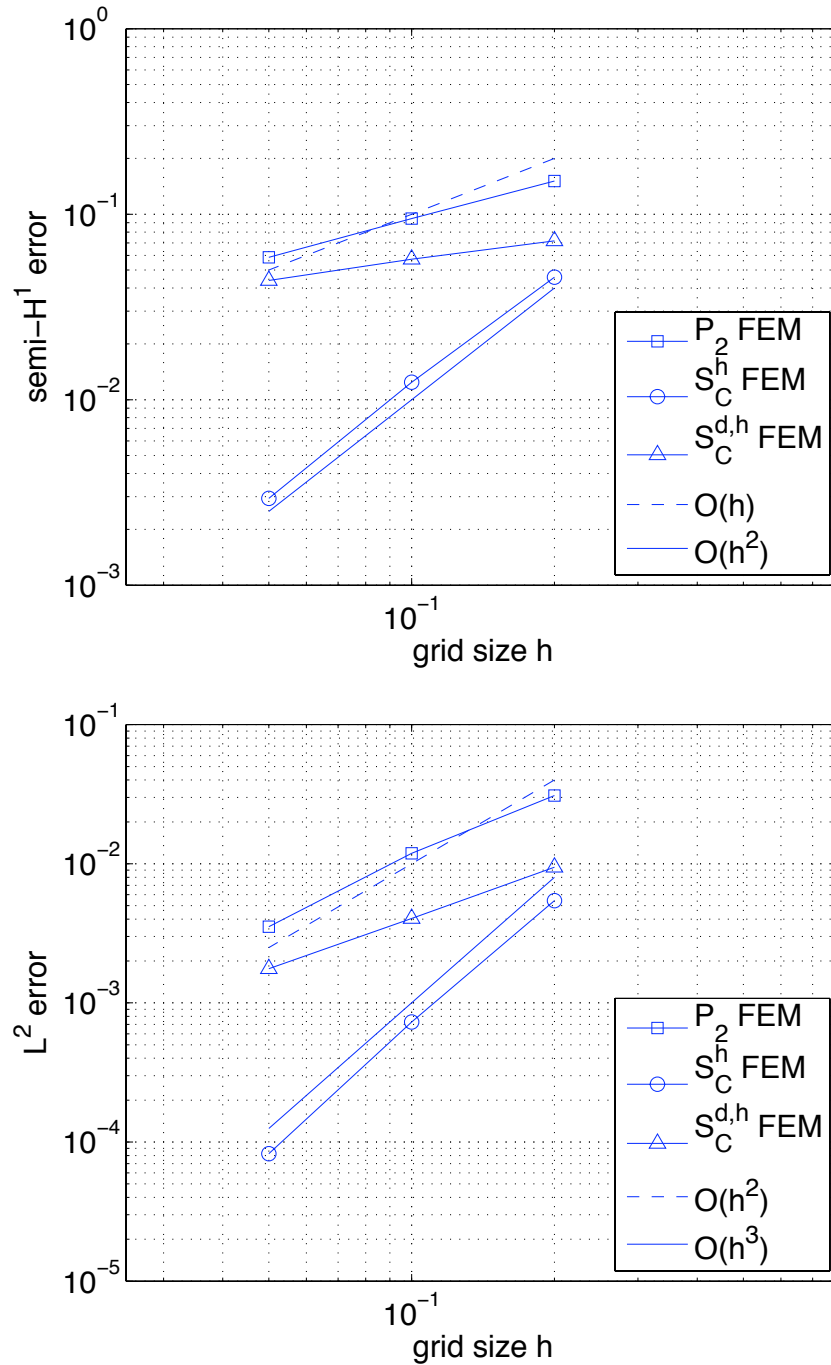


**Figure 4.12:** Convergence tests for the checkerboard example with  $\epsilon = 0.5$ .  $P_2$  finite element space is used to construct the global transfer finite element space  $S_C^h$  defined in (4.4) as well as the damping transfer finite element space  $S_C^{d,h}$  defined in (4.9).

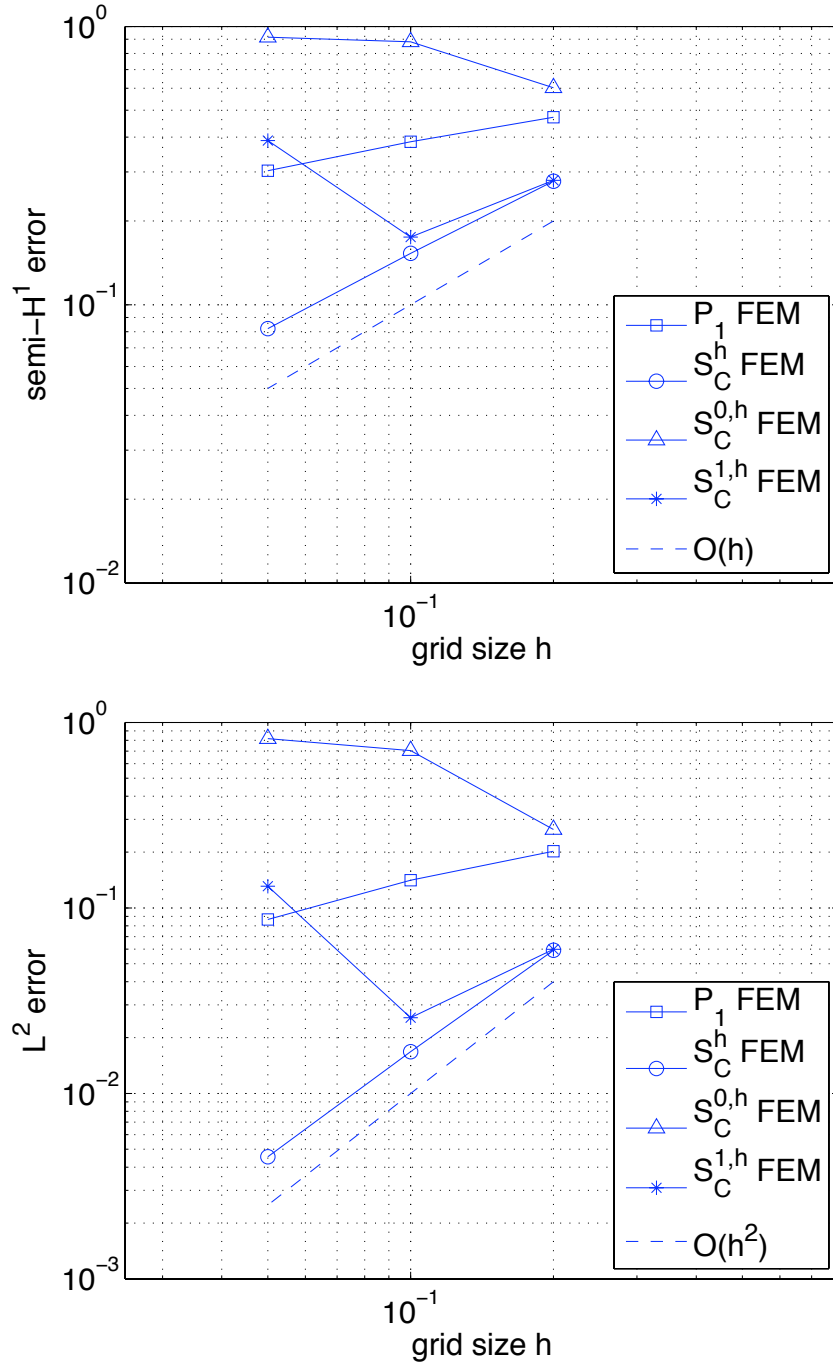


**Figure 4.13:** Convergence tests for the checkerboard example with  $\epsilon = 0.1$ .  $P_1$  finite element space is used to construct the global transfer finite element space  $S_C^h$  defined in (4.4) as well as  $S_C^{0,h}$  in (4.12) and  $S_C^{1,h}$  in (4.15).

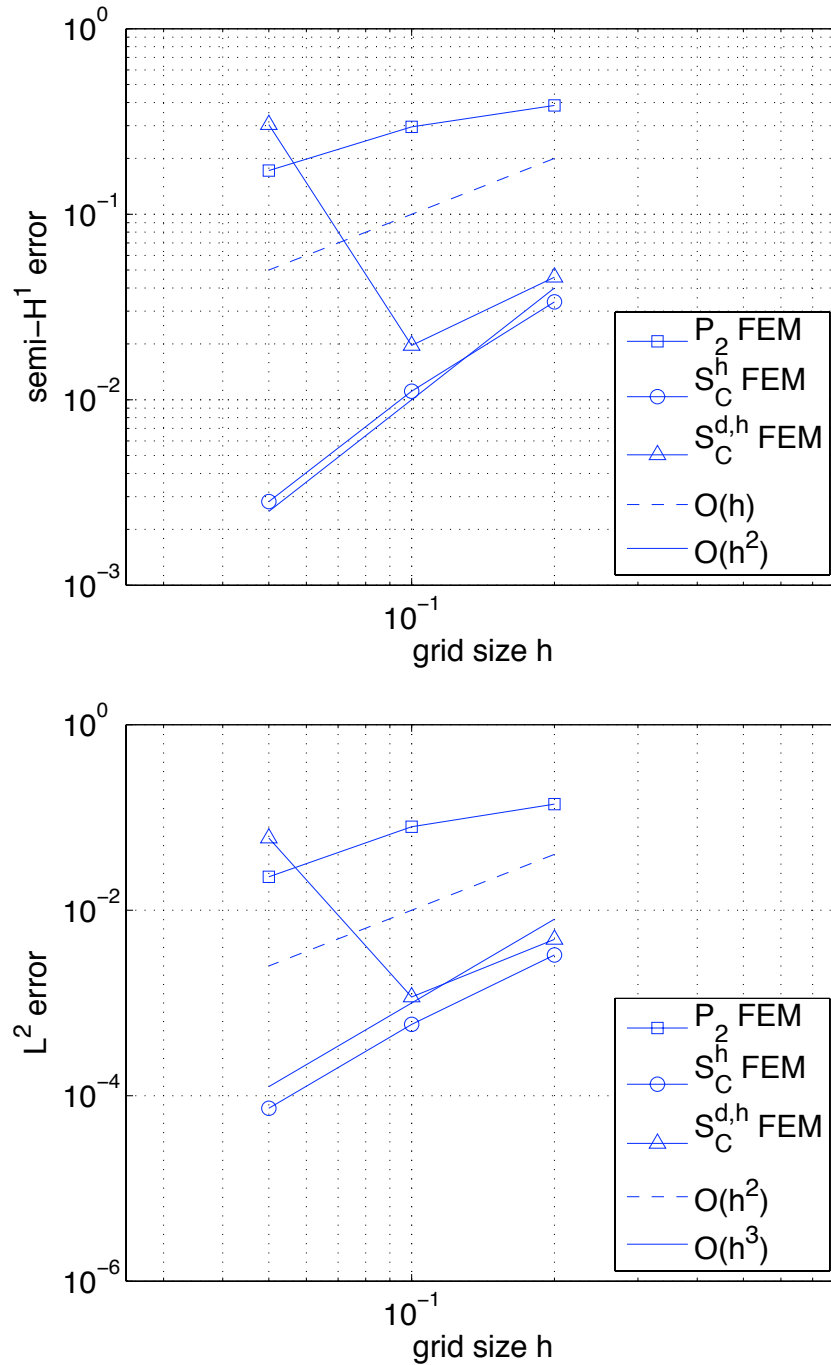


**Figure 4.14:** Convergence tests for the checkerboard example with  $\epsilon = 0.1$ .  $P_2$  finite element space is used to construct the global transfer finite element space  $S_C^h$  defined in (4.4) as well as the damping transfer finite element space  $S_C^{d,h}$  defined in (4.9).



# Chapter 5

## Harmonic Coordinate Finite Element Method

### 5.1 INTRODUCTION

In this chapter I introduce the harmonic coordinate finite element method (HCFEM). For the discussion I consider the second order elliptic boundary value problem with a variable coefficient  $C(x)$ ,

$$\begin{aligned} -\nabla \cdot C(x)\nabla u &= f \quad \text{in } \Omega \\ u(x) &= 0 \quad \text{on } \partial\Omega \end{aligned} \tag{5.1}$$

where  $\Omega$  is a bounded domain in  $\mathbb{R}^n$  ( $n = 1, 2, 3$ ),  $f$  is a function in  $L^2(\Omega)$ . The coefficient  $C(x)$  is uniformly elliptic, i.e.,  $\log C \in L^\infty(\Omega)$  with positive constants  $c_*$

and  $c^*$  such that

$$0 < c_* |\xi|^2 \leq \xi^T C(x) \xi \leq c^* |\xi|^2, \quad \forall x \in \Omega, \forall \xi \in \mathbb{R}^n. \quad (5.2)$$

Discontinuities across smooth hypersurfaces (interfaces) as well as very fine scale structures in  $C(x)$  lead to similar features in the solution of (5.1). For example, discontinuities across interfaces in  $C(x)$  imply jumps in first derivative of  $u$  in order to assure the weak differentiability of  $C\nabla u$ . Such characteristics are poorly approximated in numerical solutions produced by conventional Galerkin-type methods without using domain partitions adapted to discontinuous surfaces in  $C(x)$ , such as interface-fitting meshes or mesh refinement around singularities of coefficients. For interface problems, the immersed finite element method in Li and Ito (2006) offers a method to preserve the feature of solutions on regular meshes. The key is to build non-standard finite element bases that have appropriate jumps across interfaces so that the FE approximation to  $C\nabla u$  is weakly differentiable.

Babuška et al. (1994) constructed special finite elements for rapidly varying coefficient  $C(x)$  depending only on one spatial coordinate, perhaps after a coordinate transformation. In the geophysical literature, such models are known as *layered media*. The special finite elements are composition of  $P_1$  elements with a  $C$ -harmonic function, that is, a solution of  $\nabla \cdot C\nabla F = 0$ . For layered media, the  $C$ -harmonic function may be constructed by quadrature.

Ohwadi and Zhang (2007) extended the harmonic coordinate idea to problems with general bounded and measurable coefficients. Their idea, similar to Babuška et al. (1994), is to construct special basis functions that are adapted to the solution

of the problem. The non-conforming finite element method proposed in Ohwadi and Zhang (2007) achieves a sub-optimal convergence order due to truncating the basis functions. Binford (2011) showed that by using full, untruncated basis functions the harmonic coordinate finite element method recovers the optimal order of convergence on triangular meshes for 2D static interface problems.

In the following I first introduce the harmonic coordinates and the harmonic grid associated with a regular grid. Then I discuss the transformation of the elliptic bounded value problem to a non-divergence form with the harmonic coordinate mapping. Next I describe the construction of the harmonic coordinate finite element space. With the transfer property introduced in Chapter 3 I prove that the harmonic coordinate finite element method achieves optimal second order convergence for the elliptic boundary value problem. I also discuss the error component in HCFEM arising from the harmonic coordinates' approximation. At the end of this section numerical experiments for elliptic boundary value problems are presented to manifest the analysis for HCFEM.

## 5.2 HARMONIC COORDINATES

Components of global  $C$ -harmonic coordinates  $\mathbf{F} \in H^1(\Omega, \mathbb{R}^n)$  for (5.1) are the weak solutions of

$$\begin{aligned} \nabla \cdot C(x)\nabla F_j &= 0 & \text{in } \Omega \\ F_j(x) &= x_j & \text{on } \partial\Omega \end{aligned} \tag{5.3}$$

for  $j = 1, \dots, n$ .

Figure (5.1) shows an example of  $C(x)$  with a circular interface at radius  $r_0 = 1/\sqrt{2\pi}$  in Binford (2011). Figure (5.2) shows a regular grid  $\mathcal{T}$  and its corresponding harmonic grid  $\tilde{\mathcal{T}} = \mathbf{F}(\mathcal{T})$  associated with the coefficient in Figure (5.1). Vertices in the harmonic grid  $\tilde{\mathcal{T}}$  are images of those in the regular grid  $\mathcal{T}$  under the harmonic coordinate mapping  $\mathbf{F}$ . The connectivity relation between vertices in both grids are the same.

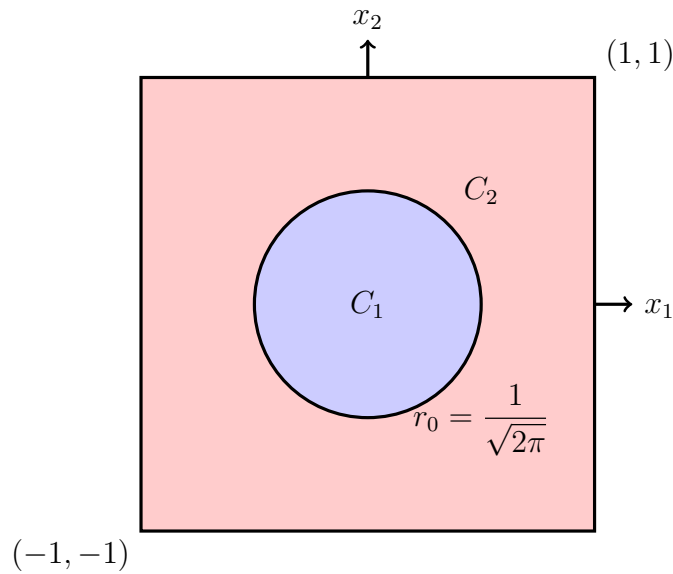


**Figure 5.1:** An example of  $C(x)$

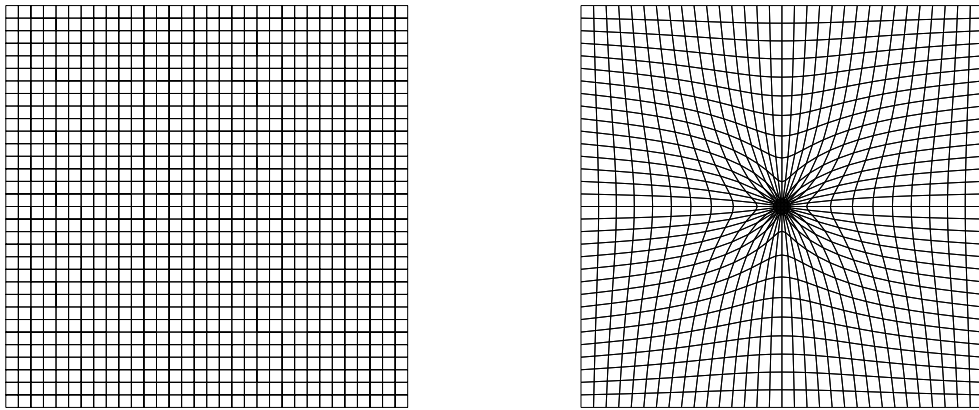


**Figure 5.2:** Left: regular grid  $(x_1, x_2) = (jh_x, kh_y)$ . Right: harmonic grid  $(y_1, y_2) = (F_1(jh_x, kh_y), F_2(jh_x, kh_y))$ . The coefficient  $C(x)$  in equation (5.3) is showed in Figure (5.1), and  $C_1 = 20, C_2 = 1$

Alessandrini and Nesi (2003) proved that if  $n = 2$  and  $\Omega \subset \mathbb{R}^2$  is a bounded and simply connected open set, then  $\mathbf{F}$  is a homeomorphism of  $\bar{\Omega}$  onto  $\bar{\Omega}$ . For  $n = 3$  Briane et al. (2004) showed that this may not hold. Since the homeomorphism is very important for deriving the harmonic coordinate finite element method (recall that  $T$  is required to be an isomorphism in Theorem (3.6)), from now on I assume  $n = 2$ .

### 5.3 ELLIPTIC EQUATION IN NON-DIVERGENCE FORM

As mentioned before the elliptic equation (5.1) with a non-smooth bounded and measurable coefficient has a solution that belongs to  $H_0^1(\Omega)$ . In theory its approximation in a polynomial subspace of  $H^1(\Omega)$  does not achieve the optimal order of convergence. Consequently the standard finite element method produces poor numerical results. The discussion below converts equation (5.1) to a non-divergence form, for which the solution has more smoothness property (Bernstein, 1910; Maugeri et al., 2000).

Assume that  $\mathbf{F}$  is a  $C^2(\Omega, \mathbb{R}^2)$  mapping. I then express  $u$  as a composite function, that is,

$$u(x) = \tilde{u} \circ \mathbf{F}(x) := \tilde{u}(y) \tag{5.4}$$

with the dummy variable  $y = \mathbf{F}(x)$ .

Applying *chain rule* to formally  $\tilde{u} \circ \mathbf{F}(x)$  yields,

$$\frac{\partial u}{\partial x_i} = \sum_{j=1}^2 \frac{\partial F_j}{\partial x_i} \frac{\partial}{\partial y_j} \tilde{u} \circ \mathbf{F}. \tag{5.5}$$

Then by *chain rule* the left hand in equation (5.1) becomes,

$$\begin{aligned} -\nabla \cdot C(x)\nabla u(x) &= -\sum_{j=1}^2 \left[ \nabla \cdot C\nabla F_j \right] \frac{\partial \tilde{u}}{\partial y_j} \circ \mathbf{F}(x) - \sum_{j,k=1}^2 [\sigma_{j,k}] \frac{\partial^2 \tilde{u}}{\partial y_j \partial y_k} \circ \mathbf{F}(x) \\ &= -\sum_{j,k=1}^2 [\sigma_{j,k}] \frac{\partial^2 \tilde{u}}{\partial y_j \partial y_k} \circ \mathbf{F}(x) \end{aligned} \quad (5.6)$$

with  $\sigma = (\sigma_{j,k}) = \nabla \mathbf{F} C(x) (\nabla \mathbf{F})^T$ .

For  $F \in H^1(\Omega, \mathbb{R}^2)$ , I make the hypothesis that equation (5.6) holds. Actually it is possible to justify (5.6) for  $F \in C^1(\Omega, \mathbb{R}^2)$ , or  $F \in W^{1,\infty}(\Omega, \mathbb{R}^2)$  in a weak sense, i.e., for any  $v \in H^1(\Omega)$ ,

$$\int_{\Omega} v(x) \nabla \cdot C(x) \nabla u(x) \, dx = \int_{\Omega} v \circ F^{-1}(y) \sum_{j,k=1}^2 [\sigma_{j,k}] \frac{\partial^2 \tilde{u}}{\partial y_j \partial y_k} \, dy \quad (5.7)$$

Substituting equation (5.6) in equation (5.1) yields the elliptic equation in *non-divergence form*,

$$\begin{aligned} -\sum_{j,k=1}^2 [\tilde{\sigma}_{j,k}] \frac{\partial^2 \tilde{u}}{\partial y_j \partial y_k} &= (|\det \nabla \mathbf{F}|^{-1} f) \circ \mathbf{F}^{-1} := \tilde{f} \quad \text{in } \Omega \\ \tilde{u} &= 0 \quad \text{on } \partial \Omega \end{aligned} \quad (5.8)$$

where  $\tilde{\sigma}(y) = (\tilde{\sigma}_{j,k}(y)) = (|\det \nabla \mathbf{F}|^{-1} \nabla \mathbf{F} C(\nabla \mathbf{F})^T) \circ \mathbf{F}^{-1}(y)$ .

Obviously the transformation from equation (5.1) to equation (5.8) discussed above relies on the validity of applying the *chain rule*, which is implied by assuming the harmonic coordinates  $\mathbf{F}$  are a  $C^2$  mapping. However since the components of  $\mathbf{F}$  are weak solutions of equation (5.3), without further assumptions on the coefficient  $C(x)$  we can only retain the fact that  $\mathbf{F} \in (H^1(\Omega))^2$ .

In the following we assume  $\mathbf{F} \in (H^1(\Omega))^2$ . Let's verify the *chain rule*

$$\nabla(\tilde{u} \circ \mathbf{F}) = \nabla \mathbf{F}^T (\nabla \tilde{u} \circ \mathbf{F}) \quad (5.9)$$

is valid for any  $\tilde{u} \in W^{2,p}(\Omega)$ ,  $p > 2$ . I conjecture that the *chain rule* holds also for  $p = 2$  without providing a proof.

For any  $\tilde{u} \in W^{2,p}(\Omega)$ ,  $p > 2$ ,  $\nabla \tilde{u} \in (W^{1,p}(\Omega))^2$ . So its components are Hölder continuous whence bounded by Morrey's inequality (Evans and Gariepy (1992), pp. 143ff). The right hand side of (5.9) makes sense and belongs to  $L^2(\Omega)$  because  $\nabla \tilde{u} \circ \mathbf{F} \in (L^\infty(\Omega))^2$ .

Denote by  $\eta$  the *standard mollifier* on the unit ball. Define the mollification  $\tilde{u}_\epsilon := \eta_\epsilon * \tilde{u}$  in  $\Omega_\epsilon = \{x \in \Omega \mid \text{dist}(x, \partial\Omega) > \epsilon\}$  where  $\eta_\epsilon := 1/\epsilon^2 \eta(x/\epsilon)$  (Evans (1998), pp 629ff). By chain rule (Theorem 4.(ii) in Evans and Gariepy (1992), pp 130ff)

$$\nabla(\tilde{u}_\epsilon \circ \mathbf{F}) = \nabla \mathbf{F}^T (\nabla \tilde{u}_\epsilon \circ \mathbf{F}) \quad a.e. \mathbf{F}^{-1}(\Omega_\epsilon). \quad (5.10)$$

By the properties of mollifiers (Evans (1998), pp 630ff) and Morrey's inequality,

$$\nabla \mathbf{F}^T (\nabla \tilde{u}_\epsilon \circ \mathbf{F}) \rightarrow \nabla \mathbf{F}^T (\nabla \tilde{u} \circ \mathbf{F}) \quad \text{in } (L^2_{\text{loc}}(\Omega))^2, \quad (5.11)$$

and

$$\nabla(\tilde{u}_\epsilon \circ \mathbf{F}) \rightarrow \nabla(\tilde{u} \circ \mathbf{F}) \quad \text{in } (L^2_{\text{loc}}(\Omega))^2. \quad (5.12)$$

Combining (5.10), (5.11) and (5.12) verifies the *chain rule* (5.9) for any  $\tilde{u} \in W^{2,p}(\Omega)$ ,  $p > 2$ .

## Regularity

For the general two dimension elliptic boundary value equation in non-divergence form,

$$\begin{aligned} -c_{11}(x, y) \frac{\partial^2 u}{\partial x^2} - 2c_{12}(x, y) \frac{\partial^2 u}{\partial x \partial y} - c_{22}(x, y) \frac{\partial^2 u}{\partial y^2} &= f \quad \text{in } \Omega \\ u &= 0 \quad \text{on } \partial\Omega, \end{aligned} \quad (5.13)$$

Babuška et al. (1994) employed a theorem of Bernstein (1910) to show the smoothness property of the solution.

**Theorem 5.1.** (Theorem (2.1) in Babuška et al. (1994)) *Let  $\Omega$  be a bounded and convex domain in  $\mathbb{R}^2$  with a Lipschitz and piecewise  $C^2$  boundary  $\partial\Omega$ . Assume the coefficient  $c_{ij} \in L^\infty(\Omega)$  satisfy*

$$\alpha|\xi|^2 \leq c_{11}(x_1, x_2)\xi_1^2 + 2c_{12}(x_1, x_2)\xi_1\xi_2 + c_{22}(x_1, x_2)\xi_2^2 \leq \beta|\xi|^2, \quad \forall (x_1, x_2) \in \Omega, \quad \forall \xi \in \mathbb{R}^2,$$

for positive constants  $\alpha, \beta$ . For each  $f \in L^2(\Omega)$ , equation (5.13) has a unique solution  $u \in H^2(\Omega) \cap H_0^1(\Omega)$ . Furthermore, there is a constant  $K(\alpha, \beta)$ , independent of  $f$ , such that

$$\|u\|_{H^2(\Omega)} \leq K(\alpha, \beta) \|f\|_{L^2(\Omega)}.$$

The solvability and regularity of equation (5.8) are deeply discussed in Maugeri et al. (2000). For completeness I include the Cordes conditions and the corresponding theorem ( Theorem 1.2.1 in Maugeri et al. (2000)) that states the regularity of the solution of (5.8).

**Definition 5.2.**  $\sigma$  satisfies the Cordes condition if  $\log \sigma \in L^\infty(\Omega, \mathbb{R}^{2 \times 2})$  and there

exists a positive constant  $\epsilon < 1$  such that

$$\frac{\sum_{i,j=1}^2 \sigma_{ij}(x)^2}{\left(\sum_{i=1}^2 \sigma_{ii}(x)\right)^2} \leq \frac{1}{1 + \epsilon}, \quad a.e. \Omega. \quad (5.14)$$

If in addition  $C(x)$  is symmetric (so is  $\sigma(x)$ ), (5.14) rewrites as

$$\frac{\lambda_1^2 + \lambda_2^2}{(\lambda_1 + \lambda_2)^2} \leq \frac{1}{1 + \epsilon}, \quad (5.15)$$

where  $\lambda_1(x), \lambda_2(x)$  are eigenvalues of the matrix  $\sigma(x)$ .

**Theorem 5.3.** (Theorem 1.2.1 in Maugeri et al. (2000)): *Suppose  $\Omega \in \mathbb{R}^2$  to be a bounded and convex domain of class  $C^2$  and that the Cordes condition holds for  $\sigma(x)$ .*

*Then there exists a unique solution  $\tilde{u}$  to the problem (5.8) and*

$$\|\tilde{u}\|_{H^2(\Omega)} \leq \frac{\text{esssup}_\Omega \alpha(x)}{1 - \sqrt{1 - \epsilon}} \|\tilde{f}\|_{L^2(\Omega)}$$

where  $\alpha(x) = \sum_{i=1}^2 \sigma_{ii}(x) / \sum_{i,j=1}^2 \sigma_{ij}(x)^2$ .

That  $\sigma$  in (5.8) satisfies the *Cordes condition* is implied by the facts that  $C$  is uniformly elliptic described in equation (3.2), and  $\mathbf{F}$  is *K-quasiregular*, meaning that for some  $K > 1$ ,  $\lambda_{max}(x) \leq K^{-2} \lambda_{min}(x), \forall x \in \Omega$ , where  $\lambda_{min}$  and  $\lambda_{max}$  are the minimal and maximal eigenvalues of  $\nabla \mathbf{F}(\nabla \mathbf{F})^T$  (see Alessandrini and Nesi (2003)). The *Cordes condition* is generally also a condition on  $C(x)$ . If  $C(x) = c(x)I$ , i.e., the isotropic case, then it is a condition only on  $\mathbf{F}$ . The *Cordes condition* measures the anisotropy of the system in harmonic coordinates, and if the physical system is isotropic then all of the anisotropy comes from  $\nabla \mathbf{F}$ . Also note that *K-quasiregularity* only guarantees that  $\sigma \in L^\infty(\Omega, \mathbb{R}^{2 \times 2})$  for  $n = 2$ . For  $n = 3$  we have to make other

assumptions.

## 5.4 HARMONIC COORDINATE FINITE ELEMENT METHOD

The construction of the harmonic coordinate finite element space can be described as following:

1. prepare a regular (rectangular) triangulation  $\mathcal{T}^h$  of diameter  $h$  that partitions the domain  $\Omega$ ;
2. construct the harmonic grid  $\tilde{\mathcal{T}}^h = \mathbf{F}(\mathcal{T}^h)$  as described in Section 5.2;
3. construct the isoparametric bilinear ( $Q_1$ ) finite element space on  $\tilde{\mathcal{T}}^h$  (Ciarlet, 2002)

$$\tilde{S}^h = \text{span}\{\tilde{\phi}_i^h(x), i = 0, \dots, N^h\};$$

4. the harmonic coordinate finite element space is then defined by

$$S^h = \text{span}\{\tilde{\phi}_i^h \circ \mathbf{F}(x), i = 0, \dots, N^h\} \quad (5.16)$$

Note that  $\tilde{\mathcal{T}}^h$  is not generally regular.  $\tilde{S}^h$  in turn is an isoparametric finite element space. Since in seismic applications the parameter contrast (e.g., density) is  $O(1)$ , we can assume that the largest grid size in  $\tilde{\mathcal{T}}^h$  is about  $O(h)$  in the analysis. Also refining  $\mathcal{T}^h$  results in refining  $\tilde{\mathcal{T}}^h$ . We can expect the usual convergence history shown up for HCFEM.

Figure (5.3) shows the HCFE bases for a 1D elliptic interface problem,

$$\begin{aligned} -(\beta(x)u_x)_x &= f \quad 0 \leq x \leq 1 \\ u(0) &= u(1) = 0, \end{aligned} \tag{5.17}$$

where the coefficient has a jump at  $x = \alpha$ . Away from the interface HCFE bases are the same as standard linear bases. Within the interval that contains the jump, HCFE bases are adapted to the solution of the problem (5.17) such that the normal stress  $\beta u_x$  is continuous at  $\alpha$ .

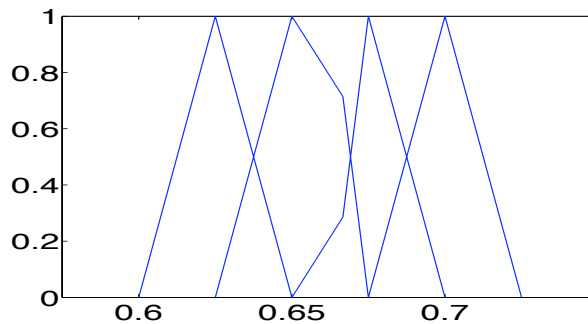


**Figure 5.3:** Illustration of 1D HCFE bases

In two dimension, the support region of a HCFE basis could be complicated, for that  $\text{supp}(\tilde{\phi}_i^h \circ \mathbf{F}) = \mathbf{F}^{-1}(\text{supp}(\tilde{\phi}_i^h))$ . Fortunately since  $\mathbf{F}$  is an isomorphism, the sparsity pattern of stiffness and mass matrices deriving from the HCFE space  $S^h$  is the same as that from the isoparametric bilinear finite element space  $\tilde{S}^h$ .

### Approximation property of $S^h$

Recall Theorem 3.6 and discussion in Section 3.4. Approximate solutions of the elliptic boundary value problem (5.1) and the transferred non-divergence form in (5.8) have

mutually equivalent errors provided that approximation spaces are the HCFE space  $S^h$  and the isoparametric bilinear finite element space  $\tilde{S}^h$ , respectively.

By Theorem 5.3 the solution  $\tilde{u}$  of equation (5.8) is twice weakly differentiable whereas  $u$ , the solution of equation (5.1), is only weakly differentiable. For the isoparametric bilinear finite element space  $\tilde{S}^h$  approximation theory (see Ciarlet (2002)) yields,

$$\inf_{\tilde{v} \in \tilde{S}^h} \|\tilde{v} - \tilde{u}\|_{H^1(\Omega)} = O(h). \quad (5.18)$$

Then by Theorem 3.6 and Corollary 3.8 we have the following approximation property for  $S^h$ ,

$$\inf_{v \in S^h} \|v - u\|_{H^1(\Omega)} = O(h).$$

This discussion can be summarize as follows.

**Theorem 5.4.** *Assume  $u$  is the solution of equation (5.1). The harmonic coordinates  $\mathbf{F} \in W^{1,\infty}(\Omega, \mathbb{R}^2)$  and the chain rule is justified for  $\mathbf{F}$ , and equation (5.6) is correct in the sense of distribution (5.7).  $\mathcal{T}^h$  is a regular triangulation of diameter  $h$  over  $\Omega$ . The harmonic grid  $\tilde{\mathcal{T}}^h = \mathbf{F}(\mathcal{T}^h)$  as described in Section 5.2.  $\tilde{S}^h$  is the isoparametric bilinear  $(Q_1)$  finite element space on  $\tilde{\mathcal{T}}^h$ , with bases  $\tilde{\phi}_i^h, i = 0, \dots, N^h$ . Define the harmonic coordinate finite element space  $S^h$  as in equation (5.16). Then*

$$\inf_{v \in S^h} \|v - u\|_{H^1(\Omega)} = O(h). \quad (5.19)$$

In above the analytical harmonic coordinates  $\mathbf{F}$  are used to construct the harmonic

coordinate basis. Except for simple cases (e.g.,  $C(x)$  varies along one direction) we can only obtain approximations of  $\mathbf{F}$ . Therefore the harmonic grid and the HCFE space defined in (5.16) are theoretical, but not used in practice.

### Approximation property of the practical HCFE space

In practice we usually don't have the mathematical formulation of the harmonic coordinates  $\mathbf{F}$ . An approximation has to be used to construct the harmonic grid and the HCFE space. In the following I analyze how the approximation error of  $\mathbf{F}$  affects the overall approximation property of the HCFE space.

Denote by  $\mathbf{F}_\delta = [F_{1,\delta}, F_{2,\delta}]$  an approximation to the harmonic coordinates  $\mathbf{F}$ . The harmonic grid under the mapping  $\mathbf{F}_\delta$  is  $\tilde{\mathcal{T}}_\delta^h = \mathbf{F}_\delta(\mathcal{T}^h)$ . Then we construct the isoparametric bilinear  $Q_1$  finite element space  $\tilde{S}^h$  on  $\tilde{\mathcal{T}}_\delta^h$ . Finally the practical HCFE space  $S_\delta^h$  is defined as,

$$S_\delta^h = \text{span}\{\tilde{\phi}_i^h \circ \mathbf{F}_\delta(x), i = 0, \dots, N^h\}. \quad (5.20)$$

Denote by  $u$  the solution of equation (5.1).  $u^h = \sum_{j=0}^{N^h} U_j^h \tilde{\phi}_j^h \circ \mathbf{F}(x)$  the Galerkin approximation to  $u$  in  $S^h$ . By (5.19) and Céa's Lemma (Ciarlet, 2002) we have

$$\|u - u^h\|_{H^1(\Omega)} = O(h). \quad (5.21)$$

Write  $\tilde{u}^h = \sum_{j=0}^{N^h} U_j^h \tilde{\phi}_j^h$ . By triangle inequality and (5.21) we have

$$\begin{aligned}
\inf_{v_\delta \in S_\delta^h} \|u - v_\delta\|_{H^1(\Omega)} &\leq \inf_{v_\delta \in S_\delta^h} \|v_\delta - u^h\|_{H^1(\Omega)} + \|u^h - u\|_{H^1(\Omega)} \\
&= \inf_{v_\delta \in S_\delta^h} \|v_\delta - u^h\|_{H^1(\Omega)} + O(h) \\
&\leq \left\| \sum_{j=0}^{N^h} U_j^h (\tilde{\phi}_j^h \circ \mathbf{F} - \tilde{\phi}_j^h \circ \mathbf{F}_\delta) \right\|_{H^1(\Omega)} + O(h) \\
&\leq K \sqrt{\sum_{i=1}^2 \|\nabla_y \tilde{u}^h \cdot \nabla (F_i - F_{i,p})\|_{L^2(\Omega)}^2} + O(h)
\end{aligned}$$

for some constant  $K$  related to applying the Poincare inequality.

Suppose that  $\|\mathbf{F} - \mathbf{F}_\delta\|_{H^1(\Omega)} = O(h)$  and  $\tilde{u}^h \in W^{1,\infty}(\Omega)$ . Then we prove that

$$\inf_{v_\delta \in S_\delta^h} \|v_\delta - u\|_{H^1(\Omega)} = O(h) \quad (5.22)$$

Finally by Céa's Lemma (Ciarlet, 2002) the Galerkin approximation  $u_\delta^h \in S_\delta^h$  to the elliptic problem solution  $u$  has the optimal error estimate,

$$\|u - u_\delta^h\|_{H^1(\Omega)} = O(h). \quad (5.23)$$

## 5.5 APPROXIMATION ERROR OF THE HARMONIC COORDINATES

In order to show the approximation property of the practical HCFE space in (5.22), we have to approximate the harmonic coordinates with error of order  $h$ . For a general coefficient  $C(x)$  a standard FEM converges very slowly when solving equation (5.3). In

other words we need spend many effort on the harmonic coordinates' approximation. This is an inevitable cost for a numerical upscaling approach. For interface problems where the coefficient varies slowly with jumps across interfaces, the adaptive FEM is accurate and efficient for the harmonic coordinates' approximation. By the following analysis I present a criteria of local mesh refinement in the harmonic coordinates' approximation for achieving the optimal order convergence of HCFEM.

I first consider 1D elliptic interface problem (5.17), where  $f \in L^2([0, 1])$  and the coefficient  $\beta$  is assumed to be positive and have a discontinuity at  $x = \alpha$ ,

$$\beta(x) = \begin{cases} \beta^- & x \leq \alpha \\ \beta^+ & x > \alpha \end{cases}$$

The solution  $u \in H_0^1([0, 1]) \cap H^2([0, \alpha]) \cap H^2([\alpha, 1])$ , and hence  $u \in C^1([0, \alpha]) \cap C^1([\alpha, 1])$ . The jump condition can be deduced from the continuity of  $u$  and  $\beta u_x$  at  $x = \alpha$ ,

$$u^+(\alpha) = u^-(\alpha), \quad \beta^+ u_x^+(\alpha) = \beta^- u_x^-(\alpha).$$

For simplicity I use a uniform grid  $x_i = ih, i = 0, 1, \dots, N$ , with  $x_0 = 0$  and  $x_N = 1$  and then  $h = 1/N$ . The standard linear basis function  $\phi_i$  satisfies,

$$\phi_i(x_k) = \delta_{ik}.$$

Suppose that for some  $j$ ,  $x_j < \alpha < x_{j+1}$ . Denote by  $\tilde{\phi}_j, \tilde{\phi}_{j+1}$  the modified basis

function associated with  $x_j, x_{j+1}$ , respectively.

$$\tilde{\phi}_j(x) = \begin{cases} 0, & x \leq x_{j-1} \\ \frac{x - x_{j-1}}{h}, & x_{j-1} \leq x \leq x_j \\ \frac{\alpha - x}{\alpha - x_j}, & x_j \leq x \leq \alpha \\ 0, & x \geq \alpha \end{cases} \quad \tilde{\phi}_{j+1}(x) = \begin{cases} 0, & x \leq \alpha \\ \frac{x - \alpha}{x_{j+1} - \alpha}, & \alpha \leq x \leq x_{j+1} \\ \frac{x_{j+2} - x}{h}, & x_{j+1} \leq x \leq x_{j+2} \\ 0, & x \geq x_{j+1} \end{cases}$$

Define an auxiliary basis  $\tilde{\phi}_\beta$  as,

$$\tilde{\phi}_\alpha(x) = \begin{cases} 0, & x \leq x_j \\ \frac{x - x_j}{\alpha - x_j}, & x_j \leq x \leq \alpha \\ \frac{x_{j+1} - x}{x_{j+1} - \alpha}, & \alpha \leq x \leq x_{j+1} \\ 0, & x \geq x_{j+1} \end{cases}$$

Denote by  $V^h$  the linear finite element space on the uniform grid  $\{x_i\}_{i=0}^N$  and  $\tilde{V}^h$  the linear finite element space on the interface-fitting grid  $\{x_0, \dots, x_j, \alpha, x_{j+1}, \dots, x_N\}$ ,

$$V^h = \text{span}\{\phi_i\}_{i=1}^{N-1}, \quad \tilde{V}^h = \text{span}\{\phi_1, \dots, \phi_{j-1}, \tilde{\phi}_j, \tilde{\phi}_\alpha, \tilde{\phi}_{j+1}, \dots, \phi_{N-1}\}.$$

Let  $u^h \in V^h$  be the finite element solution such that,

$$\int_0^1 \beta(u^h)'(v^h)' dx = \int_0^1 f v^h dx, \quad \forall v^h \in V^h.$$

By Céa's lemma, we have for some constant  $C_1$  dependent of  $\beta$ ,

$$|u - u^h|_{H^1([0,1])} \leq C_1 \inf_{v^h \in V^h} |u - v^h|_{H^1([0,1])} \leq C_1 (|u - \tilde{u}_I|_{H^1([0,1])} + |u_I - \tilde{u}_I|_{H^1([0,1])}), \quad (5.24)$$

where  $u_I = \sum_{i=1}^{N-1} u(x_i)\phi_i = \sum_{i=1}^{N-1} u_i\phi_i$  and  $\tilde{u}_I = \sum_{\substack{i=1, \\ i \neq j, j+1}}^{N-1} u_i\phi_i + u_j\tilde{\phi}_j + u(\alpha)\tilde{\phi}_\alpha + u_{j+1}\tilde{\phi}_{j+1}$

are interpolants of  $u$  on  $V^h$  and  $\tilde{V}^h$ , respectively. Since  $u \in H_0^1([0, 1]) \cap H^2([0, \alpha]) \cap H^2([\alpha, 1])$ , there exists a constant  $C_2$  such that

$$|u - \tilde{u}_I|_{H^1([0,1])} \leq C_2 h (\|u\|_{H^2([0,\alpha])} + \|u\|_{H^2([\alpha,1])}).$$

Since  $u \in C^1([0, \alpha]) \cap C^1([\alpha, 1])$ , there exist some  $\xi_h^- \in (x_j, \alpha)$  and  $\xi_h^+ \in (\alpha, x_{j+1})$ , such that,

$$u_{j+1} - u(\alpha) = u'(\xi_h^+)(x_{j+1} - \alpha), \quad u(\alpha) - u_j = u'(\xi_h^-)(\alpha - x_j).$$

Also notice that  $u_I$  and  $\tilde{u}_I$  are only distinguished in  $[x_j, x_{j+1}]$ . Therefore

$$\begin{aligned}
|u_I - \tilde{u}_I|_{H^1([0,1])} &= \left( \int_{x_j}^{x_{j+1}} ((u_I)' - (\tilde{u}_I)')^2 dx \right)^{1/2} \\
&= \left( \left( \frac{u_{j+1} - u_j}{h} - \frac{u(\alpha) - u_j}{\alpha - x_j} \right)^2 (\alpha - x_j) \right. \\
&\quad \left. + \left( \frac{u_{j+1} - u_j}{h} - \frac{u_{j+1} - u(\alpha)}{x_{j+1} - \alpha} \right)^2 (x_{j+1} - \alpha) \right)^{1/2} \\
&= |u'(\xi_h^+) - u'(\xi_h^-)| \left( \frac{(x_{j+1} - \alpha)^2 (\alpha - x_j)}{h^2} + \frac{(x_{j+1} - \alpha)(\alpha - x_j)^2}{h^2} \right)^{1/2} \\
&= |u'(\xi_h^+) - u'(\xi_h^-)| \sqrt{\frac{(x_{j+1} - \alpha)(\alpha - x_j)}{h}} \\
&\leq \frac{|u'(\xi_h^+) - u'(\xi_h^-)|}{2} \sqrt{h}.
\end{aligned}$$

In summary, we have

$$|u - u^h|_{H^1([0,1])} \leq C_1 C_2 h (\|u\|_{H^2([0,\alpha])} + \|u\|_{H^2([\alpha,1])}) + C_1 \frac{|u'(\xi_h^+) - u'(\xi_h^-)|}{2} \sqrt{h}. \quad (5.25)$$

Note that the second term on the right hand side of the above priori estimate is  $O(\sqrt{h})$ , which lower the convergence order of the  $P_1$  finite element method . A simple but effective cure to recover optimal a priori estimate is to locally refine the grid such that near interfaces the grid size is of order  $h^2$ .

To check the validity of the above analysis, take  $\beta^- = 1, \beta^+ = 10, f = 1, \alpha = \frac{1}{2} + \frac{1}{80}$ . The analytical solution of (5.17) for this case is

$$u(x) = \begin{cases} -\frac{x^2}{2} + \frac{21529}{71840}x & x \leq \frac{1}{2} + \frac{1}{80} \\ -\frac{x^2}{20} + \frac{21529}{71840}x + \frac{14391}{718400} & x > \frac{1}{2} + \frac{1}{80} \end{cases}$$

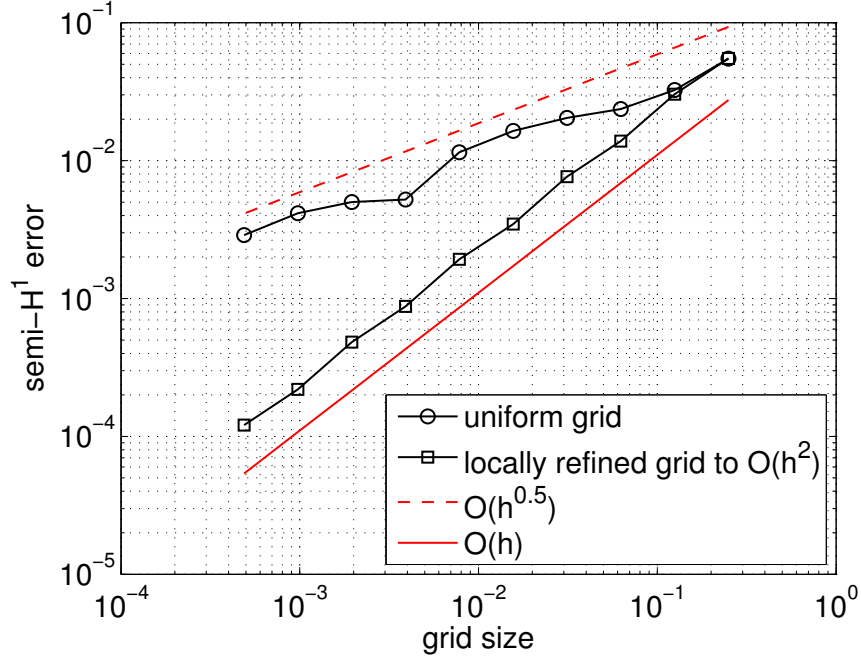


**Figure 5.4:** Convergence test for 1D interface problem using  $P_1$  finite element method.

Figure (5.4) shows the errors  $|u - u^h|_{H^1([0,1])}$  using  $P_1$  FEM. On the locally refined grids  $P_1$  FEM achieves the optimal order convergence, while on uniform grids  $P_1$  FEM converges in the order of  $1/2$ .

For 2D/3D elliptic interface problems Li et al. (2010) provides an optimal a priori estimates as follows. Suppose  $\Omega$  is composed of subdomains  $\Omega_k$  with piecewise constant media. Denote by  $\mathcal{T}_\delta^h$  a triangulation of  $\Omega$ , where the grid diameter is  $h$  within each subdomain  $\Omega_k$  and  $\delta$  quantifies the grid size around interfaces. Let  $\mathbf{F}_\delta^h = [F_{1,\delta}^h, F_{2,\delta}^h]$  be the  $Q_1$  finite element solution of the harmonic coordinates  $\mathbf{F}$  on  $\mathcal{T}_\delta^h$ . Then for  $i = 1, 2$ ,

$$\|F_i - F_{i,\delta}^h\|_{H^1(\Omega)} \leq K_i \left\{ h \|F_i\|_{H^2(\cup_k \Omega_k)} + \sqrt{\delta} \|\nabla F_i\|_{B_{2,1}^{1/2}(\cup_k \Omega_k)} \right\}, \quad (5.26)$$

for some constant  $K_i$ .  $B_{2,1}^{1/2}(\omega) = (L^2(\omega), H^1(\omega))_{1/2,1}$  is a Besov space (Tartar, 2007). As mentioned in Li et al. (2010)  $H^{1/2+\epsilon}(\Omega_k)$  is compactly embedded into  $B_{2,1}^{1/2}(\Omega_k)$  for any  $\epsilon > 0$ . So we can substitute  $\|\nabla F_i\|_{B_{2,1}^{1/2}(\cup_k \Omega_k)}$  with  $\|F_i\|_{H^{3/2+\epsilon}(\cup_k \Omega_k)}$  for any  $\epsilon > 0$ .

The above error estimate suggests that by setting  $\delta \leq h^2$  we have as in 1D case, for  $i = 1, 2$

$$\|F_i - F_{i,\delta}^h\|_{H^1(\Omega)} = O(h). \quad (5.27)$$

For elliptic interface problem the adaptive FEM is an accurate and efficient numerical method for the harmonic coordinates' approximation. We first partition the domain with a regular grid of diameter  $h$ , then locally refine the grid near interfaces such that the grid size there is  $h^2$ . With the approximation of the harmonic coordinates on this locally refined grid by the  $Q_1$  finite element method, HCFEM can achieve the optimal order convergence.

It is worth pointing out that the above discussion is valid only if equation (5.19) in Theorem 5.4 is true. For the 1D interface case,  $F \in W^{1,\infty}$  ( $F$  is Lipschitz). So the change of variable formula holds (Evans and Gariepy (1992), pp. 99ff). For 2D, I am not sure whether the Besov space is embedded in  $W^{1,\infty}$ , but it is better than  $H^1$  according to the above discussion.

## 5.6 NUMERICAL RESULTS FOR ELLIPTIC INTERFACE PROBLEMS

In this section I show the numerical results for elliptic interface problems. Two models are employed. One is the square-circle model, in which the interface is a circle. The other is two-layer model, in which the interface is a straight line. For the square-circle model, I compare the HCFEM, with the  $Q_1$  FEM. I also show how the approximation error of the harmonic coordinates affect the overall error of HCFEM. For the two-layer model, I show the convergence test of HCFEM, and compare it with the  $Q_1$  FEM.

The implementation of HCFEM is based on deal.II (Bangerth et al., 2007), a C++ program library for solving partition differential equations with adaptive finite element methods.

### Square-circle model

I consider the elliptic boundary value problem,

$$-\nabla \cdot C(x)\nabla u = -9\sqrt{x_1^2 + x_2^2} \quad \text{in } \Omega, \quad u|_{\partial\Omega} = u_0$$

in which the coefficient  $C(x)$  and the domain  $\Omega$  are shown in Figure (5.1). The interface lies on a circle of radius  $r_0 = 1/\sqrt{2\pi}$  centered at origin. The coefficient  $C(x)$  is piecewise constant inside and outside the circular region. The analytical solution for this problem is,

$$u = u_0 = \frac{1}{C(x)}((x_1^2 + x_2^2)^3 - r_0^3).$$

- $C_1 = 20, C_2 = 1$ : Figure (5.5) shows the convergence test of HCFEM. Fig-

ure (5.6) shows the convergence test of the  $Q_1$  FEM. Apparently HCFEM achieves the optimal convergence order in both  $L^2$ -error and semi- $H^1$  error, while the  $Q_1$  FEM loses its convergence rate. Figure (5.7) shows the error effect of harmonic coordinates' approximation to HCFEM. As the grid size  $\delta$  near the interface goes to  $h^2$ , the numerical error stabilizes, and can not be improved by decreasing  $\delta$ .

- $C_1 = 2, C_2 = 1$ : Figure (5.8) shows the convergence test of HCFEM. Figure (5.9) shows the convergence test of the  $Q_1$  FEM. HCFEM achieves the optimal convergence order in both  $L^2$ -error and semi- $H^1$  error. Though the  $Q_1$  FEM is not of optimal order, it produces solutions almost as accurate as HCFEM for this low contrast case. Figure (5.10) shows the error effect of harmonic coordinates' approximation to HCFEM. As the grid size  $\delta$  near the interface goes to  $h^2$ , the numerical error stabilizes, and can not be improved by decreasing  $\delta$ .

## Two-layer model

The test elliptic problem is

$$-\nabla \cdot C(x)\nabla u = 0 \quad \text{in } \Omega, \quad u|_{\partial\Omega} = u_0.$$

The coefficient  $C(x)$  shown in Figure (5.11) is piecewise constant with an interface lying on the line  $x_1 \sin \theta + x_2 \cos \theta = b$ . The analytical solution is,

$$u = u_0 = \frac{1}{C(x)}(x_1 \sin \theta + x_2 \cos \theta - b).$$

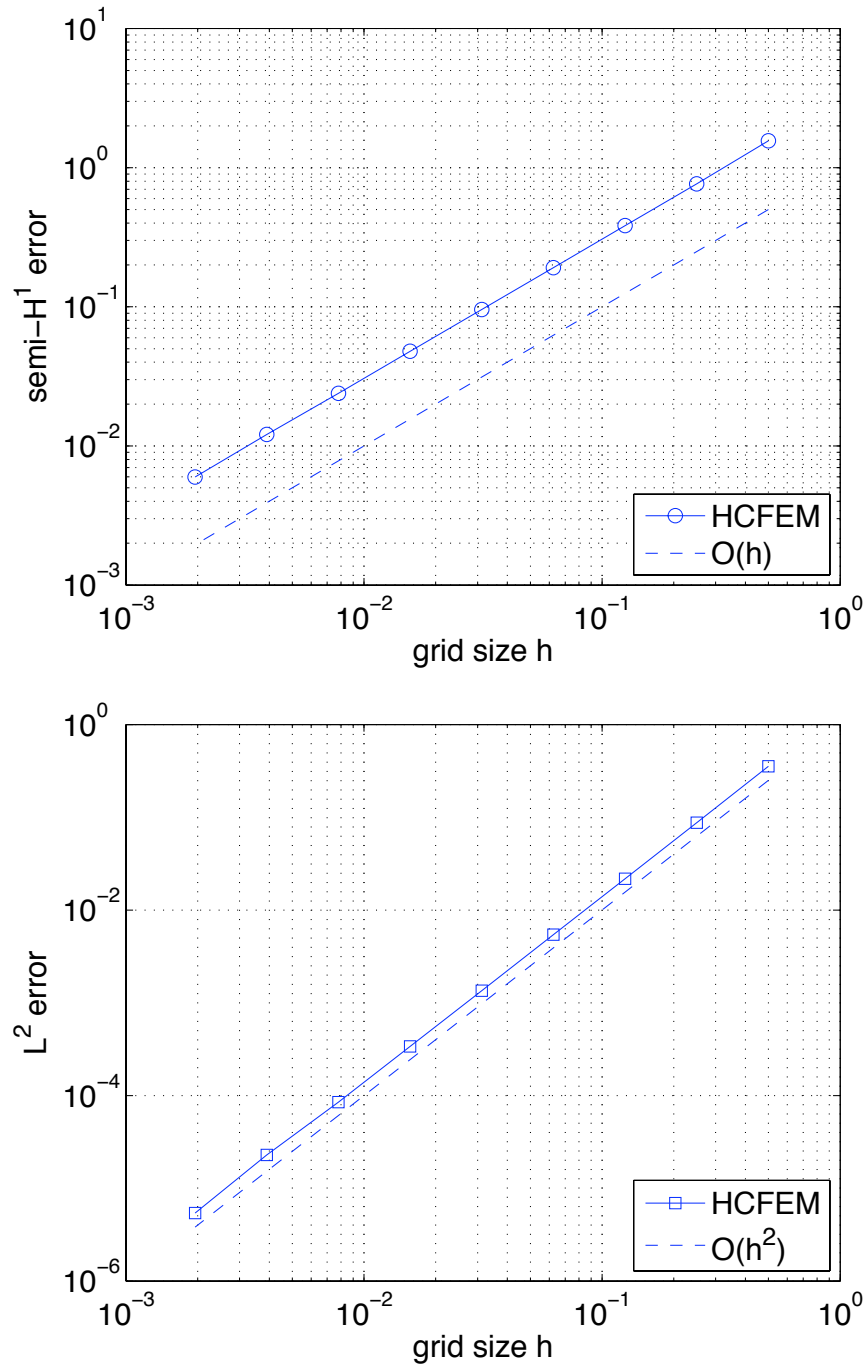


**Figure 5.5:** Convergence test of HCFEM for the square-circle model when  $C_1 = 20, C_2 = 1$ . HCFEM is applied on the regular grid of diameter  $h$ . Harmonic coordinates are approximated on the locally refined grid, in which the grid size is  $\delta$  ( $\delta = h^2$ ) near interfaces.

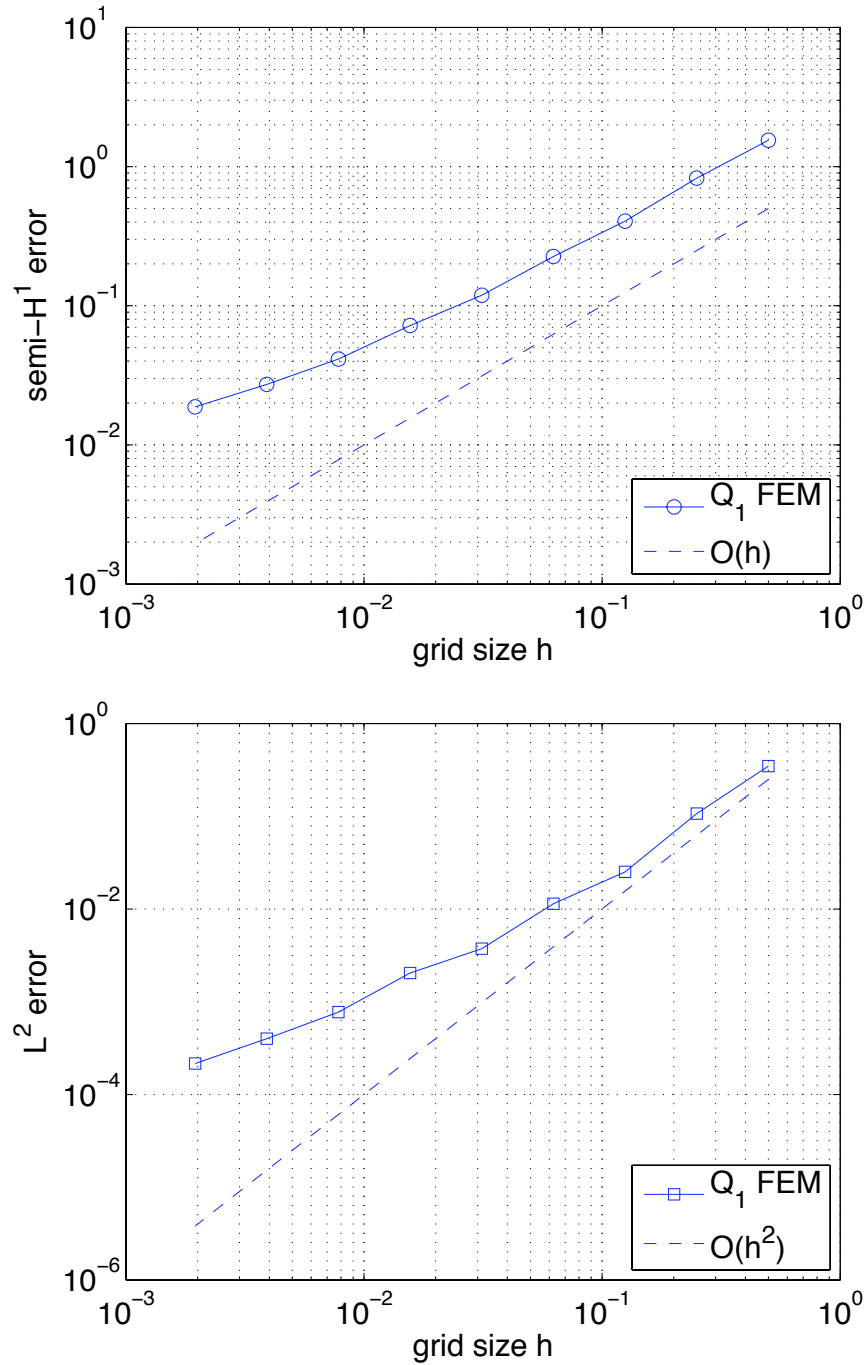


**Figure 5.6:** Convergence test of the standard  $Q_1$  FEM for the square-circle model when  $C_1 = 20, C_2 = 1$ .

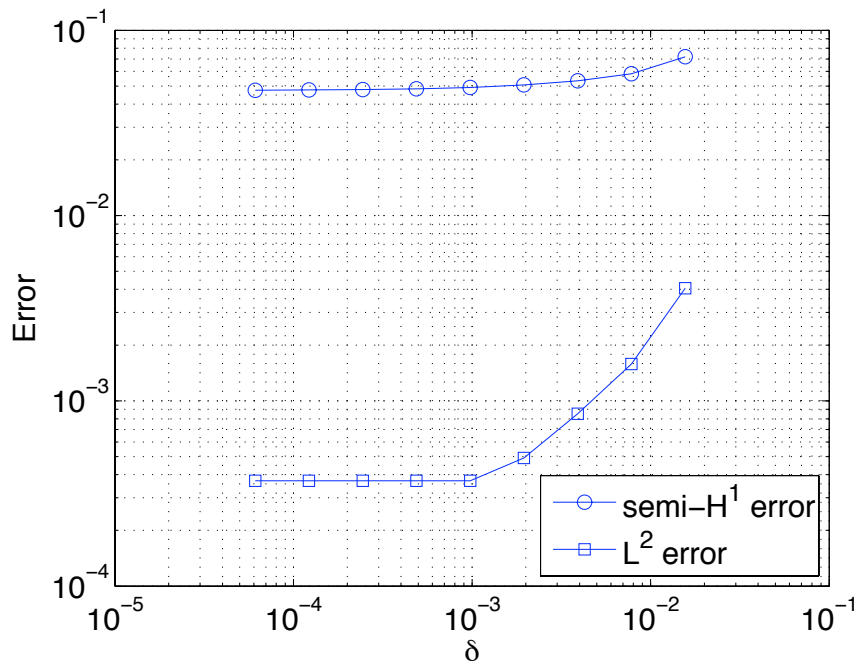


**Figure 5.7:** HCFEM is applied on a regular grid of diameter  $h = 2^{-6}$  for the square-circle model when  $C_1 = 20, C_2 = 1$ . Different locally refined grids of diameter  $\delta$  near the interface are tested to show the error effect of harmonic coordinates' approximation.

In the following test I choose  $\theta = 30^\circ, b = -0.02345$ . Table (5.1) shows the convergence test of HCFEM. Table (5.2) shows the convergence test of the  $Q_1$  FEM. Again HCFEM achieves the optimal convergence order in both  $L^2$ -error and semi- $H^1$  error, while the  $Q_1$  FEM loses its convergence rate.

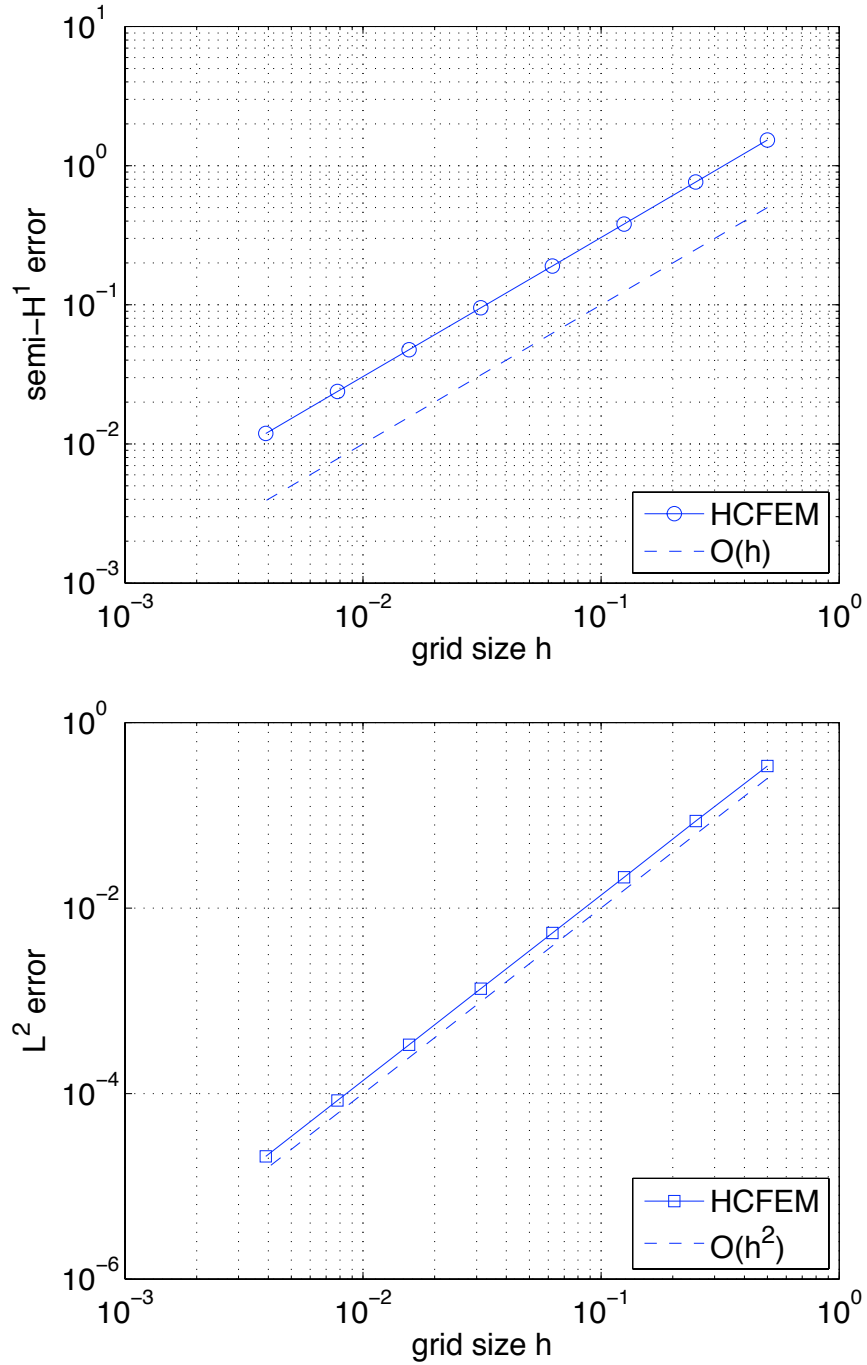


**Figure 5.8:** Convergence test of HCFEM for the square-circle model when  $C_1 = 2, C_2 = 1$ . HCFEM is applied on the regular grid of diameter  $h$ . Harmonic coordinates are approximated on the locally refined grid, in which the grid size is  $\delta$  ( $\delta = h^2$ ) near interfaces.

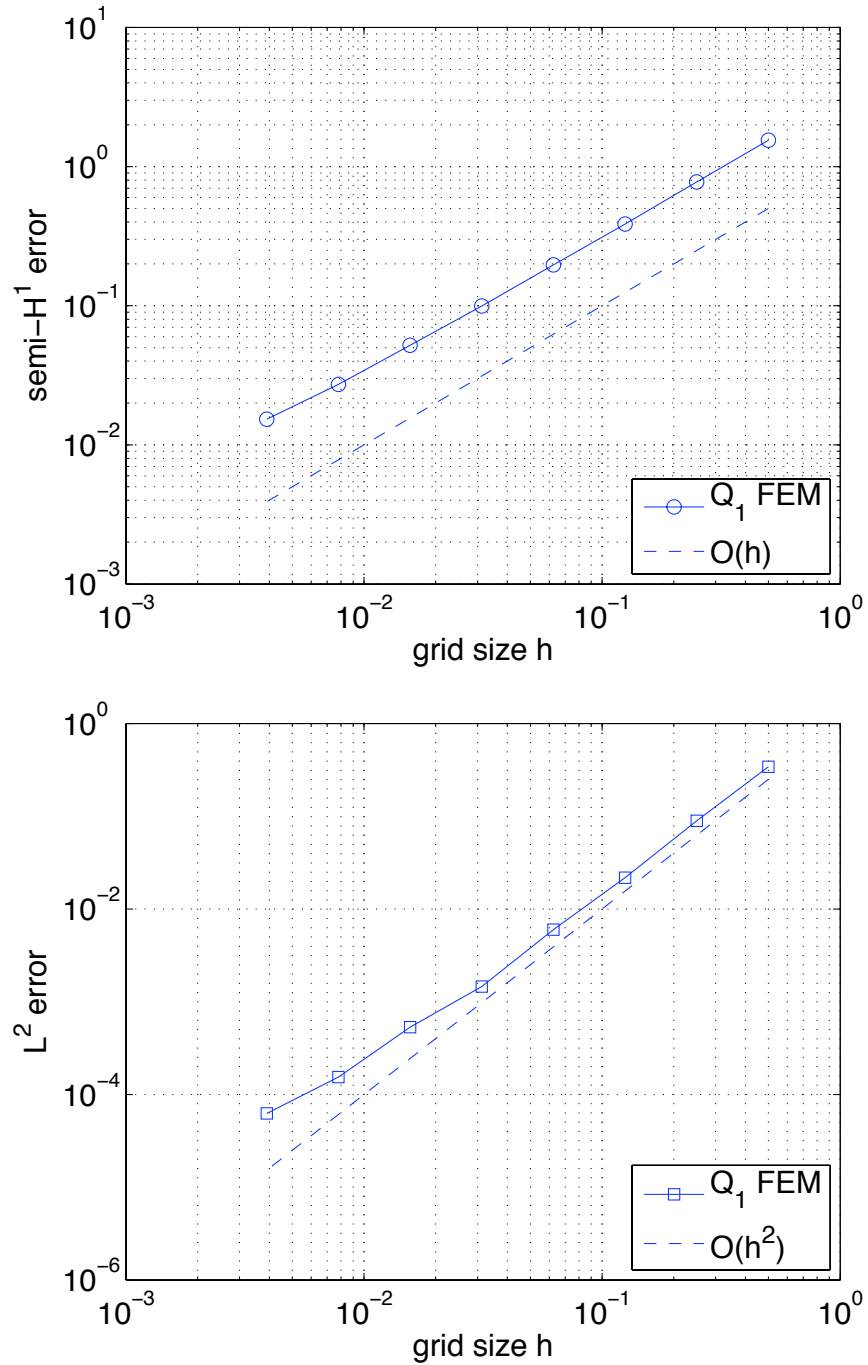


**Figure 5.9:** Convergence test of the standard  $Q_1$  FEM for the square-circle model when  $C_1 = 2$ ,  $C_2 = 1$ .

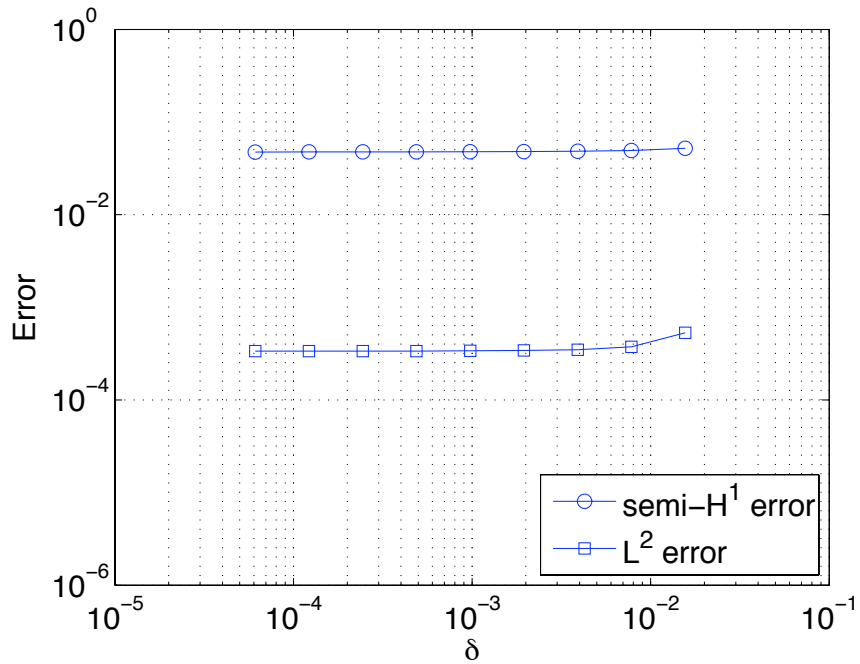


**Figure 5.10:** HCFEM is applied on a regular grid of diameter  $h = 2^{-6}$  for the square-circle model when  $C_1 = 2, C_2 = 1$ . Different locally refined grids of diameter  $\delta$  near the interface are tested to show the error effect of harmonic coordinates' approximation.

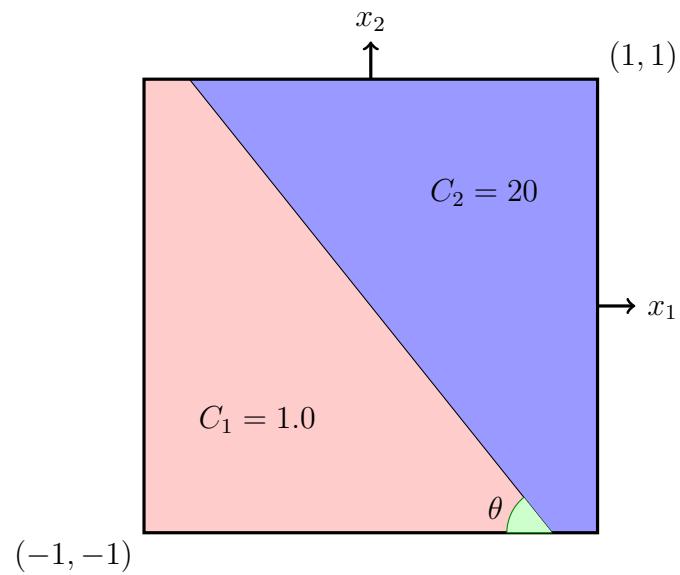


**Figure 5.11:** Two-layer dip model.

$h$	$H^1$ -error	$H^1$ -rate	$L^2$ -error	$L^2$ -rate
$2^{-3}$	1.13e-1	-	3.74e-3	-
$2^{-4}$	5.82e-2	0.96	9.44e-4	1.99
$2^{-5}$	3.19e-2	0.87	2.35e-4	2.01
$2^{-6}$	1.67e-2	0.93	6.02e-5	1.96
$2^{-7}$	9.73e-3	0.78	1.64e-5	1.88
$2^{-8}$	5.12e-3	0.93	3.28e-6	2.32

**Table 5.1:** Convergence test of HCFEM for the two-layer dip model. HCFEM is applied on the regular grid of diameter  $h$ . Harmonic coordinates are approximated on the locally refined grid, in which the grid size is  $\delta$  ( $\delta = h^2$ ) near interfaces.

$h$	$H^1$ -error	$H^1$ -rate	$L^2$ -error	$L^2$ -rate
$2^{-3}$	2.87e-1	-	2.59e-2	-
$2^{-4}$	2.05e-1	0.49	1.31e-2	0.98
$2^{-5}$	1.40e-1	0.55	6.66e-3	0.98
$2^{-6}$	9.97e-2	0.49	3.33e-3	1.00
$2^{-7}$	6.99e-2	0.51	1.68e-3	0.99
$2^{-8}$	4.95e-2	0.52	8.41e-4	1.01

**Table 5.2:** Convergence test of the standard  $Q_1$  FEM for the two-layer dip model.



# Chapter 6

## HCFEM for Scalar Wave Equation

### 6.1 INTRODUCTION

Chapter 5 shows in theory and numerical results that HCFEM achieves the optimal order convergence for 2D elliptic problems on regular rectangular meshes at the additional cost of solving two auxiliary elliptic boundary value problems for the harmonic coordinates. Such additional cost becomes negligible when solutions of the same elliptic system for many different right hand side are needed. For the scalar wave equation, HCFEM is efficient and accurate for that we solve the harmonic coordinates once, and can use them in thousands of time updates.

This chapter discusses the application of HCFEM to the scalar wave equation (3.11). I first recall the theory developed in Chapter 3 to show that HCFEM achieves optimal second order convergence for the scalar wave equation. Then I discuss the mass-lumping technique that maintains the optimal convergence order and overcomes the numerical obstacle of solving a large lines system every time update. At the end of

this chapter numerical results of HCFEM for the scalar wave equation are presented.

## 6.2 ERROR ESTIMATE OF HCFEM FOR SCALAR WAVE EQUATION

For the scalar wave equation, components of the harmonic coordinates  $\mathbf{F}$  are weak solutions of,

$$-\nabla \cdot \frac{1}{\rho} \nabla F_i = 0 \quad \text{in } \Omega, \quad F_i|_{\partial\Omega} = x_i \quad i = 1, 2. \quad (6.1)$$

Again write  $u$  as a composite function, that is,  $u(x) = \tilde{u} \circ \mathbf{F}(x) := \tilde{u}(y)$ . We conclude that  $\tilde{u}$  solve the scalar wave equation in non-divergence form,

$$\frac{\partial^2 \tilde{u}}{\partial t^2} - \sum_{j,k=1}^2 \sigma_{j,k} \circ \mathbf{F}^{-1} \frac{\partial^2 \tilde{u}}{\partial y_j \partial y_k} = f \circ \mathbf{F}^{-1} := \tilde{f}. \quad (6.2)$$

where  $\sigma = \frac{1}{\rho} \nabla \mathbf{F} (\nabla \mathbf{F})^T$ . By Theorem 1.2.1 in Maugeri et al. (2000)  $\tilde{u}(t) \in H_0^1(\Omega) \cap H^2(\Omega)$  for each  $t$ .

Denote by  $\tilde{S}^h$  the bilinear  $Q_1$  finite element space on a regular rectangular triangulation  $\tilde{\mathcal{T}}^h$  of diameter  $h$  over  $\Omega$ ,

$$\tilde{S}^h = \text{span}\{\tilde{\phi}_j^h(x), j = 0, \dots, N^h\}.$$

Then the harmonic coordinates finite element space  $S^h = \text{span}\{\tilde{\phi}_j^h \circ \mathbf{F}(x), i = 0, \dots, N^h\}$ .

Notice that here I assume that the harmonic grid  $\tilde{\mathcal{T}}^h$  is regular. Such assumption doesn't affect the approximation property of  $S^h$ . Denote by  $A = -\nabla \cdot \frac{1}{\rho} \nabla$ . By

Theorem 3.6 and Corollary 3.8 we have that for any  $g \in L^2(\Omega)$

$$\inf_{v \in S^h} \|v - A^{-1}g\|_{H^1(\Omega)} = O(h).$$

Denote by  $u^h \in C^2([0, T], S^h)$  the Galerkin approximation, satisfying

$$\frac{d^2}{dt^2} \langle \kappa^{-1}u^h, \phi^h \rangle + \langle \rho^{-1}\nabla u^h, \nabla \phi^h \rangle = \langle f, \phi^h \rangle, \quad \phi^h \in S^h. \quad (6.3)$$

By Theorem 3.9 we have

- if  $f \in H^3(\mathbb{R}, L^2(\Omega))$ ,  $e_{\kappa, \rho}[u - u^h]^{1/2}(t) \leq K_T h \left\| \frac{\partial^3 f}{\partial t^3} \right\|_{L^2(\Omega \times [0, T])}$ ;
- if  $f \in H^5(\mathbb{R}, L^2(\Omega))$ ,  $\|u - u^h\|_{L^2(\Omega)}(t) \leq K_T h^2 \left\| \frac{\partial^5 f}{\partial t^5} \right\|_{L^2(\Omega \times [0, T])}$ ,

where  $e_{\kappa, \rho}[u](t)$  denotes the energy at time  $t$ ,

$$e_{\kappa, \rho}[u](t) = \frac{1}{2} \left( \left\| \frac{1}{\sqrt{\kappa}} \frac{\partial u}{\partial t}(t) \right\|_{L^2(\Omega)}^2 + \left\| \frac{1}{\sqrt{\rho}} \nabla u \right\|_{L^2(\Omega)} \right),$$

### 6.3 HCFEM GALERKIN APPROXIMATION

Write

$$u^h(t, x) = \tilde{u}^h \circ \mathbf{F}(x) = \sum_{j=0}^{N^h} U_j^h(t) \tilde{\phi}_j^h \circ \mathbf{F}(x).$$

Note  $\tilde{u}^h$  is not the Galerkin approximation to  $\tilde{u}$  of equation (6.2), but simply the composition of  $u^h$  with  $\mathbf{F}^{-1}$ .

Then the Galerkin system (6.3) is a system of ODEs

$$M^h \frac{d^2 U^h}{dt^2} + K^h U^h = F^h \quad (6.4)$$

where  $U^h(t) = [U_0^h, \dots, U_{N^h}^h]^T$ . The components in  $M^h, N^h, F^h$  are defined by,

$$\begin{aligned} M_{ij}^h &= \int_{\Omega} \frac{1}{\kappa} (\tilde{\phi}_i^h \circ \mathbf{F}(x)) \times (\tilde{\phi}_j^h \circ \mathbf{F}(x)) \, dx, \\ N_{ij}^h &= \int_{\Omega} \frac{1}{\rho} \nabla(\tilde{\phi}_i^h \circ \mathbf{F}(x)) \cdot \nabla(\tilde{\phi}_j^h \circ \mathbf{F}(x)) \, dx, \\ F_i^h(t) &= \int_{\Omega} f(x, t) \tilde{\phi}_i^h \circ \mathbf{F}(x) \, dx. \end{aligned}$$

Since

$$\begin{aligned} M_{i,j}^h &= \int_{\Omega} \frac{1}{\kappa} (\tilde{\phi}_i^h \circ \mathbf{F}(x)) \times (\tilde{\phi}_j^h \circ \mathbf{F}(x)) \, dx \\ &= \int_{\Omega} \frac{1}{\kappa} \tilde{\phi}_i^h(y) \tilde{\phi}_j^h(y) (|\det \nabla \mathbf{F}|^{-1} \circ \mathbf{F}^{-1}(y)) \, dy \end{aligned}$$

there exists  $0 < K_1 \leq K_2$  (independent of  $h$ ) so that  $hK_1 I \leq M^h \leq hK_2 I$ . This implies that

$$K_1 h (U^h)^T U^h \leq \|u^h\|^2 \leq K_2 h (U^h)^T U^h.$$

Define the discretized energy as

$$e_{\kappa, \rho}[u^h] = \frac{1}{2} \left( \left( \frac{dU^h}{dt} \right)^T M^h \frac{dU^h}{dt} + (U^h)^T N^h U^h \right) := E[U^h]$$

An argument similar to (3.12) yields

$$E[U^h] \leq K_T \int_0^T d\tau \|f\|^2, \quad t \leq T \quad (6.5)$$

## 6.4 MASS-LUMPING FOR HCFEM

The major obstacle of applying finite element methods to time-dependent PDEs is that every time update the mass matrix has to be inverted. To overcome it, I propose to use the mass-lumping for HCFEM. The main result of this section can be summarized by the following theorem, which shows that the lumped mass solution is as accurate as the consistent mass solution and converges at optimal order.

**Theorem 6.1.** *Assume  $u$  is the solution of equation (3.11). The harmonic coordinates  $\mathbf{F} \in W^{1,\infty}(\Omega, \mathbb{R}^2)$  and the chain rule is justified for  $\mathbf{F}$ , and equation (5.6) holds in the sense of distribution (5.7).  $\tilde{\mathcal{T}}^h$  is a regular triangulation of diameter  $h$  over  $\Omega$ .  $\tilde{S}^h$  is the isoparametric bilinear ( $Q_1$ ) finite element space on  $\tilde{\mathcal{T}}^h$ , with bases  $\tilde{\phi}_i^h, i = 0, \dots, N^h$ . Let  $\hat{u}^h = \sum_{\alpha} \hat{U}_{\alpha}^h(t) \tilde{\phi}_{\alpha}^h \circ \mathbf{F}$ , where  $\hat{U}^h$  is the solution of equation (6.10). Then*

$$e_{\kappa,\rho}[\hat{u}^h - u](t) \leq K_T h^2 \int_0^T d\tau \left\| \frac{\partial^3 f}{\partial t^3} \right\|^2, \quad 0 \leq t \leq T, \quad (6.6)$$

The proof below follows the one given by Symes and Terentyev (2009a) for  $Q_1$  finite elements and constant density acoustics, with necessary modifications to apply to HCFEM.

I assume  $\Omega = [0, l_1] \times [0, l_2]$ . I first extend the solution  $u$  of the acoustic wave equation (3.11) on  $[0, T] \times \Omega$  to  $[0, T] \times \mathbb{R}^2$ . To do so, I make the coefficients  $\kappa, \rho$  periodic even functions with multiperiod  $[2l_1, 2l_2]$  and  $f$  periodic odd functions with multiperiod  $[2l_1, 2l_2]$ . Then the solution  $u$  can be proved to reside in the odd subspace of  $H_{\text{per}}^1(\mathbb{R}^2)$  with multiperiodicity  $[2l_1, 2l_2]$ . I also extend the harmonic coordinate

mapping to  $\mathbb{R}^2$  as for all  $m, n \in \mathbb{Z}$ ,

$$\mathcal{F}_1(x_1, x_2) = \begin{cases} F_1(x_1 - 2ml_1, x_2 - 2nl_2) + 2ml_1, & [x_1, x_2] \in \Omega_1^{m,n} \\ F_1(x_1 - 2ml_1, 2nl_2 - x_2) + 2ml_1, & [x_1, x_2] \in \Omega_4^{m,n} \\ -F_1(2ml_1 - x_1, x_2 - 2nl_2) + 2ml_1, & [x_1, x_2] \in \Omega_2^{m,n} \\ -F_1(2ml_1 - x_1, 2nl_2 - x_2) + 2ml_1, & [x_1, x_2] \in \Omega_3^{m,n} \end{cases} \quad (6.7)$$

$$\mathcal{F}_2(x_1, x_2) = \begin{cases} F_2(x_1 - 2ml_1, x_2 - 2nl_2) + 2nl_2, & [x_1, x_2] \in \Omega_1^{m,n} \\ F_2(2ml_1 - x_1, x_2 - 2nl_2) + 2nl_2, & [x_1, x_2] \in \Omega_2^{m,n} \\ -F_2(2ml_1 - x_1, x_2 - 2nl_2) + 2nl_2, & [x_1, x_2] \in \Omega_3^{m,n} \\ -F_2(x_1 - 2ml_1, 2nl_2 - x_2) + 2nl_2, & [x_1, x_2] \in \Omega_4^{m,n} \end{cases}.$$

where  $\mathbf{F} = [F_1, F_2]$  are the harmonic coordinates satisfying equation (6.1) in  $\Omega$ , and

$$\begin{aligned} \Omega_1^{m,n} &= [2ml_1, 2ml_1 + l_1] \times [2nl_2, 2nl_2 + l_2], \\ \Omega_2^{m,n} &= [2ml_1 - l_1, 2mL] \times [2nl_2, 2nl_2 + l_2], \\ \Omega_3^{m,n} &= [2ml_1 - l_1, 2ml_1] \times [2nl_2 - l_2, 2nl_2], \\ \Omega_4^{m,n} &= [2ml_1, 2ml_1 + l_1] \times [2nl_2 - l_2, 2nl_2]. \end{aligned}$$

which is shown in Figure (6.1).

With the coordinate change of  $\mathcal{F}$ , the solution  $\tilde{u}$  of equation (6.2) is also extend to a function in  $H_{\text{per}}^2(\mathbb{R}^2)$ . Let  $\tilde{\mathcal{T}}_{\mathbb{R}^2}^{\mathbf{h}}$  be a regular rectangular grid over  $\mathbb{R}^2$ , and  $\mathbf{h} = [h_1, h_2]$  denote the vector of cell side lengths. I number the nodal point  $[\alpha_1 h_1, \alpha_2 h_2]$  in  $\tilde{\mathcal{T}}_{\mathbb{R}^2}^{\mathbf{h}}$  with the index  $\alpha = [\alpha_1, \alpha_2]$ . Associated with each node there is a  $Q_1$  finite element  $\tilde{\phi}_{\alpha}^{\mathbf{h}}$ .

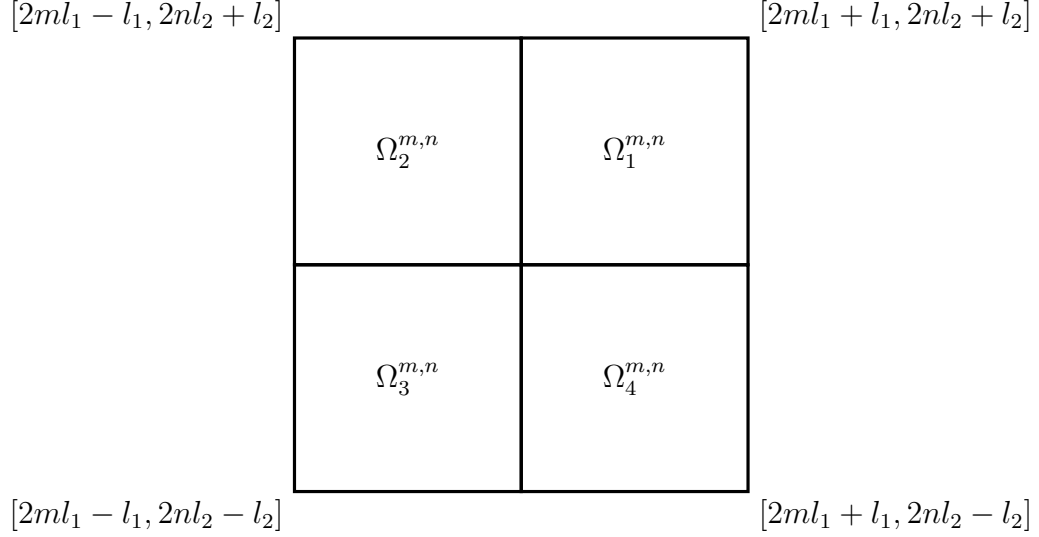


**Figure 6.1:** Illustration of  $\Omega_1^{m,n}, \Omega_2^{m,n}, \Omega_3^{m,n}, \Omega_4^{m,n}$

The harmonic coordinate finite element solution of equation (3.11) that is extended to the entire  $\mathbb{R}^2$  can be expressed as

$$u^{\mathbf{h}}(x, t) = \sum_{\alpha} U_{\alpha}^{\mathbf{h}}(t) \tilde{\phi}_{\alpha}^{\mathbf{h}} \circ \mathcal{F}(x)$$

Using a second order differencing scheme for the time derivative yields the full discretization of the scalar wave equation (3.11) within  $\Omega$ ,

$$M^{\mathbf{h}} \frac{U^{\mathbf{h}}(t + \delta t) - 2U^{\mathbf{h}}(t) + U^{\mathbf{h}}(t - \delta t)}{\delta t^2} + N^{\mathbf{h}} U^{\mathbf{h}}(t) = F^{\mathbf{h}}(t), \quad (6.8)$$

where  $U^{\mathbf{h}}(t)$  is a vector function of time  $t$  enumerating all  $U_{\alpha}^{\mathbf{h}}$  where  $(\alpha_1 h_1, \alpha_2 h_2) \in \Omega$ .

The components in  $N^{\mathbf{h}}, M^{\mathbf{h}}, F^{\mathbf{h}}$  are defined by

$$\begin{aligned} N_{\alpha,\beta}^{\mathbf{h}} &= \int_{\Omega} \frac{1}{\rho} \nabla(\tilde{\phi}_{\alpha}^{\mathbf{h}} \circ \mathcal{F}(x)) \cdot \nabla(\tilde{\phi}_{\beta}^{\mathbf{h}} \circ \mathcal{F}(x)) \, dx, \\ M_{\alpha,\beta}^{\mathbf{h}} &= \int_{\Omega} \frac{1}{\kappa} (\tilde{\phi}_{\alpha}^{\mathbf{h}} \circ \mathcal{F}(x)) \times (\tilde{\phi}_{\beta}^{\mathbf{h}} \circ \mathcal{F}(x)) \, dx, \\ F_{\alpha}^{\mathbf{h}}(t) &= \int_{\Omega} f(x, t) \tilde{\phi}_{\alpha}^{\mathbf{h}} \circ \mathcal{F}(x) \, dx. \end{aligned}$$

Clearly every time update in equation (6.8) involves solving a linear system

$$\begin{aligned} M^{\mathbf{h}} U^{\mathbf{h}}(t + \delta t) &= 2M^{\mathbf{h}} U^{\mathbf{h}}(t) - M^{\mathbf{h}} U^{\mathbf{h}}(t - \delta t) \\ &\quad + \delta t^2 (F^{\mathbf{h}} - N^{\mathbf{h}} U^{\mathbf{h}}(t)). \end{aligned} \tag{6.9}$$

To overcome this numerical obstacle I replace  $M^{\mathbf{h}}$  on the left hand side in equation (6.9) by a diagonal matrix  $D^{\mathbf{h}}$ , where

$$D_{\alpha,\alpha}^{\mathbf{h}} = \sum_{\beta} M_{\alpha,\beta}^{\mathbf{h}}.$$

Since  $\tilde{\phi}_{\alpha}^{\mathbf{h}}$  is a  $Q_1$  element,  $M_{\alpha,\beta}^{\mathbf{h}} = 0$  if  $|\alpha_1 - \beta_1| > 1$  or  $|\alpha_2 - \beta_2| > 1$ . Define  $\Delta = \{\gamma \in \mathbb{Z}^2 : |\gamma_i| \leq 1, i = 1, 2\}$ . Then

$$D_{\alpha,\alpha}^{\mathbf{h}} = \sum_{\gamma \in \Delta} M_{\alpha,\alpha+\gamma}^{\mathbf{h}},$$

and

$$(M^{\mathbf{h}} U^{\mathbf{h}})_{\alpha} = \sum_{\gamma \in \Delta} M_{\alpha,\alpha+\gamma}^{\mathbf{h}} U_{\alpha+\gamma}^{\mathbf{h}} = \sum_{\gamma \in \Delta} M_{\alpha,\alpha+\Delta}^{\mathbf{h}} (U_{\alpha+\Delta}^{\mathbf{h}} - U_{\alpha}^{\mathbf{h}}) + D_{\alpha,\alpha}^{\mathbf{h}} U_{\alpha}^{\mathbf{h}}$$

Let  $\hat{U}^{\mathbf{h}}$  be the solution of the mass-lumped Galerkin system

$$D^{\mathbf{h}} \frac{d^2 \hat{U}^{\mathbf{h}}}{dt^2} + K^{\mathbf{h}} \hat{U}^{\mathbf{h}} = F^{\mathbf{h}} \quad (6.10)$$

For any solution of such a system, an energy inequality similar to (6.5) holds,

$$\hat{E}[\hat{U}^{\mathbf{h}}](t) \equiv \frac{1}{2} \left( \left( \frac{dU^{\mathbf{h}}}{dt} \right)^T D^{\mathbf{h}} \frac{dU^{\mathbf{h}}}{dt} + (U^{\mathbf{h}})^T K^{\mathbf{h}} U^{\mathbf{h}} \right) (t) \leq K_T \int_0^T dt \|f\|_{L^2(\Omega)}^2, \quad t \leq T \quad (6.11)$$

The difference between  $\hat{U}^{\mathbf{h}}$  and  $U^{\mathbf{h}}$  satisfies,

$$\left[ D^{\mathbf{h}} \frac{d^2}{dt^2} (U^{\mathbf{h}} - \hat{U}^{\mathbf{h}}) + K^{\mathbf{h}} (U^{\mathbf{h}} - \hat{U}^{\mathbf{h}}) \right]_{\alpha} = - \sum_{\gamma \in \Delta} M_{\alpha, \alpha + \gamma}^{\mathbf{h}} \left( \frac{d^2 U_{\alpha, \alpha + \gamma}^{\mathbf{h}}}{dt^2} - \frac{d^2 U_{\alpha}^{\mathbf{h}}}{dt^2} \right)$$

According to (6.11)

$$\begin{aligned} \hat{E}[U^{\mathbf{h}} - \hat{U}^{\mathbf{h}}] &\leq K_T \int_0^T d\tau \\ &\times \sum_{\gamma \in \Delta} M_{\cdot, \cdot + \gamma}^{\mathbf{h}} \left( \frac{d^2 U_{\cdot, \cdot + \gamma}^{\mathbf{h}}}{dt^2} - \frac{d^2 U_{\cdot}^{\mathbf{h}}}{dt^2} \right) (D^{\mathbf{h}})^{-1} \sum_{\gamma \in \Delta} M_{\cdot, \cdot + \gamma}^{\mathbf{h}} \left( \frac{d^2 U_{\cdot, \cdot + \gamma}^{\mathbf{h}}}{dt^2} - \frac{d^2 U_{\cdot}^{\mathbf{h}}}{dt^2} \right) \\ &\leq K K_T h \sum_{\gamma \in \Delta} \int_0^T d\tau \left| \frac{d^2 U_{\cdot, \cdot + \gamma}^{\mathbf{h}}}{dt^2} - \frac{d^2 U_{\cdot}^{\mathbf{h}}}{dt^2} \right|^2 \end{aligned} \quad (6.12)$$

in which  $h = \max(h_1, h_2)$  and  $K$  from now on denotes a constant depending on the coefficients and  $\Omega$ , but not on  $h$ .

Define the unitary translation operator  $T_{\gamma}^{\mathbf{h}} : L_{\text{per}}^2(\mathbb{R}^2) \rightarrow L_{\text{per}}^2(\mathbb{R}^2)$  by

$$T_{\gamma}^{\mathbf{h}} v(y) = v(y - \text{diag}(\gamma) \mathbf{h}).$$

Since  $\tilde{\phi}_{\alpha+\gamma}^{\mathbf{h}} = T_{\gamma}^{\mathbf{h}} \tilde{\phi}_{\alpha}^{\mathbf{h}}$ ,

$$\sum_{\alpha} \left( \frac{d^2 U_{\alpha+\gamma}^{\mathbf{h}}}{dt^2} - \frac{d^2 U_{\alpha}^{\mathbf{h}}}{dt^2} \right) \tilde{\phi}_{\alpha}^{\mathbf{h}} = \sum_{\alpha} \left[ \frac{d^2 U_{\alpha}^{\mathbf{h}}}{dt^2} \tilde{\phi}_{\alpha-\gamma}^{\mathbf{h}} - \frac{d^2 U_{\alpha}^{\mathbf{h}}}{dt^2} \tilde{\phi}_{\alpha}^{\mathbf{h}} \right] = (T_{-\gamma}^{\mathbf{h}} - I) \frac{\partial^2 \tilde{u}^{\mathbf{h}}}{\partial t^2}.$$

Denote by  $\tilde{M}^{\mathbf{h}}$  the mass matrix of the bilinear  $Q_1$  finite element space  $\tilde{S}^h$  on  $\Omega$ . For some constant  $K$  independent of  $h$

$$hI \leq K\tilde{M}^{\mathbf{h}}.$$

Thus

$$\begin{aligned} \left| \frac{d^2 U_{\cdot+\gamma}^{\mathbf{h}}}{dt^2} - \frac{d^2 U_{\cdot}^{\mathbf{h}}}{dt^2} \right|^2 &\leq Kh^{-1} \left\| \sum_{\alpha} \left( \frac{d^2 U_{\alpha+\gamma}^{\mathbf{h}}}{dt^2} - \frac{d^2 U_{\alpha}^{\mathbf{h}}}{dt^2} \right) \tilde{\phi}_{\alpha}^{\mathbf{h}} \right\|_{L^2(\Omega)}^2 \\ &= Kh^{-1} \left\| (T_{-\gamma}^{\mathbf{h}} - I) \frac{\partial^2 \tilde{u}^{\mathbf{h}}}{\partial t^2} \right\|_{L^2(\Omega)}^2 \end{aligned} \quad (6.13)$$

Combining (6.12) and (6.13) gives

$$\hat{E}[U^{\mathbf{h}} - \hat{U}^{\mathbf{h}}](t) \leq K_T \sum_{\gamma \in \Delta} \int_0^T d\tau \left\| (T_{-\gamma}^{\mathbf{h}} - I) \frac{\partial^2 \tilde{u}^{\mathbf{h}}}{\partial t^2} \right\|_{L^2(\Omega)}^2 \quad (6.14)$$

Suppose that in addition to the previous hypotheses,  $f \in H^4([0, T], L^2(\Omega))$ . Theorem 3.9 applied to the  $\partial u / \partial t$  gives

$$\left\| \frac{\partial^2 u}{\partial t^2} - \frac{\partial^2 u^{\mathbf{h}}}{\partial t^2} \right\|_{L^2(\Omega)}^2 (t) \leq K_T h^2 \int_0^T d\tau \left\| \frac{\partial^4 f}{\partial t^4} \right\|_{L^2(\Omega)}^2, \quad t \leq T. \quad (6.15)$$

An integration by substitution yields

$$\left\| \frac{\partial^2 \tilde{u}}{\partial t^2} - \frac{\partial^2 \tilde{u}^{\mathbf{h}}}{\partial t^2} \right\|_{L^2(\Omega)}^2 (t) \leq \sup_{x \in \Omega} |\det \nabla \mathbf{F}| \left\| \frac{\partial^2 u}{\partial t^2} - \frac{\partial^2 u^{\mathbf{h}}}{\partial t^2} \right\|_{L^2(\Omega)}^2 (t)$$

whence

$$\hat{E}[U^{\mathbf{h}} - \hat{U}^{\mathbf{h}}](t) \leq K_T \left( \sum_{\alpha \in \Delta} \int_0^T d\tau \left\| (T_{-j}^{\mathbf{h}} - I) \frac{\partial^2 \tilde{u}}{\partial t^2}(\tau) \right\|_{L^2(\Omega)}^2 + h^2 \int_0^T d\tau \left\| \frac{\partial^4 f}{\partial t^4}(\tau) \right\|_{L^2(\Omega)}^2 \right).$$

When  $f \in H^3([0, T], L^2(\Omega))$  Theorem 3.9 applied to  $\frac{\partial^3 u}{\partial t^3}$  gives

$$\left\| \frac{\partial^4 u}{\partial t^4} \right\|_{L^2(\Omega)}^2(t) \leq K_T \int_0^T d\tau \left\| \frac{\partial^3 f}{\partial t^3} \right\|_{L^2(\Omega)}^2, \quad 0 \leq t \leq T$$

whence

$$\left\| \frac{\partial^4 \tilde{u}}{\partial t^4} \right\|_{L^2(\Omega)}^2(t) \leq \sup_{x \in \Omega} |\det \nabla \mathbf{F}| \left\| \frac{\partial^4 u}{\partial t^4} \right\|_{L^2([0, l])}^2(t) \leq K_T \int_0^T d\tau \left\| \frac{\partial^3 f}{\partial t^3} \right\|_{L^2(\Omega)}^2, \quad 0 \leq t \leq T$$

Taking the 2nd time derivative of (6.2) and using the elliptic regularity in Theorem 1.2.1 in Maugeri et al. (2000) for the spatial operator yield,  $\partial^2 \tilde{u} / \partial t^2 \in C^0([0, T], H^2(\Omega))$ , and even  $\in C^0([0, T], H_{\text{per}}^2(\mathbb{R}))$  and in fact

$$\left\| \frac{\partial^2 \tilde{u}}{\partial t^2} \right\|_{H^2(\Omega)}^2(t) \leq K_T \int_0^T d\tau \left( \left\| \frac{\partial^2 f}{\partial t^2} \right\|_{L^2(\Omega)}^2 + \left\| \frac{\partial^4 \tilde{u}}{\partial t^4} \right\|_{L^2(\Omega)}^2 \right) \leq K_T \int_0^T d\tau \left\| \frac{\partial^3 f}{\partial t^3} \right\|_{L^2(\Omega)}^2 \quad (6.16)$$

For  $w \in C_{\text{per}}^2(\mathbb{R}^2)$ , Taylor's formula gives for  $i = 1, 2$  ( $e_1 = [1, 0]$ ,  $e_2 = [0, 1]$ ),

$$(T_{-e_i}^{\mathbf{h}} - I)w(x) = w(x + \text{diag}(e_i)\mathbf{h}) - w(x) = h_i \frac{\partial w}{\partial x_i}(x) + \int_0^{h_i} dk (h_i - k) \frac{\partial^2 w}{\partial x_i^2}(x + ke_i)$$

whence

$$\begin{aligned}
\|(T_{-e_i}^{\mathbf{h}} - I)w\|_{L^2(\Omega)}^2 &\leq 2\left(h_i^2 \left\| \frac{\partial w}{\partial x_i} \right\|_{L^2(\Omega)}^2 \right. \\
&\quad \left. + \int_{\Omega} dx \int_0^{h_i} \int_0^{h_i} dk_1 dk_2 (h_i - k_1) \frac{\partial^2 w}{\partial x_i^2}(x + k_1 e_i) (h_i - k_2) \frac{\partial^2 w}{\partial x_i^2}(x + k_2 e_i) \right) \\
&\leq 4h^2 \|w\|_{H^2(\Omega)}^2
\end{aligned}$$

Taking limits, the same argument is true for  $w \in H_{\text{per}}^2$ .

For each  $\gamma \in \Delta$ , i.e.,  $|\gamma_i| \leq 1, i = 1, 2$ , write  $\gamma = \gamma - \gamma_1 e_1 + \gamma_1 e_1$ .

$$T_{-\gamma}^{\mathbf{h}} - I = T_{-\gamma}^{\mathbf{h}} - T_{-\gamma_1 e_1}^{\mathbf{h}} + T_{-\gamma_1 e_1}^{\mathbf{h}} - I$$

By periodicity of  $\tilde{u}$ ,

$$\left\| (T_{-\gamma}^{\mathbf{h}} - T_{-\gamma_1 e_1}^{\mathbf{h}}) \frac{\partial^2 \tilde{u}}{\partial t^2}(t) \right\|_{L^2(\Omega)} \leq \left\| (T_{-\gamma_2 e_2}^{\mathbf{h}} - I) \frac{\partial^2 \tilde{u}}{\partial t^2}(t) \right\|_{L^2(\Omega)}.$$

For any  $\gamma \in \Delta$

$$\begin{aligned}
\left\| (T_{-\gamma}^{\mathbf{h}} - I) \frac{\partial^2 \tilde{u}}{\partial t^2}(t) \right\|_{L^2(\Omega)}^2 &\leq 2 \left\| (T_{-\gamma}^{\mathbf{h}} - T_{-\gamma_1 e_1}^{\mathbf{h}}) \frac{\partial^2 \tilde{u}}{\partial t^2}(t) \right\|_{L^2(\Omega)}^2 + 2 \left\| (T_{-\gamma_1 e_1}^{\mathbf{h}} - I) \frac{\partial^2 \tilde{u}}{\partial t^2}(t) \right\|_{L^2(\Omega)}^2 \\
&\leq 2 \left\| (T_{-\gamma_2 e_2}^{\mathbf{h}} - I) \frac{\partial^2 \tilde{u}}{\partial t^2}(t) \right\|_{L^2(\Omega)}^2 + 2 \left\| (T_{-\gamma_1 e_1}^{\mathbf{h}} - I) \frac{\partial^2 \tilde{u}}{\partial t^2}(t) \right\|_{L^2(\Omega)}^2 \\
&\leq 4K_T h^2 \int_0^T d\tau \left\| \frac{\partial^3 f}{\partial t^3} \right\|_{L^2(\Omega)}^2, \quad 0 \leq t \leq T.
\end{aligned}$$

Combining these inequalities yields

$$\begin{aligned} e_{\kappa,\rho}[\hat{u}^{\mathbf{h}} - u](t) &\leq K(\hat{E}[U^{\mathbf{h}} - \hat{U}^{\mathbf{h}}] + e_{\kappa,\rho}[u^{\mathbf{h}} - u]) \\ &\leq K_T h^2 \int_0^T d\tau \left\| \frac{\partial^3 f}{\partial t^3} \right\|^2, \quad 0 \leq t \leq T, \end{aligned}$$

where  $\hat{u}^h = \sum_{\alpha} \hat{U}_{\alpha}^h \tilde{\phi}_{\alpha}^h \circ \mathbf{F}$  is the HCFEM solution of equation (3.11) via mass-lumping.

In summary the above inequality justifies the error in the lumped mass Galerkin approximation by HCFEM is of the same order as in the consistent mass Galerkin approximation by HCFEM.

## 6.5 NUMERICAL RESULTS FOR SCALAR WAVE EQUATION

The following two numerical examples are similar to those in Symes and Terentyev (2009b). In both examples, I set  $f = 0$  in equation (3.11). Waves are triggered by the initial conditions,

$$u(\mathbf{x}, 0) = g(\mathbf{x}, 0), \quad \frac{\partial u}{\partial t}(\mathbf{x}, 0) = \frac{\partial g}{\partial t}(\mathbf{x}, 0), \quad (6.17)$$

where

$$g(\mathbf{x}, t) = \frac{1}{r} \left(1 - 2\left(\pi f_0 \left(t + \frac{1.45}{f_0} - \frac{r}{c_s}\right)\right)^2\right) \exp\left(-\left(\pi f_0 \left(t + \frac{1.45}{f_0} - \frac{r}{c_s}\right)\right)^2\right)$$

with  $r = \|\mathbf{x} - \mathbf{x}_s\|_2$ .  $\mathbf{x}_s$  are the center of the radiation field.  $f_0$  denotes the central frequency.  $c_s = \sqrt{\frac{\kappa(\mathbf{x}_s)}{\rho(\mathbf{x}_s)}}$  is the sound velocity at  $\mathbf{x}_s$ .

The implementation of HCFEM is based on deal.II (Bangerth et al., 2007), a C++ program library for solving partial differential equations with adaptive finite element methods.

Figure (6.2) shows the dipping model. In this example  $f_0 = 10$  Hz.  $x_s = [-300\sqrt{3} \text{ m}, -300 \text{ m}]$ . Figure (6.5), (6.6), (6.7) shows the wave field snapshot at  $T = 0.75$  s. Figure 6.5 and 6.6 show the  $Q_1$  finite element solutions. The difference is, to produce the solution in Figure 6.5 mass and stiffness matrices are calculated with regular grid quadrature, while accurate quadrature for mass and stiffness matrices' computation with mass lumping (this is similar to Symes and Terentyev (2009b)) is applied to obtain the solution in Figure 6.6. Figure 6.7 shows the numerical solution by HCFEM on the same regular grid as in Figure 6.5 and 6.6. For the dipping model as shown in Figure 6.6 and 6.7 HCFEM is at least as good as the  $Q_1$  FEM with accurate quadrature for mass and stiffness matrices' computation when the density contrasts are low. Both methods seem to get rid of the staircase diffraction, which is shown in Figure 6.5. Table (6.1) shows the RMS error of the  $Q_1$  FEM and HCFEM in the region within the red box shown in Figure (6.6) and (6.7). The  $Q_1$  FEM here is with accurate quadrature for mass and stiffness matrices' computation. This table shows that the estimated convergence rate of HCFEM is about second-order while the  $Q_1$  FEM loses some convergence rate. This implies that HCFEM is somewhat more accurate.

The second example is the dome model, the velocity and density of which are illustrated in Figure (6.3), (6.4) respectively. The initial radiation field is centered at  $\mathbf{x}_s = [3920 \text{ m}, 3010 \text{ m}]$  with  $f_0 = 15$  Hz. Since the locally refined grid around interfaces reduces the first order interface error in acoustic wave simulations, we use

the  $Q_1$  FEM solution on a locally refined grid as the reference solution. Figure 6.8 shows the difference of the  $Q_1$  FEM solutions on a regular grid  $\mathcal{T}^h$  and on a locally refined grid  $\mathcal{T}_\delta^h$  around interfaces. Figure 6.9 shows the difference of HCFEM solution on  $\mathcal{T}^h$  and the  $Q_1$  FEM solution on the same locally refined grid  $\mathcal{T}_\delta^h$ . We use the same time stepping restricted by the smallest grid size in  $\mathcal{T}_\delta^h$ , so that the difference shown in Figure 6.8 and 6.9 reflects the distinction of the spatial discretization. In the dome model, since several interfaces are presented instead of one, the interface error becomes more severe and is gradually accumulated as time goes by. It turns out that the HCFEM solution is closer to the refined-grid FEM solution.

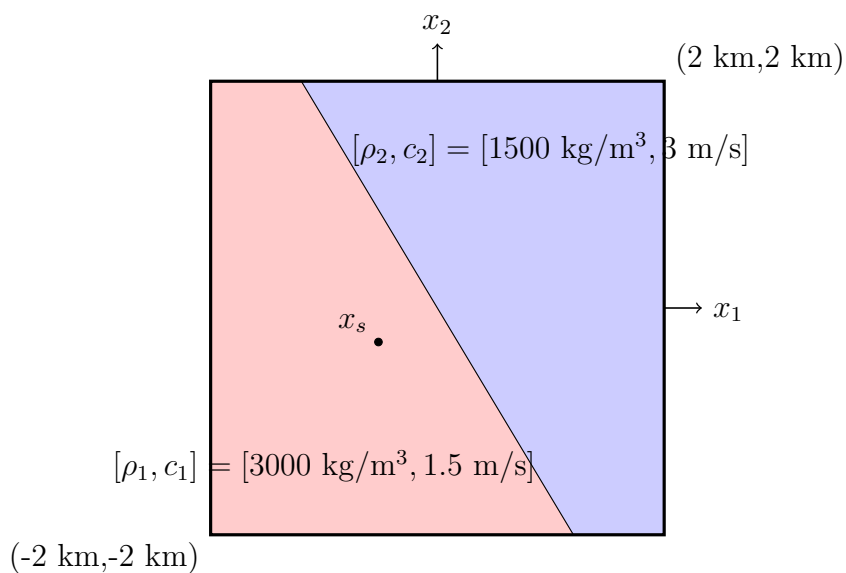


**Figure 6.2:** Dipping model

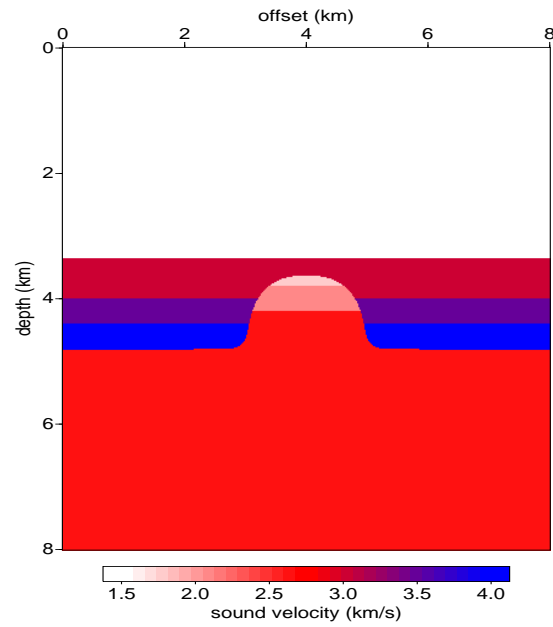


**Figure 6.3:** Velocity model for dome model

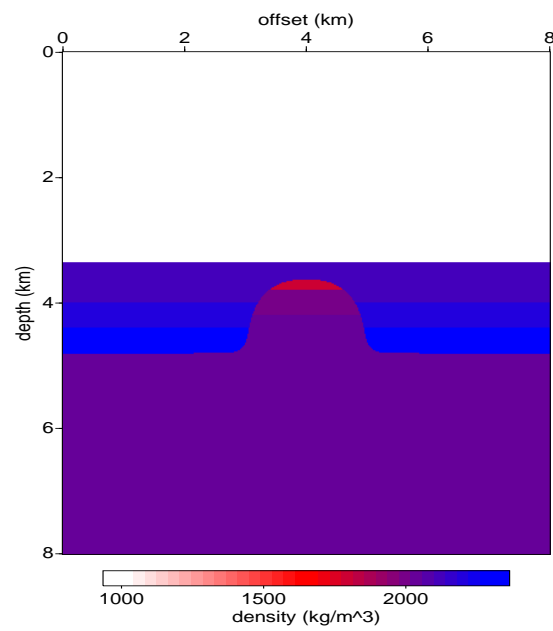


**Figure 6.4:** Density model for dome model



**Figure 6.5:**  $Q_1$  FEM solution snapshot at  $T = 0.75$  s on the dipping model, regular grid quadrature for mass and stiffness matrices.

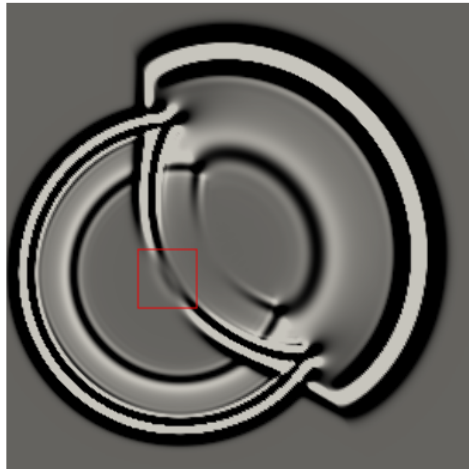


**Figure 6.6:**  $Q_1$  FEM solution snapshot at  $T = 0.75$  s on the dipping model, accurate quadrature for mass and stiffness matrices.

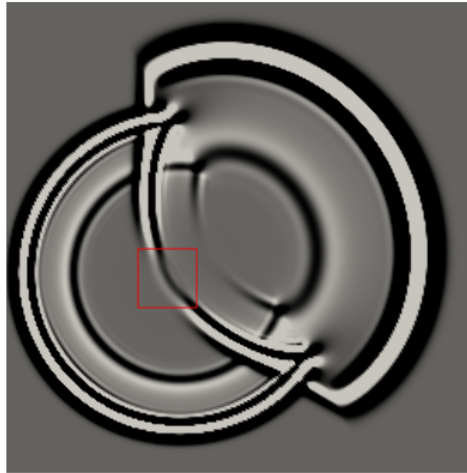


**Figure 6.7:** HCFEM solution snapshot at  $T = 0.75$  s on the dipping model.

RMS error			
$h$	7.8125 m	3.90625 m	1.953125 m
$Q_1$ FEM	4.23e-1	1.49e-1	5.72e-2
HCFEM	2.79e-1	7.64e-2	1.94e-2
convergence rate			
$h$	7.8125 m	3.90625 m	1.953125 m
$Q_1$ FEM	-	1.51	1.38
HCFEM	-	1.87	1.97

**Table 6.1:** RMS error and estimated convergence rate over the region within the red box shown in Figure (6.6) and (6.7). The  $Q_1$  FEM here is the one with accurate quadrature for mass and stiffness matrices

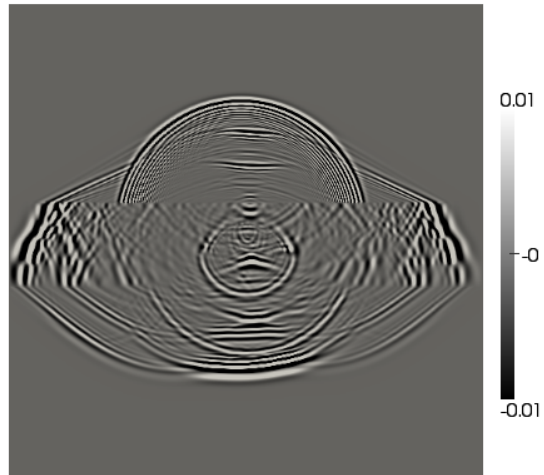


**Figure 6.8:** Difference of  $Q_1$  FEM solution on a regular grid  $\mathcal{T}^h$  and on a locally refined grid  $\mathcal{T}_\delta^h$  around interfaces at  $T = 1.3$  s on the dome model.

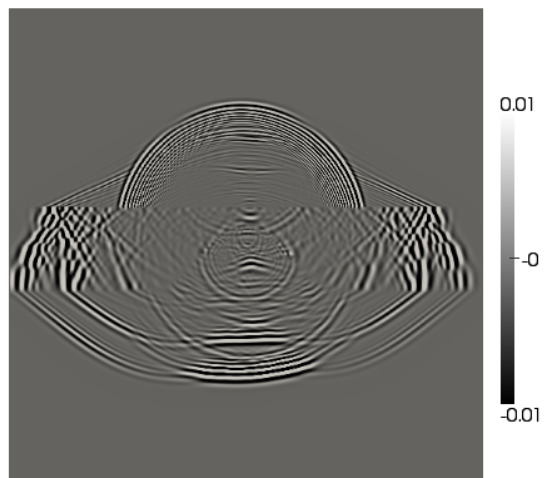


**Figure 6.9:** Difference of HCFEM solution on  $\mathcal{T}^h$  and  $Q_1$  FEM solution on  $\mathcal{T}_\delta^h$  at  $T = 1.3$  s on the dome model.



# Chapter 7

## Conclusion

I propose the transfer-of-approximation finite element method and harmonic coordinate finite element method based on the transfer-of-approximation property. These two methods achieve the optimal convergence rate on regular grids. The transfer-of-approximation finite element method is theoretically attractive, but it is not very practical due to the prohibitive cost of basis construction and the dense property of the resulting stiffness and mass matrices. The 2D harmonic coordinate finite element method (HCFEM) on regular grids achieves optimal second-order convergence for static and dynamic acoustic boundary value problems with spatially heterogeneous bulk modulus and density, at the additional cost of solving two auxiliary elliptic boundary value problems. HCFEM stiffness and mass matrices are constructed in a systematic procedure, and have the same sparsity pattern as those in the standard regular grid FEM. Mass-lumping in HCFEM is proved to preserve the optimal convergence order, due to the smoothness of acoustic solutions in harmonic coordinates, and results in an efficient, explicit time step.

## Contribution

In Chapter 3 I summarize the transfer-of-approximation results first proposed by Berlyand and Owhadi (2010) and later generalized by Symes (2011, 2012). I manage to show that under certain assumptions, the HCFEM for scalar elliptic problems with  $L^\infty$  coefficients achieves the optimal order convergence due to Corollary 3.8, Theorem 5.4. I also present a modified proof of approximation theorem for the scalar wave equation, patterned after the one given by Symes and Terentyev (2009a). In this proof I show that an approximation property for solutions of an elliptic equation (Theorem 3.9), rather than the specific finite element spaces, is the key assumption.

In Chapter 4 I implement the simple transfer-of-approximation FEM for elliptic and scalar wave interface problems, and through numerical experiments discover that even with the localization strategy suggested by Owhadi and Zhang (2011) its cost is prohibitive for use in practice.

In Chapter 5 I present an analysis for HCFEM including the effect of errors from the harmonic coordinates' approximation for first time. The results completely justify the HCFEM in 1D. For 2D interface problems I propose and implement the HCFEM with adaptive gridding for the harmonic coordinates' computation. Numerical results show that the convergence is as the theory suggests.

In Chapter 6 the results of Symes and Terentyev (2009a) on mass lumping with  $Q_1$  finite element space for constant density acoustic wave equation are extended to HCFEM for variable density acoustics. I show that the lumped mass solution has the same accuracy as the consistent mass solution asymptotically. My numerical experiments of the lumped mass HCFEM for 2D acoustics verify the theoretical result,

and suggest that standard lumped mass  $Q_1$  Galerkin is as accurate as lumped mass HCFEM when the density contrasts are small. This observation suggests we can avoid the expensive harmonic coordinates' computation for problems of sedimentary rocks in which the density contrasts are typically small.

## 7.1 FUTURE WORK

There are still some interesting questions left. In the following I list them in the chronological order of this thesis as a reference for future work.

### Transfer basis construction error

In Chapter 4 the transfer basis satisfies equation (4.3). Since the right hand side  $\Delta\phi_i^h \in H^{-1}(\Omega)$ , there is no error estimate for any finite element method applied to this problem. So it would be good to know how much effort we should put into solving this problem in order to maintain the optimal convergence rate of the transfer-of-approximation finite element method.

### Questions about HCFEM

Though I try to make the analysis of HCFEM as robust as possible, there are still questions for future work.

Starting from deriving the non divergence form, we need the regularity of the harmonic coordinates to apply the chain rule. For  $\mathbf{F} \in H^1(\Omega, \mathbb{R}^2)$  I prove the change rule (5.9) is valid for any  $\tilde{u} \in W^{2,p}(\Omega)$ ,  $p > 2$ . Maugeri et al. (2000) prove that the

solution  $\tilde{u}$  of equation (5.8) belongs to the space  $H_0^1(\Omega) \cap H^2(\Omega)$ . So does the chain rule also hold for  $p = 2$ ?

In the error estimate (5.26) (Li et al., 2010) for the harmonic coordinates' approximation, it is assumed that  $\nabla F_i \in B_{2,1}^{1/2}(\bigcup_k \Omega_k), i = 1, 2$  in order to obtain the desirable error estimate. Does this holds for interface problems generally, or other assumptions on the coefficient have to be made? Is there a similar analysis for the texture problems where the coefficient varies on many scales?

## Extension to elasticity

The transfer-of-approximation finite element method works for the elastic problem and can achieves optimal convergence rate in theory. But it is not practical due to the prohibitive numerical cost. The change-of-variable trick in HCFEM doesn't work in the elastic case. Therefore the direct extension of HCFEM for elasticity is not possible. Other ideas have to be explored.

In Berlyand and Owhadi (2010) they mentioned to construct the harmonic displacements by solving,

$$\begin{aligned} -\nabla \cdot C[\epsilon(\mathbf{F}^{kl})] &= 0 \quad \text{in } \Omega \\ \mathbf{F}^{kl} &= \frac{x_k \mathbf{e}_l + x_l \mathbf{e}_k}{2} \quad \text{on } \partial\Omega. \end{aligned} \tag{7.1}$$

for  $k, l = 1, 2, 3$ . For displacements  $\mathbf{u}$  of the original elasticity problem under any force density, they observed that  $\epsilon(\mathbf{F})^{-1}[\epsilon(\mathbf{u})]$  has smoothness regularity (Hölder continuity) like in the scalar elliptic case. Berlyand and Owhadi (2010) claimed the strain  $\epsilon(\mathbf{u})$  then can be approximated well enough by a special finite element space. How-

ever they didn't provide any detailed proof for elasticity as for acoustics in Owhadi and Zhang (2008), and didn't even describe an algorithm. The elasticity upscaling is a long term goal and deserves more efforts.



# BIBLIOGRAPHY

- Alessandrini, G. and V. Nesi, 2003, Univalent  $\sigma$ -harmonic mappings: connections with quasiconformal mappings: *Journal d'Analyse Mathématique*, **90**, 197–215.
- Alford, R., R. Kelly, and D. M. Boore, 1974, Accuracy of the finite difference modelling of the acoustic wave equation: *Geophysics*, **39**, 834–842.
- Allaire, G. and R. Brizzi, 2005, A multiscale finite element method for numerical homogenization: *SIAM Journal on Multiscale Modeling and Simulation*, **4**, 790–812.
- Auriault, J. L., C. Boutin, and C. Geindreau, 2009, Homogenization of coupled phenomena in heterogeneous media: ISTE Ltd and John Wiley & Sons, Inc.
- Babuška, I., G. Caloz, and J. E. Osborn, 1994, Special finite element methods for a class of second order elliptic problems with rough coefficients: *SIAM Journal on Numerical Analysis*, **31**, 945–981.
- Backus, G., 1962, Long wavelength elastic anisotropy produced by horizontal layering: *Journal of Geophysical Research*, **67**, 4427–4440.
- Bangerth, W., R. Hartmann, and G. Kanschat, 2007, deal.II – a general purpose object oriented finite element library: *ACM Transactions on Mathematical Software*, **33**, 24/1–24/27.
- Bensoussan, A., J.-L. Lions, and G. Papanicolau, 1978, Asymptotic analysis for peri-

- odic structures: North-Holland, Amsterdam New York Oxford.
- Berlyand, L. and H. Owhadi, 2010, Flux norm approach to finite dimensional homogenization approximations with non-separated scales and high contrast: *Archive for Rational Mechanics and Analysis*, **198**, 677–721.
- Bernstein, S. N., 1910, Sur la généralisation du problème de Dirichlet: *Math. Ann.*, **62**, 253–271.
- Binford, T. L., J., 2011, Applications of harmonic coordinate finite element method to 2d interface problems: Department of Computational and Applied Math, Rice University, Houston, Texas, USA. (PHD thesis).
- Briane, M., G. W. Milton, and V. Nesi, 2004, Change of sign of the corrector’s determinant for homogenization in three-dimensional conductivity: *Arch. Ration. Mech. Anal*, **173**, 133–150.
- Brown, D., 1984, A note on the numerical solution of the wave equation with piecewise smooth coefficients: *Mathematics of Computation*, **42**, 369–391.
- Ciarlet, P., 2002, *The finite element method for elliptic problems*: SIAM, Philadelphia.
- Craster, R. V. and Y. V. Obnosov, 2001, Four-phase checkerboard composites: *SIAM Journal on Applied Mathematics*, **61**, 1839–1856.
- E, W. and B. Engquist, 2003, Multiscale modeling and computation: *Notices of the AMS*, **50**, 1062–1070.
- Efendiev, Y. and T. Hou, 2009, *Multiscale finite element methods: theory and applications*: Springer, New York.
- Engquist, B., H. Holst, and O. Runborg, 2011, Multiscale methods for wave propagation in heterogeneous media: *Communications in Mathematical Sciences*, **9**, 33–56.
- Evans, L. C., 1998, *Partial differential equations*: American Mathematical Society,

- Providence, Rhode Island.
- Evans, L. C. and R. F. Gariepy, 1992, Measure theory and fine properties of functions: CRC Press, Boca Raton London New York Washington, D.C.
- Fehler, M. and P. Keliher, 2011, SEAM Phase I: Challenges of Subsalt Imaging in Tertiary Basins, with Emphasis on Deepwater Gulf of Mexico: Society of Exploration Geophysicists.
- Hou, T. and X. Wu, 1997, A multiscale finite element method for elliptic problems in composite materials and porous media: *Journal of Computational Physics*, **134**, 169–189.
- Hou, T. Y., X.-H. Wu, and Z. Cai, 1999, Convergence of a multiscale finite element method for elliptic problems with rapidly oscillating coefficients: *Mathematics of Computation*, **68**, 913–943.
- Kozlov, S., 1980, Averaging of random operators: *Mathematics of the USSR-Sbornik*, **37**, 167–180.
- Leveque, R. J. and Z. Li, 1994, The immersed interface method for elliptic equations with discontinuous coefficients and singular sources: *SIAM Journal on Numerical Analysis*, **31**, 1019–1044.
- Li, J., J. Melenk, B. Wohlmuth, and J. Zou, 2010, Optimal a priori estimates for higher order finite elements for elliptic interface problems: *Applied Numerical Mathematics*, **60**, no. 1-2, 19–37.
- Li, Z. and K. Ito, 2006, The immersed interface method: numerical solution of PDEs involving interfaces: SIAM, Philadelphia.
- Lions, J.-L. and E. Magenes, 1972, Non-homogeneous boundary value problems and applications: Springer, New York.
- Maugeri, A., D. K. Palagachev, and L. G. Softova, 2000, Elliptic and parabolic equations with discontinuous coefficients, volume **109** of *Mathematical Research*: Wiley-

- VCH, Berlin, New York.
- Melenk, J. and I. Babuška, 1996, The partition of unity finite element method: Basic theory and applications: *Computer Methods in Applied Mechanics and Engineering*, **139**, 289314.
- Muir, F., J. Dellinger, J. Etgen, and D. Nichols, 1992, Modeling elastic fields across irregular boundaries: *Geophysics*, **57**, 1189–1193.
- Ohwadi, H. and L. Zhang, 2007, Metric based upscaling: *Communications in Pure and Applied Mathematics*, **60**, 675–723.
- Owhadi, H. and L. Zhang, 2008, Homogenization of the acoustic wave equations with a continuum of scales: *Computer Methods in Applied Mechanics and Engineering*, **198**, 397–406.
- , 2011, Localized bases for finite dimensional homogenization approximations with non-separated scales and high contrast: *SIAM Journal on Multiscale Modeling and Simulation*, **9**, no. 4, 1373–1398.
- Schoenberg, M. and F. Muir, 1989, A calculus for finely layered anisotropic media: *Geophysics*, **54**, 581–589.
- Stolk, C. C., 2000, On the modeling and inversion of seismic data: PhD thesis, Universiteit Utrecht.
- Strang, G. and G. J. Fix, 1973, *An analysis of the finite element method*: Prentice-Hall, New York.
- Symes, W., 2006, CAAM 436 Notes: Partial Differential Equations of Mathematics Physics: Department of Computational and Applied Mathematics, Rice University.
- Symes, W. W., 2011, Numerical upscaling by transfer of approximation: Presented at the , Presented at Baylor workshop on splitting and multiscale methods for computational PDEs, Waco, TX.
- , 2012, Transfer of approximation and numerical homogenization of hy-

- parabolic boundary value problems with a continuum of scales: **TR12-20**, Department of Computational and Applied Mathematics, Rice University, [http://www.caam.rice.edu/tech\\_reports.html](http://www.caam.rice.edu/tech_reports.html).
- Symes, W. W. and I. Terentyev, 2009a, Mass lumping for constant-density acoustics: **09-06**, Department of Computational and Applied Mathematics, Rice University, [http://www.caam.rice.edu/tech\\_reports.html](http://www.caam.rice.edu/tech_reports.html).
- , 2009b, Subgrid modeling via mass lumping in constant density acoustics: 79th Annual International Meeting, Expanded Abstracts, 2572–2576, Society of Exploration Geophysicists.
- Symes, W. W. and T. Vdovina, 2009, Interface error analysis for numerical wave propagation: *Computational Geosciences*, **13**, 363–371.
- Tartar, L., 2007, *An introduction to Sobolev spaces and interpolation spaces vol.3 of Lecture Notes of the Unione Matematica Italiana*: Springer.
- Vdovina, T., S. Minkoff, and O. Korostyshevskaya, 2005, Operator upscaling for the acoustic wave equation: *SIAM Journal on Multiscale Modeling and Simulation*, **4**, 1305–1338.
- Wang, X., 2010, Discontinuous Galerkin time domain methods for acoustics and comparison with finite difference time domain methods: Department of Computational and Applied Mathematics, Rice University, Houston, Texas, USA.
- Yosida, K., 1996, *Functional analysis*: Springer Verlag.
- Zhang, C. and R. J. LeVeque, 1997, The immersed interface method for acoustic wave equations with discontinuous coefficients: *Wave Motion*, **25**, 237–263.
- Zhang, C. and W. W. Symes, 1998, Fourth order methods for acoustic waves with discontinuous material: *Mathematical and Numerical Aspects of Wave Propagation*, 652–656, SIAM, Philadelphia.